Dissertation

submitted to the
Combined Faculty for the Natural Sciences and for Mathematics
of the Ruperto Carola University of Heidelberg, Germany
for the degree of
Doctor of Natural Sciences

presented by

M.Sc. Britta Ismer

born in: Bochum, Germany
Oral examination: 5th December 2018

Novel gene fusions identified as new drug targets in paediatric glioma and their pre-clinical characterisation

Referees: Prof. Dr. Peter Angel
Prof. Dr. Stefan Pfister

Für Onkel Kai,

“My childhood-hero
Will always be you
And no one else comes close

I thought you’d lead me
When life’s misleading
That’s when I miss you most

Every now and then I’m drawn to places
Where I hear your voice and see your face and
Every little thought will lead me right back to you

You were born from one love of two hearts
You were three kids and a loving mum
You made this place a home
A shelter from the storm
You said I had life and a true heart
I tried my best and I came so far
But you will never know…”

The work and results of the following dissertation were performed and obtained from October 2015 until August 2018 under the supervision of Dr. David Jones and Prof. Dr. Stefan Pfister in the Paediatric Glioma Research Group and Division of Paediatric Neurooncology, respectively, at the German Cancer Research Center (DKFZ), Heidelberg, Germany and Hopp Children's Cancer Center at the NCT Heidelberg (KiTZ), Heidelberg, Germany.

Content

Abbreviations

ANTCN	Anaplastic Neuroepithelial Tumour with Condensed Nuclei
ALCL	Anaplastic large-cell lymphoma
ALK	Anaplastic Lymphoma Kinase
ASAP	Adaptable System for Assembly of multiplex Plasmids
BBB	Blood-brain barrier
BCA	Bicinchoninic Acid
BSA	Bovine Serum Albumin Fraction V
Cdkn2a	Cyclin-dependent kinase inhibitor 2A
CNS	Central Nervous System
DNA	Deoxyribonucleic acid
DNET	Dysembroplastic NEuroepithelial Tumour
E14.5	Embryonic day 14.5 after conception
EMA	European Medicines Agency
EML4	Echinoderm microtubule-associated protein-like 4
EP	Electroporation
EtOH	Ethanol
FCS	Fetal Calf Serum
FDA	Food and Drug Administration
FFPE	Formalin-Fixed Paraffin-Embedded
FGFR	Fibroblast Growth Factor Receptor
FGFR1mut546	FGFR1 mutation: amino acid substitution of N to K at position 546
FGFR1mut656	FGFR1 mutation: amino acid substitution of K to E at position 656
GBM	Glioblastoma
GEMM	Genetically engineered mouse model
gRNA	Guide RNA
H&E	Haematoxylin & Eosin
HA	human influenza hemagglutinin
HDR	Homology-Directed Repair
HGG	High-Grade Glioma

ICGC	International Cancer Genome Consortium
IF	Immunofluorescence
IHC	Immunohistochemistry
Indels	Insertions and deletions
INFORM	INdividualized Therapy FOr Relapsed Malignancies in Childhood
LB	Miller's Luria-Butani Broth
LGG	Low-Grade Glioma
MHLW	Japanese Ministry of Health, Labor and Welfare
MNP	Molecular Neuropathology
MRI	Magnetic Resonance Imaging
mTOR	Mammalian (or mechanistic) Target Of Rapamycin
NHEJ	Non-Homologous End Joining
NPM	Nucleophosmin
NSCLC	Non-small-cell lung cancer
NTRK	Neurotrophic Tyrosine Kinase
N-tva	*Tva* receptor under nestin promoter
ORR	Objective Response Rate
P/S	Penicillin & Streptomycin
PBS	Phosphate-Buffered Saline
PCR	Polymerase Chain Reaction
PDX	Patient-Derived Xenograft
PFS	Progression-free survival
PI	Propidium Iodide
PS	Phosphatidylserine
PTT	Paediatric Targeted Therapy
RCAS	Replication-Competent ASLV long terminal repeat (LTR) with a Splice acceptor
RNA	Ribonucleic acid
Ros1	C-ros oncogene 1
sgcdkn2a	Single guide RNA against cdkn2a
sgp53	Single guide RNA against p53

TMZ	Temozolomide
WHO	World Health Organization

Summary

Gliomas are the most common paediatric brain tumours, accounting for about 50% of all brain tumours in children. They are typically classified by the putative cell type they arise from based on morphology, the location they are found and malignancy grade. The most common glioma found in adults is glioblastoma, which is a WHO grade IV tumour with an average survival of less than 15 months. Extensive work has gone into characterising, modelling and treating this tumour *in vivo* and *in vitro*, but it is now clear that glioblastoma in children is biologically very different from that in adults. Paediatric high-grade gliomas do, however, share their aggressiveness with their adult counterparts, with few patients achieving long-term survival - dictating an urgency to find more precise therapies for these patients.

Additionally, relatively little work has focused on low-grade gliomas to date. Nevertheless, these tumours also deserve a lot of attention, because low-grade gliomas make up 30-50% of all paediatric brain tumours and more than half of all paediatric gliomas. Although the tumour itself does not necessarily lead to a massively reduced life span and should rather be considered a chronic disease, the impact on the patients' and families' lives caused by the therapy load and possible recurrences remains a major clinical burden. Unlike high-grade gliomas, which are very heterogeneous with multiple oncogenic drivers, most low-grade gliomas are driven by alterations in the mitogen-activated protein kinase (MAPK) pathway through different mechanisms. Examples are *BRAF* alterations, *FGFR1* mutations, and *NTRK* or *MYB* fusions.

After analysing around 200 paediatric glioma samples by whole-genome/whole-exome and RNA sequencing within the ICGC PedBrain Tumour Project and the INFORM personalised medicine study, fusions involving an additional candidate gene (*ALK*) were found to be of interest in terms of their pattern of occurrence and availability of targeted inhibitors. Clinically these fusions arose in an interesting patient population, affecting infants (<2 years old) with histologically malignant tumours that however showed outcomes more similar to low-grade glioma than glioblastoma.

PPP1CB:ALK was the most common gene fusion found in this context, which was then modelled *in vivo* using two different state-of-the-art methodologies: *in utero* electroporation and p0 injection using the RCAS-tva system. Through *in utero* electroporation, a novel mouse

model was generated that nicely recapitulates the human tumours. Different ALK-specific inhibitors already used in clinical trials for other tumours, like non-small cell lung cancer or neuroblastoma, were tested on the tumour cells in an *in vitro* sphere culture setting and in addition also *in vivo* on allografted tumour cells. The results show a promising effect of the third-line, blood-brain-barrier penetrant ALK inhibitor lorlatinib, with IC50 values below 1.3nM and a significant increase in lifespan with a decrease in tumour signal, respectively.

Thus, the project led from the genomic discovery of a novel driving event in paediatric glioma through to its modelling and identification of a promising new option for therapy. Further proof-of-concept application with other oncogenic combinations leads to the conclusion that the mouse model strategy and the methodology behind this can be further applied to test other candidate genes and specific inhibitor therapies. The overall aim is thus to accelerate the approval of targeted drugs by authorities after running a stratified clinical trial on a small infant patient population carrying the gene of interest, to enable patients to get the most potent therapy with the fewest side effects.

Zusammenfassung

Gliome sind mit ca. 50% die am häufigsten auftretenden pädiatrischen Hirntumore und werden normalerweise nach dem Zelltyp, von dem der Tumor vermutlich entstanden ist, klassifiziert. Diese Klassifizierung basiert auf der Morphologie, der Lage und der Malignität des Tumors. Bei Erwachsenen ist das Glioblastom das prävalenteste Gliom, welches nach WHO Klassifizierung als Grad IV eingestuft ist und die durchschnittliche Überlebenszeit beträgt weniger als 15 Monate. Umfangreiche Charakterisierung, Modelletablierung und Behandlungen wurden *in vitro* und *in vivo* durchgeführt bevor sich nun herausgestellt hat, dass sich pädiatrische Glioblastome biologisch stark von denen in Erwachsenen unterscheiden. Hochgradige pädiatrische Gliome zeigen die gleiche Aggressivität wie die adulte Form, da nur wenige Patienten lange überleben und somit die Dringlichkeit für präzisere Therapien für solche Patienten verdeutlicht.

Aber es wird auch vergleichsweise wenig Arbeit in niedriggradige Gliome investiert. Nichtsdestotrotz verdienen diese Tumore ebenso viel Aufmerksamkeit, da mehr als die Hälfte aller pädiatrischen Hirntumore (30-50%) niedriggradige Gliome sind. Obwohl der Tumor an sich die Lebensdauer nicht zwangsläufig drastisch reduziert und er dadurch eher als chronische Krankheit angesehen werden sollte, haben die Therapiefolgen und mögliche Rezidive trotzdem sehr drastische Auswirkungen auf die Patienten und deren Familien, und bleiben somit eine bedeutende klinische Belastung. Anders als hochgradige Gliome, welche aufgrund ihrer vielen onkogenen Auslöser sehr heterogen sind, entstehen die meisten niedriggradigen Gliome durch verschiedene Veränderungen im mitogen-activated protein kinase (MAPK) Signalweg. Beispiele hierfür sind *BRAF* Modifikationen, *FGFR1* Mutationen, und *NTRK* oder *MYB* Fusionen.

Nachdem ca. 200 pädiatrische Gliomproben im Rahmen des ICGC PedBrain Tumour Projekts und der INFORM personalisierten Medizinstudie mittels Ganzgenom/Ganzexon- und RNA-Sequenzierung analysiert wurden, sind wiederholt Fusionen eines zusätzlichen Kandidatengens (*ALK*) aufgetreten, welche aufgrund ihres aufgetretenen Musters und der Verfügbarkeit gezielter Inhibitoren interessant wurden. In der Klinik wurden diese Tumore in einer interessanten Patientenpopulation (< 2 Jahre) gefunden, da sie histologisch auf einen malignen Tumor hinweisen, aber die Überlebensdaten der Patienten eher zu niedriggradigen Gliomen als zu Glioblastomen passen.

PPP1CB:ALK war die am meisten gefundene Genfusion, die in diesem Zusammenhang aufgetreten ist, woraufhin diese *in vivo* mit zwei verschiedenen Methoden nach dem aktuellen Stand der Technik: *in utero* Elektroporation und p0 Injektion des RCAS-tva Systems, nachgestellt wurden. Durch *in utero* Elektroporation wurde ein neuartiges Mausmodell entwickelt, welche die humanen Tumore nachstellt. Verschiedene ALK-spezifische Inhibitoren, welche in klinischen Studien schon für andere Tumore wie zum Beispiel dem Neuroblastom oder nicht-kleinzelligem Lungenkrebs verwendet werden, wurden an Tumorzellesphären *in vitro* und zusätzlich noch *in vivo* an allotransplantierten Tumorzellen getestet. Die Ergebnisse zeigen eine signifikante Wirkung des third-line, Blut-Hirn-Schranke durchlässigen ALK Inhibitors Lorlatinib mit IC50 Werten unter 1.3nM und einem signifikanten Anstieg der Lebenserwartung sowie einer Reduktion des Tumorsignals.

Zusammenfassend deckt dieses Projekt alle Aspekte von genomischer Entdeckung eines neuartigen karzinogenen Kandidatengens über dessen Modellentwicklung zur Identifizierung und Testung neuer hoffnungsvoller Therapieoptionen ab. Weitere Machbarkeitsstudien mit anderen onkogenen Kombinationen ermöglichen es, das Mausmodell und die verwendeten Methoden auch für andere Kandidatengene und deren gezielte Inhibitoren einzusetzen. Dies hat als endgültiges Ziel, die zielgerichteten Inhibitoren schneller von den Behörden genehmigt zu bekommen, nachdem diese in einer stratifizierten klinischen Studie an einer kleinen Patientenzahl, die dieses Gen mutiert haben, erfolgreich getestet wurden. So kann den Patienten die bestmöglichste Therapie mit den geringsten Nebenwirkungen ermöglicht werden.

Graphical abstract

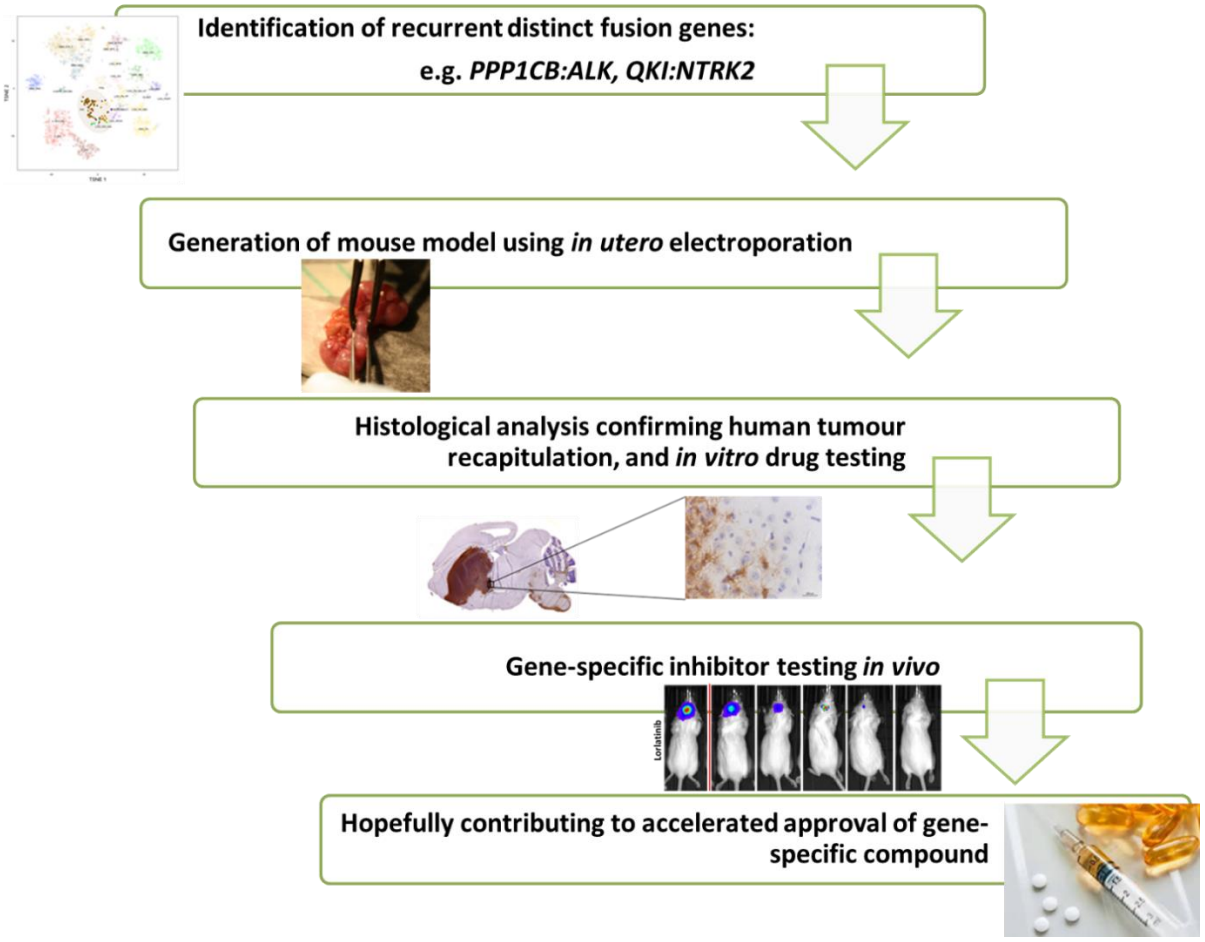

1. Introduction

1.1 Paediatric Cancer

Mutations leading to cancer growth can occur anytime in the cellular lineage from the development of the fertilised egg to the cells being sequenced in the tumour bulk[1]. These may lead to uncontrolled growth of cells caused by increased cell proliferation and decreased apoptosis. In this setting, intrinsic control mechanisms are damaged and alterations are made to the normal cell regulatory pathways. Cancer is not only a disease that occurs in adults or results from environmental exposures such as UV radiation or tobacco smoke. Although cancer is a disease of genetic and epigenetic changes accumulating over time, even children (hereafter defined as 0-18 years of age) develop neoplasms. Paediatric tumours make up 2% of all cancer cases and are the second most common cause of death in this age group, after trauma[2]. The number of genome-wide mutations and copy number changes positively correlate with patient age at diagnosis[1,3-11], with the naturally increased proliferation rate during early development potentially meaning that fewer additional alterations are required in order for a cell to become cancerous.

Paediatric central nervous system (CNS) tumours are the second most common (20-25%) tumours found in childhood[12] (Figure 1). Recently, however, statistics gathered by the Central Brain Tumor Registry of the United States (CBTRUS) and others have shown that brain and CNS tumours are now the leading cause of cancer-related death in children aged 0-19, except in 1-4 year olds, where leukaemia is still the leading cause of mortality[13].

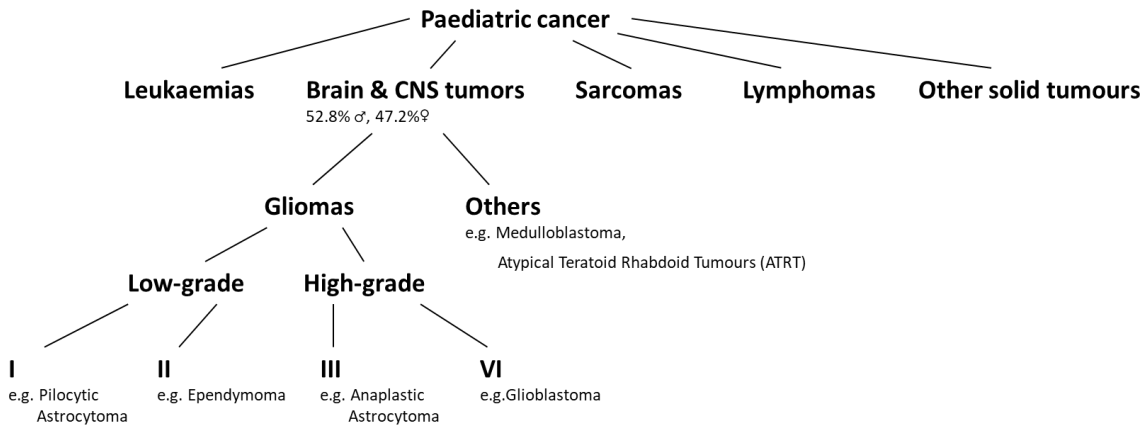

Figure 1. Hierarchial tree of paediatric cancers. Brain and CNS tumours are the second most common childhood tumour after leukaemias. These divide into gliomas and other tumours, e.g. Medulloblastoma or ATRT. The gliomas can be divided into low- and high-grade gliomas with astrocytomas being the most common glioma followed by ependymoma. Pilocytic Astrocytoma (PA) is the most common low-grade glioma.

1.2 Paediatric Neurooncology

Brain tumours have an overall lower somatic mutational burden than other human cancer types (Figure 2) with most paediatric tumours harbouring far fewer mutations compared with tumours caused by chronic mutagenic exposures such as lung cancer or melanoma (tobacco and UV, respectively)[1]. Pilocytic astrocytoma is known to be a single pathway disease[14] with few somatic mutations compared with almost all other cancers.

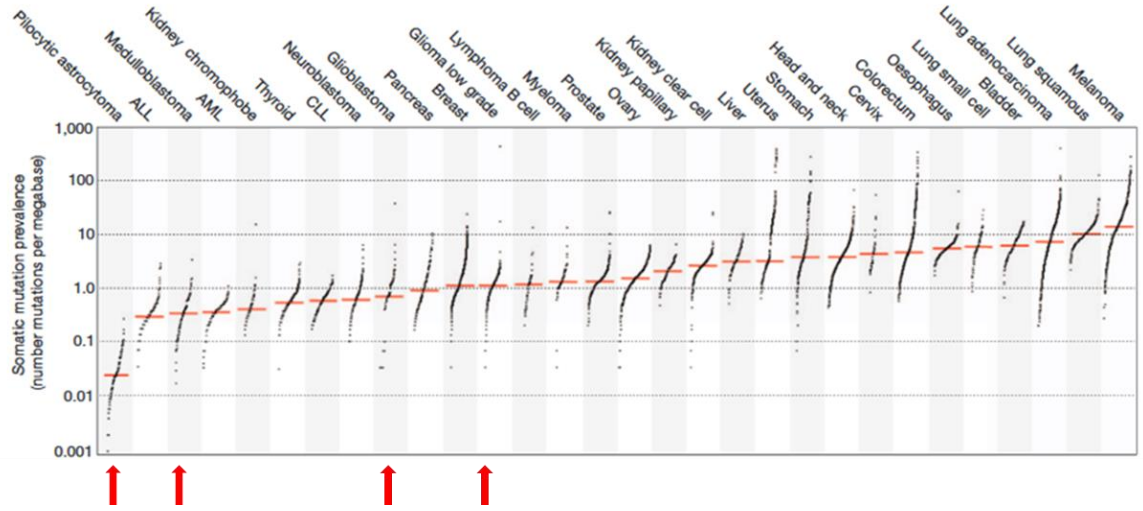

Figure 2. Somatic mutation prevalence of several different types of cancer in humans. All brain and CNS tumours (indicated by the red arrows) are found in the bottom half of the list ranked by somatic mutation prevalence. Glioblastoma and Glioma low grade refer to the adult groups. Taken from Alexandrov *et al*., 2013[1].

All brain tumour types depicted in Figure 2 are in the bottom half of all tumours listed in terms of somatic mutation prevalence, with the paediatric groups (pilocytic astrocytoma and medulloblastoma) being in the bottom three. Although the adult groups (glioblastoma and glioma low-grade) show a lower mutational burden than other cancers depicted, they have a higher mutational burden than the paediatric groups. Thus, adult low-grade gliomas have a higher mutational burden than paediatric low-grade gliomas, which are similar to pilocytic astrocytoma as displayed in Figure 2.

1.2.1 Gliomas

Gliomas are the most common CNS tumours in children and young adults[15,16] (Figure 3) and arise from an uncontrolled growth of cells from the glial lineage[16-18]. These include astrocytomas, oligodendrogliomas, mixed gliomas and ependymomas[19,20] (Figure 3) and can be classified into different grades depending on the particular type and on the presence of aggressive histopathological features in the tumour[21].

1. Introduction

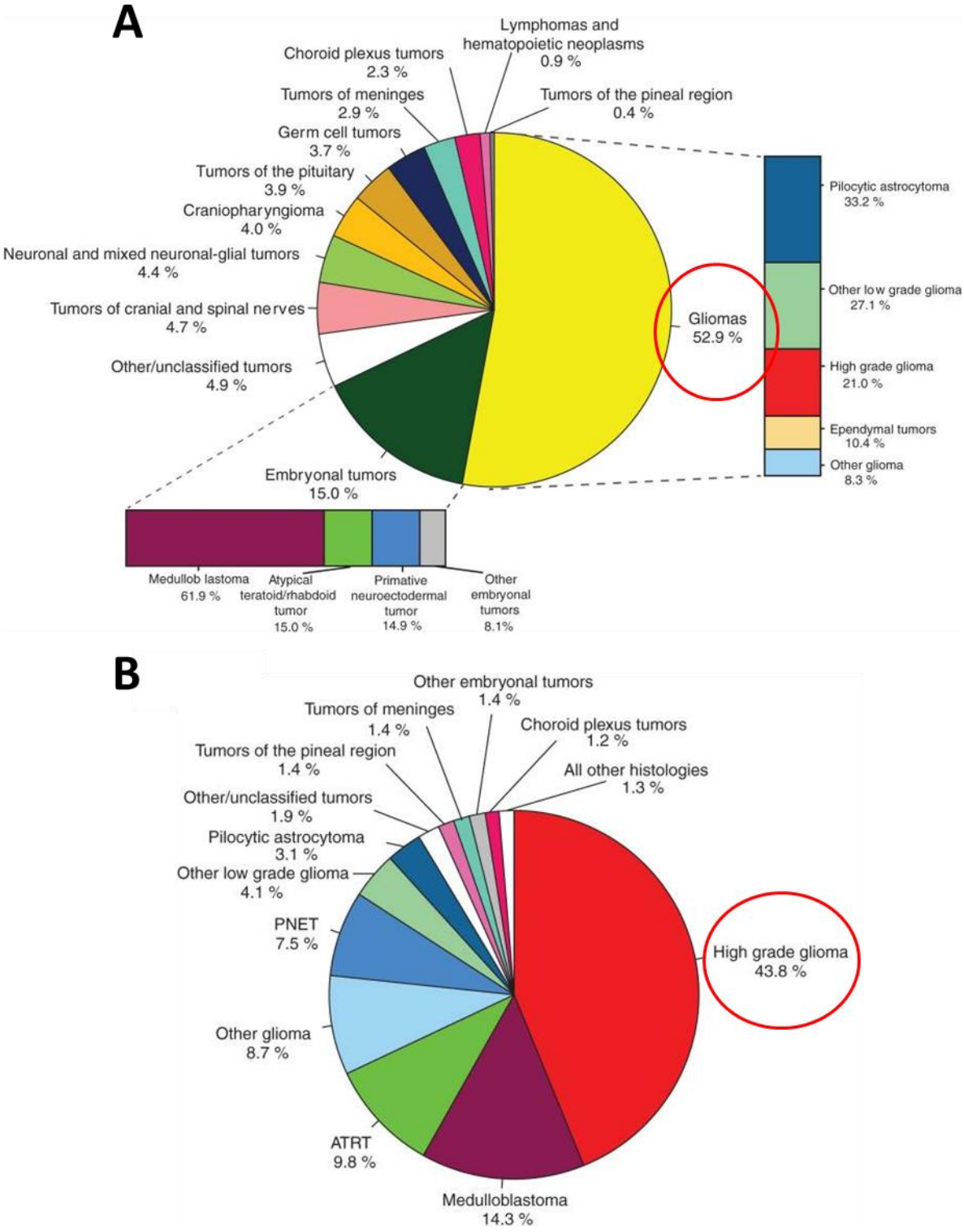

Figure 3. Tumour type incidence in children ages 0-14 and their mortality rates 2007-2011. A. Histological CNS tumour diagnoses of children ages 0-14 years of age between 2007 and 2011. B. Percentage of total deaths of children ages 0-14 caused by malignant brain and CNS tumours between 2007 and 2011. Adapted from Ostrom *et al*. 2015[13].

Grade I and II gliomas are commonly considered together and termed as low-grade glioma (LGG), with Grades III and IV belonging to the high-grade glioma (HGG) group[22,23].

LGGs have a much better prognosis than high-grade gliomas. Grading is currently based solely on histological features such as the presence of necrosis, pleomorphic nuclei, mitosis, giant cells and endothelial proliferation. However, the assessment of these can often be highly subjective, leading to different diagnoses between pathologists, often with enormous clinical consequences for patient management[24].

1.2.2 High-grade gliomas

Paediatric HGGs may occur throughout the brain. One noticeable difference from their adult counterparts, which are mostly found in the cerebral hemisphere[25], is the relatively high frequency of tumours in midline structures like the pons (diffuse intrinsic pontine glioma, DIPG) or brainstem. The latter locations make resection impossible, likely a key reason why these patients therefore have an even worse prognosis than patients with hemispheric HGGs (Figure 4).

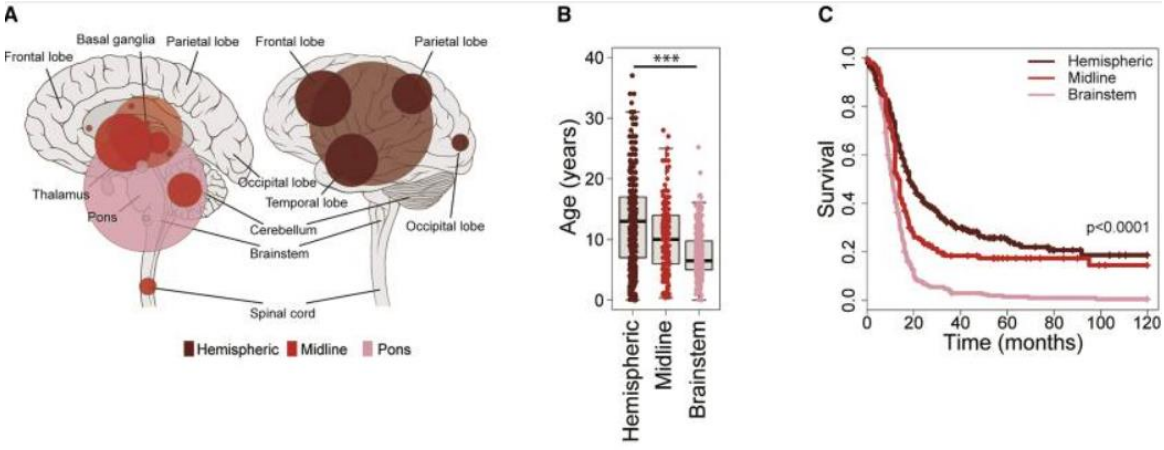

Figure 4. Location, age at diagnosis and survival of >1000 paediatric HGG and DIPG tumours. A. The left side shows an interior view of a sagittal section of the brain, and the right an external view. The different colours represent different locations. The size of the circles is proportional to the number of cases, with the lighter coloured circles having an unspecific designation. B. Boxplot of age at diagnosis separated by location of 1011 cases. ***Adjusted p< 0.0001 for all pairwise comparisons, t test. C. Kaplan-Meier survival analysis of 811 cases grouped by location. The p-value was calculated by the Log-rank test. Taken from Mackay *et al.,* 2017[26].

The diffusely infiltrative nature of HGG in general means that even hemispheric tumours are not completely resectable, also contributing to the low survival rates[27]. Luckily, LGGs occur more often than HGGs in children and the malignant transformation rate of the former is also much lower (7%) than that of adult 'LGG' (50%)[28,29]. High-grade gliomas account for around 8-12% of all paediatric CNS tumours[30] with a median overall survival of 9-15 months[31] and a 5-year survival outcome of only 15-35% [32-35] making high-grade

gliomas a key priority area for research to try to improve these statistics in the coming years. Global annual primary malignant brain and CNS tumour incidences (age-standardized) currently hold at approximately 37 males and 26 females per 1,000,000[36-38].

1.2.3 Low-grade gliomas

Patients with low-grade gliomas on the other hand have a much better survival in comparison, but nevertheless suffer from a substantial burden due to (sometimes multiple) recurrences and therapy-related side effects. PA, representing ~18% of all paediatric brain tumours, is the most common single entity[16,39] with paediatric low-grade gliomas accounting for 30-50% of all CNS tumours in children[40-42]. Low-grade gliomas are mostly found infratentorially (Figure 5), but are very rarely found in the brainstem or pons like HGGs (the most common site being the cerebellum). However, LGGs found in midline locations often cannot be completely resected, leading to a worse prognosis of patients harbouring tumours in those locations since surgical resection is the mainstay of therapy for LGGs[43].

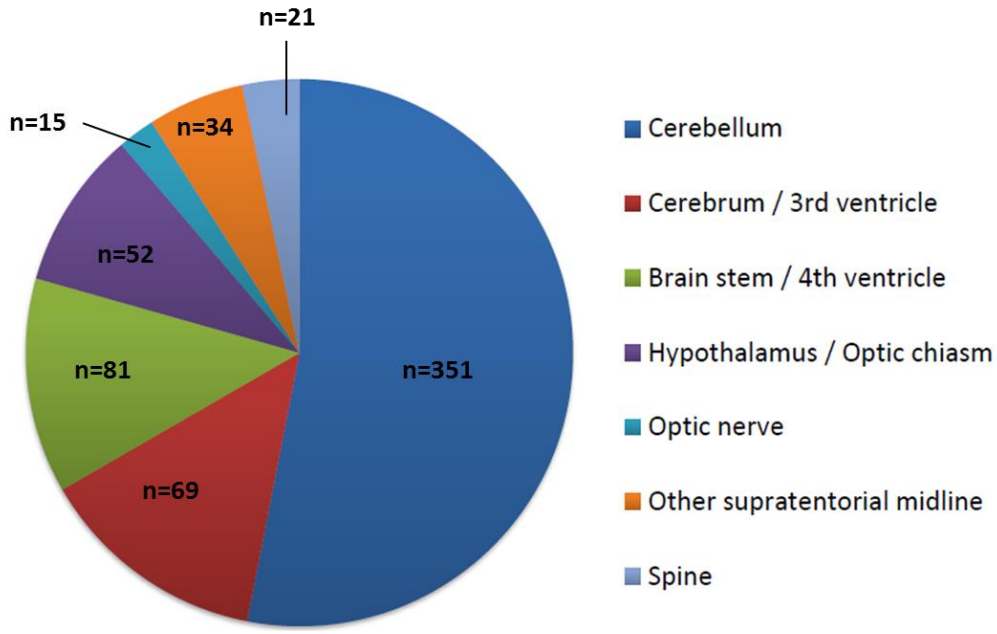

Figure 5. Location distribution of 623 paediatric low-grade gliomas (PA). PAs most often occur infratentorial. Data collected by D. Jones et al., unpublished. High-grade gliomas on the other hand are commonly found in the brainstem or pons (Figure 4).

Adult and paediatric gliomas are histologically and biologically different and should therefore not be treated the same way[44]. However, most clinical trials are focused solely

on adult patients, with different dosing and pharmacokinetics of the drugs in addition to the different biology meaning that these studies cannot easily be translated to children[45].

Luckily, the five and ten year survival of paediatric LGG patients when the tumours are completely resected lies at 97% and 95.8%[46], respectively, which is contrasting to the adult situation[47]. Adult gliomas have a more aggressive phenotype[48] with a higher tendency of malignant progression than in children[23], leading to a worse survival[49-52]. This is due to fundamental differences in biology, but also in the use of the term 'low-grade'. Adult 'LGGs' are defined by the presence of IDH mutations (very rare in children), and typically show a more diffusely infiltrating growth pattern even at WHO Grade II[53-55].

Thus, low- and high-grade gliomas can be seen as being on two sides of a coin in terms of the clinical challenge that they represent. Research on the former concentrates mostly on reducing side effects and prolonging the recurrence-free time (increasing quality rather than just quantity of survival), whereas for HGGs the main issue is the high mortality rates.

1.2.4 Problems with current therapy regimen and aims of new therapy options

One fundamental problem with current therapeutic strategies is that they remain largely based on a histopathological diagnosis of the tumour. Grading and histopathological pattern recognition are challenging, with many of the different described brain tumour types showing similar features under the microscope or in magnetic resonance imaging (MRI). This obstacle makes it difficult to produce reliable and reproducible diagnoses based on histopathology only to act as a foundation for treatment planning[56].

Beyond this, however, standard therapies might not be ideal for every tumour due to a variety of reasons as outlined below. Surgical resection is the first option for paediatric low-grade gliomas, with gross total resection being a good indicator for overall and progression-free survival[57-62]. In 90% of these cases, no recurrence was observed with a 10-year overall survival of 90% or more[57,59,62-65]. However, surgical resection is not always possible due to inaccessibility of the tumour, for example if it is located within critical surrounding brain areas[43]. Therefore, other treatment options would be used instead, with the most common alternative for LGGs being chemotherapy. However, the

slow growth of most LGGs somewhat reduces the efficacy of this treatment, because it primarily affects dividing cells. A third option, radiotherapy, is a big burden on the child. Radiation-induced side effects can result in long-term morbidity including secondary tumours, impaired cognition and vasculopathy[66]. Thus, chemotherapy and radiotherapy can cause long-term side effects in the patients, often impacting their lives as much as the tumour growth of LGGs itself, especially when repeatedly administered over the lifetime of a patient[66].

These side effects arise due to unspecific treatments, with more than just the tumour cells being affected. In addition to tumour recurrences, treatment side effects are one of the main factors which may lead to life-long quality of life problems, which is why the aim of this and other studies[39] is to reduce morbidity and tailor the treatment specifically to the molecular features in LGGs, rather than purely increasing the already good overall survival rate[67]. In fact, beyond five years after diagnosis, one-third of deaths in LGG patients are from non-tumour related causes (Table 1). Long-term therapy-related side effects and tumour-related symptoms occur in most survivors[68,69] and include: seizures (60-85% of LGG[70-73]), abnormal thyroid function and growth hormone deficiency[74]. Recurrence or progressive disease in PAs occurs in ~80% of subtotally resected patients[39,47,66] making the therapy-related side effects at least as big a burden as the tumour itself - again showing that the research aims of low- and high-grade gliomas differ and are important to keep in mind.

Table 1. Causes of death of paediatric patients with LGG. Taken from Krishnatry *et al*., 2016[69].

Cause of death	<5 y From Diagnosis	≥5 y From Diagnosis	Total
Tumor progression	10	0	10
Tumor transformation	12	14	26
Secondary malignancies	0	3	3
Acute lymphoblastic leukemia[a]	0	1	
Acute myelogenous leukemia[a]	0	1	
Primitive neuroectodermal brain tumor[b]	0	1	
Other	5	9	14
Accident	1	6	
Pneumonia	2	1	
Cystic fibrosis	0	1	
Pulmonary embolism	0	1	
Sepsis	1	0	
Juvenile myelomonocytic leukemia treatment complication	1	0	
Unknown	2	0	2
Grand total	29	26	55

[a] No history of radiation or chemotherapy use for pediatric low-grade glioma treatment.
[b] Previous radiation treatment with an in-field secondary tumor.

Less toxic and more specific treatment to attack just the tumour cells are needed to reduce these therapy-related side effects[75]. The key to an improved quality of survival is a better understanding of the molecular and genetic disposition, to identify driver mutations and tailor a patient's therapies according to that[76]. It is hoped that through such an approach, the survival rates and survival quality of children with cancer can increase again after a slow-down in survival improvement in the last 20 years. The currently best way to achieve this is through the field of personalised oncology[77], where tumours are not just diagnosed by their histological features, but molecular analysis is also taken into account in order to improve and standardise both diagnosis and treatment. Successes with BRAF and MEK inhibitors, for example, have shown great promise with this approach so far[78-81].

1.3 Personalised oncology

Recent years have shown that histological and radiological diagnosis of brain tumours are not sufficient anymore to correctly identify the tumour[82-84], because there are too many histological similarities[85] leading to tremendous inter-observer variation. PA and anaplastic astrocytoma with piloid features, for example, show histological overlaps, but

are molecularly different, have a very diverse clinical course, and thus require different treatments[86]. In recent years, many groups have worked on further breaking down tumour entities and molecularly reclassifying them[11,82,83,87-96] to further define tumour types, making the entities more specific and objectively-defined, hopefully leaving less room for discrepancies.

The most important impact on molecular classification was the implementation of molecular features into the revised World Health Organization (WHO) classification published in 2016[97-100]. The aim of including molecular markers for the diagnosis of CNS tumours was not only to standardise diagnosis and treatment, but also suggest more precisely tailored therapy and be able to more accurately predict the prognosis of the disease[101]. Many papers have evaluated the new classification and how it improved diagnosis, and also suggested future directions that should be considered for the next classification[102-104].

DNA methylation profiling is an important tool for tumour classification and identifying homogeneous molecular subclasses [85,91,105-110], which is regularly used in the clinical setting[111,112] and in personalised oncology studies like INFORM (http://pediatric-neurooncology.dkfz.de/index.php/en/diagnostics/inform) and Molecular Neuropathology (MNP)2.0 (http://pediatric-neurooncology.dkfz.de/index.php/en/diagnostics/molecular-neuropathology).

INFORM stands for INdividualized Therapy For Relapsed Malignancies in Childhood, with the aim of molecularly characterising relapsed tumours, where no further standard of care therapy is available. Recurrent and high risk tumours of different paediatric entities are being investigated on a biological level by next generation sequencing to identify the individual fingerprint of each tumour[113] (Figure 6). This is done on standard of care biopsy tissue from patients, with possible molecular drug targets being reported back to treating physicians but as yet no formal therapy recommendation given by the INFORM team.

A similar approach for relapsed tumours is taken by the Paediatric Targeted Therapy (PTT) 2.0 study (http://pediatric-neurooncology.dkfz.de/index.php/en/diagnostics/pediatric-targeted-therapy). The aim

of this study is to identify druggable molecular targets from the analysis of formalin-fixed paraffin-embedded (FFPE) tissue. A corresponding blood sample is also profiled, in order to reliably distinguish between genetic alterations arising within the tumour tissue and germline polymorphisms/mutations.

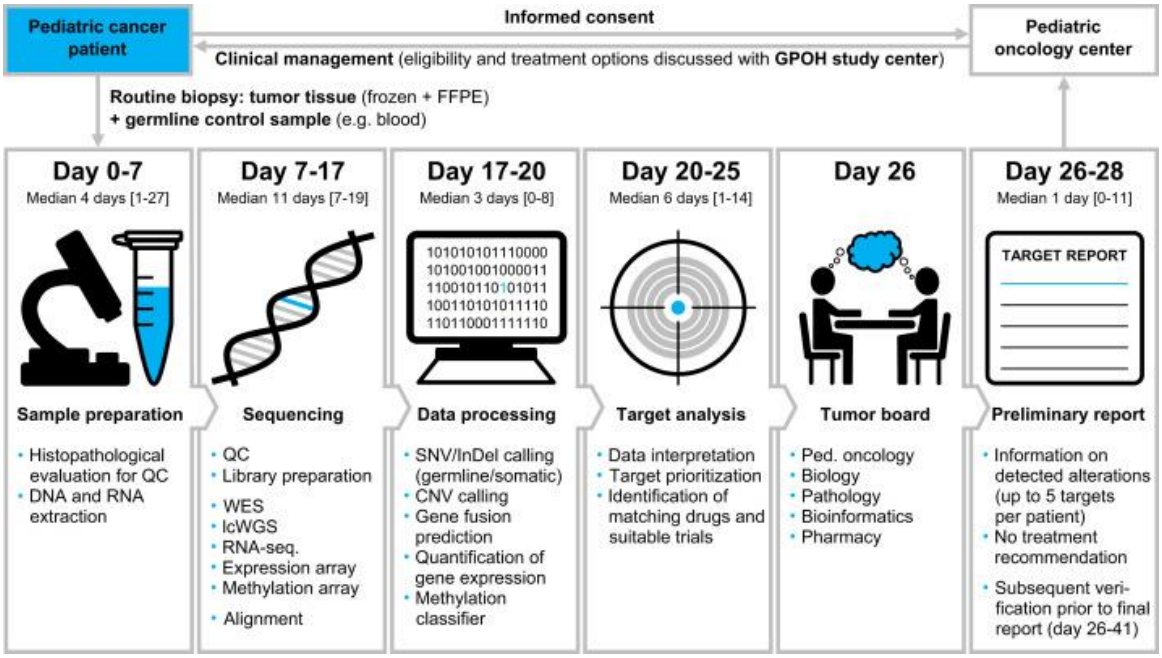

Figure 6. INFORM registry pipeline. Tumour biopsies and the corresponding blood samples are evaluated for quality and then sequenced, before the data is processed by bioinformaticians. From that, targets are identified to find matching drugs or suitable trials to treat the patients. Taken from Worst *et al.*[113].

MNP2.0 on the other hand aims at improving molecular diagnostics in newly-diagnosed childhood brain tumours. Every primary brain tumour patient in Germany is eligible to be part of this study, and more importantly 80% of them are actually recruited - showing how valuable this study is in the molecular era and how much clinicians trust in and rely on these results. Analysis is done on FFPE tissue and a corresponding blood sample.

The principle aim of INFORM and PTT2.0, and a secondary aim of MNP2.0, is to find mutational targets that may be druggable with already existing treatments either in trials or which have been approved in other tumour entities. With the growing interest from oncologists to enrol their patients in these and similar international studies, more novel molecular targets can be identified leading to a better understanding of the tumour biology and with that greater treatment options. In addition to known targets, however, a further aim of the INFORM study (together with initiatives such as the International Cancer Genome Consortium (ICGC) PedBrain Tumor Project) is to highlight

novel potential targets for intervention. The analyses conducted within these programs revealed some novel recurrent genetic fusion or mutation events that became the basis of this project. Several of these genetic alterations occur in tumours which cluster separately from other genetically distinct groups, and although many were initially thought to be HGGs, their survival is more similar to that of LGGs (Figure 7).

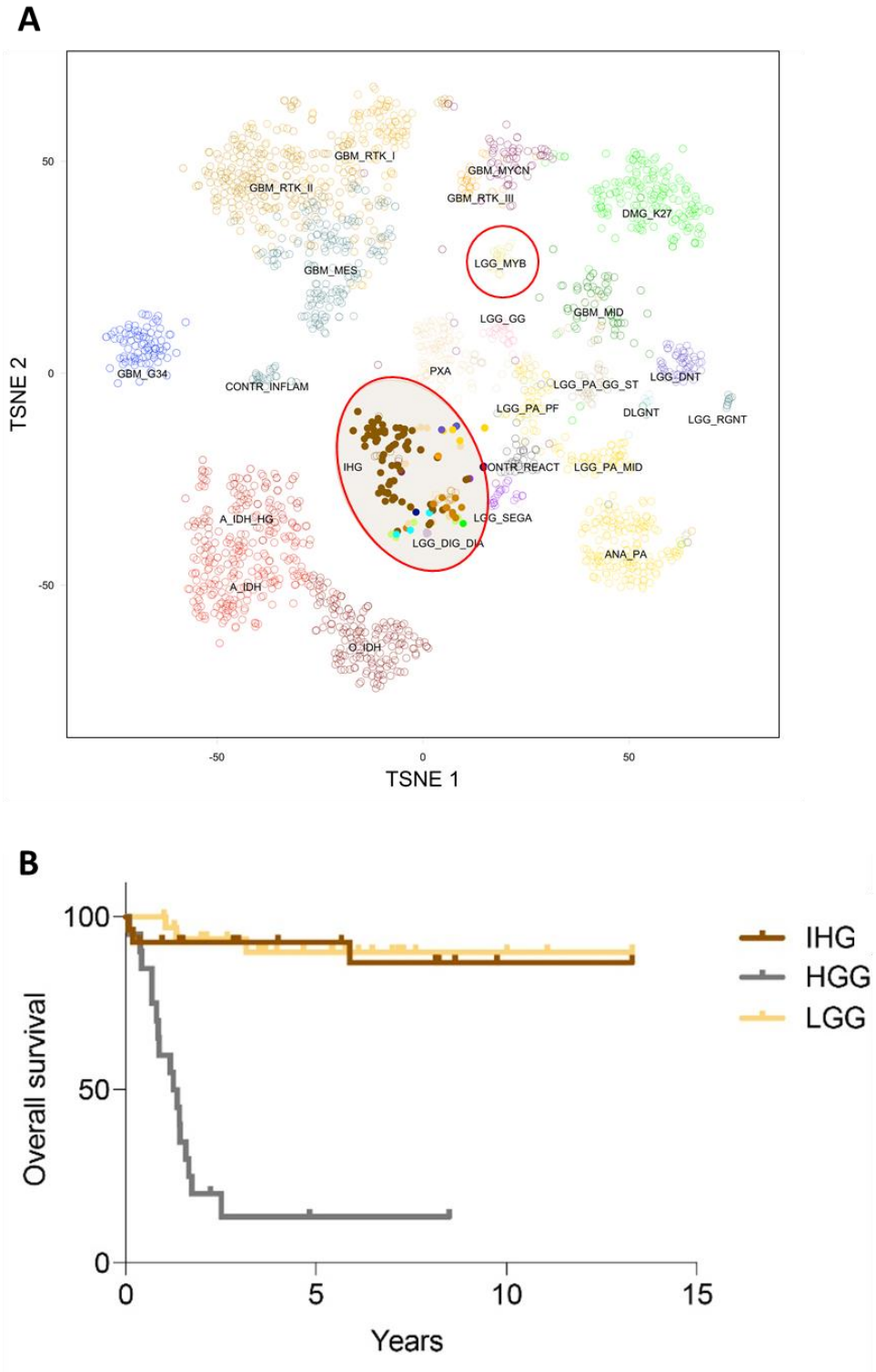

Figure 7. Identification and survival of new genetically distinct groups. A. Methylation subset of infantile 'HGG' are distinct from other gliomas indicating new molecularly defined entities. B. The prognosis of the IHG group (infantile hemispheric glioma, including many *ALK*-fused tumours) is very similar to that of LGGs. Data kindly provided by Matthew Clarke and Chris Jones, ICR, London.

Table 2 shortly describes some of these newly identified subgroups, with the main focus of this thesis being on the role of *Anaplastic Lymphoma Kinase* (*ALK*).

Table 2. Selected candidate genes as potential oncogenic drivers

Gene	CNS tumour types	Approximate prevalance	Schematic diagram of matching event modelled here
ALK	Infantile hemispheric glioma	About 20-30% of all infant 'HGG-like' tumours in patients < 2 years old (fusions)	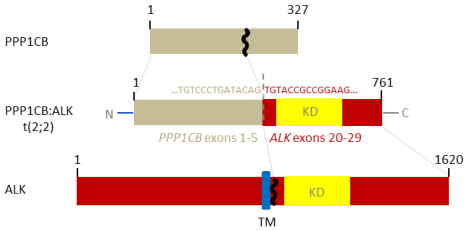
NTRK	Pilocytic astrocytoma; infantile hemispheric glioma; anaplastic neuroepithelial tumour with condensed nuclei (ANTCN)	2-3% of PA; 20-30% of infant 'HGG'; >50% of ANTCN (unpublished; fusions)	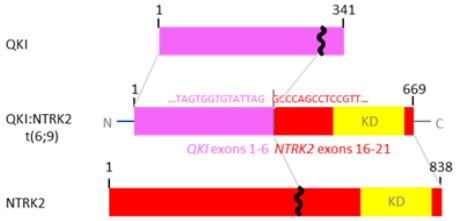
FGFR1	Pilocytic astrocytoma; dysembroplastic neuroepithelial tumour (DNET); extraventricular neurocytoma (EVN)	~5% of PA (mutation); ~60-70% of DNET (mutation & kinase dupl.); >60% of EVN (mostly *FGFR1:TACC1*)	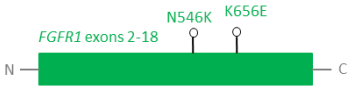
MYB/ MYBL1	Angiocentric glioma; diffuse astrocytoma; isomorphic astrocytoma	~100% pathognomonic of angiocentric glioma & isomorphic astrocytoma; ~10-20% of paediatric diff. astrocytoma (fusions)	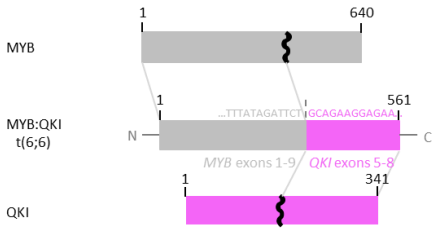

1.4 *ALK* as an oncogene

From a total of 90 tyrosine kinase genes identified in the human genome, around 60 encode for receptor tyrosine kinase proteins[114]. Receptor tyrosine kinases have been shown to not only be involved in normal cellular functions, but when dysregulated, they also play a major role in cancer development[115].

One such receptor is ALK, a member of the insulin receptor superfamily[116] originally identified in 1994 in anaplastic large-cell lymphoma[117](ALCL), hence the name, as part of the *Nucleophosmin (NPM):ALK* fusion. This alteration, where the entire *NPM* gene on chromosome 5 is fused to the *ALK* gene at the 3' position, was the starting point of many more *ALK* fusions being identified across various other tumour types.

1.4.1 *ALK* in NSCLC

With advances in sequencing technologies, more genetic aberrations involving the kinase domain of the *ALK* gene have since been found[118,119]. For example the *Echinoderm microtubule-associated protein-like 4 (EML4):ALK* fusion was first identified in non-small cell lung cancer (NSCLC) in 2007, independently by two groups[120,121]. This is the most common fusion found in NSCLC, seen in 5% of all NSCLC patients[118,120,122-130], and is caused by chromosomal rearrangement[124].

In normal tissue, ALK is minimally expressed[131] due to controlled pathway activation. As a result of a gene fusion event, however, the kinase domain is aberrantly expressed leading to an auto- phosphorylation loop and constitutively active fusion protein facilitating dimerisation of the receptor subunits and increased downstream pathway activation [120,124,125].

Our group, first within the INFORM project and subsequently in a broader molecular analysis of additional brain tumours, found recurrent fusions of *ALK* with different genes at the N –terminus, with *PPP1CB* being the most common upstream fusion partner of *ALK* (Figure 8).

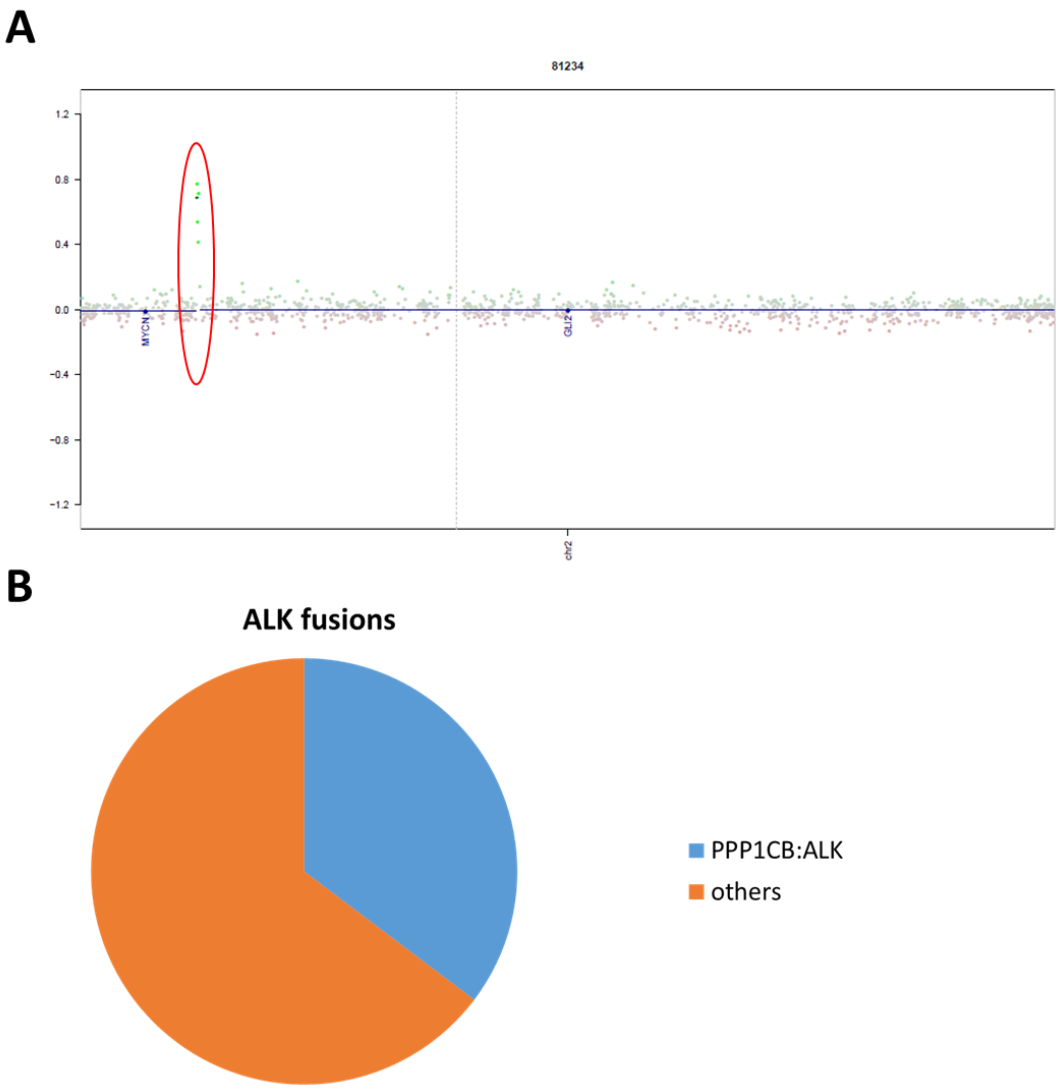

Figure 8. *ALK* fusion identification and occurrence of *PPP1CB:ALK* fusion. A. Copy number plot showing an increased signal on chromosome 2p at the position of the *PPP1CB* and *ALK* genes resulting in a fusion. RNA sequencing was used to confirm this. B. Pie chart indicating the frequency of *PPP1CB* as a fusion partner of *ALK* for 17 patients. Other *ALK* fusion partners are: *CCDC88A* (n=2), *MSI2*, *MAD1L1*, *TPM3*, *KTN1*, *EML4*, *PRKAR2A*, *CLIP2* and *SPTBN1*, with the latter all seen in only one patient each.

1.5 ALK inhibition

1.5.1 ALK inhibitor development

The ALK receptor is involved in activation of the MAPK pathway, therefore either targets downstream of ALK for which inhibitors are already available and more commonly used in brain tumours (e.g. MEK) or ALK itself represent druggable targets for inhibition[132]. An inhibitor targeting the tyrosine kinase itself might be better than inhibitors in downstream pathways, because ALK signals through additional pathways, which MEK inhibitors for example would not target (Figure 9).

Within the last seven years, several ALK inhibitors have entered the market and/or are being tested in clinical trials, which are separated into three groups: first-, second- or third-line inhibitors.

Crizotinib (PF-2341066) for example was initially developed by Pfizer as a c-Met inhibitor, but rapidly progressed in the clinic as one of the first-line ALK inhibitors[133,134]. Only four years after ALK was acknowledged as an important target in cancer with the discovery of the *EML4:ALK* fusion[120,121], crizotinib (Xalkori™) was fast-track approved for *ALK*-positive NSCLC by the Food and Drug Administration (FDA). Early successes of crizotinib in clinical studies with an objective response rate (ORR) and a median progression-free survival (PFS) of 60% and 9.7 months, respectively[135] were soon shadowed by relapses of patients caused by either *ALK* fusion gene amplification, secondary ALK kinase domain mutations (roughly 1/3 of all acquired resistance) around the ATP binding site, activation of other bypass signalling pathways (EGFR, c-KIT), and other mechanisms[116,123]. This led to demand for new generation ALK inhibitors to combat the resistance mechanisms of crizotinib.

Second line inhibitors, ceritinib (LDK-378) and alectinib (CH-5424802), were developed in 2014 by Novartis and Chugai/Roche, respectively, and approved by the FDA and Japanese Ministry of Health, Labor and Welfare (MHLW) in 2014 (ceritinib) and 2013 (alectinib). Both are used in patients showing crizotinib resistance[136], with ceritinib being effective against L1196M, G1269A, I1171T and S1206Y mutations and alectinib against L1196M, F1174L, R1275Q and C1156Y[116]. They were not specifically designed to target the resistance mutations, but nevertheless are very effective against wildtype and mutant ALK kinases[116] more than other serine/threonine or tyrosine kinases.

Alectinib incorporates a few structural changes to improve its potency, selectivity and pharmacokinetic properties over the previous inhibitors. It showed low IC50 values in *ALK*-positive cell lines and high selectivity for ALK compared to other tyrosine kinases[131,137]. According to a clinical study by Watanabe *et al.*, the PFS of *EML4-ALK* fusion-positive patients with NSCLC first treated with crizotinib followed by alectinib increased from 6.1 months to 15.2 months[138], showing that alectinib overcame the crizotinib resistance to provide additional survival benefit.

However, there was then another mutation that arose, *ALK*^{G1202R}, shown to confer resistance to all three previously described ALK inhibitors[125,139-141]. With that, there was another need for a further ALK inhibitor that would work in patients showing resistance mechanisms, or one that can be given to patients right from the start in the hope that this will not induce resistance. The third-line ALK inhibitor lorlatinib (PF-06463922) developed by Pfizer, was thus approved by the FDA in April 2017 for *ALK*-positive metastatic NSCLC patients who progressed on another ALK inhibitor[142]. It is an orally available ATP-competitive inhibitor of receptor tyrosine kinases ALK and ROS1[143] (Figure 9). Lorlatinib has cross-reactivity to ROS1 receptor kinase domain due to a phylogenetic relation to the ALK receptor kinase domain[114], and also exhibits an effect on ROS1 fusion-positive lung cancers due to this receptor homology[144,145]. Lorlatinib binds to and inhibits ALK and ROS1 kinases and inhibits growth of *ALK* or *ROS1*-overexpressing tumour cells. However, Zou *et al.*[143] showed that lorlatinib has no substantial activity against MET like crizotinib does, further suggesting differences in the mechanism of action of the two compounds.

Lorlatinib was specifically designed to cross the blood-brain barrier (BBB)[143,146,147], which is a major aspect that needs to be considered when designing compounds for brain tumours or brain metastases. The BBB makes it difficult for therapeutic compounds to reach their target, therefore it is difficult to achieve effective levels of the drug in the tumour[148,149]. Johnson *et al*. initially showed BBB penetrance in rats[147], with other *in vivo*[150] models and *in vitro*[151-157] techniques having been subsequently developed, but Collier *et al.*[146] stated that more *in vivo* models are necessary to confirm this.

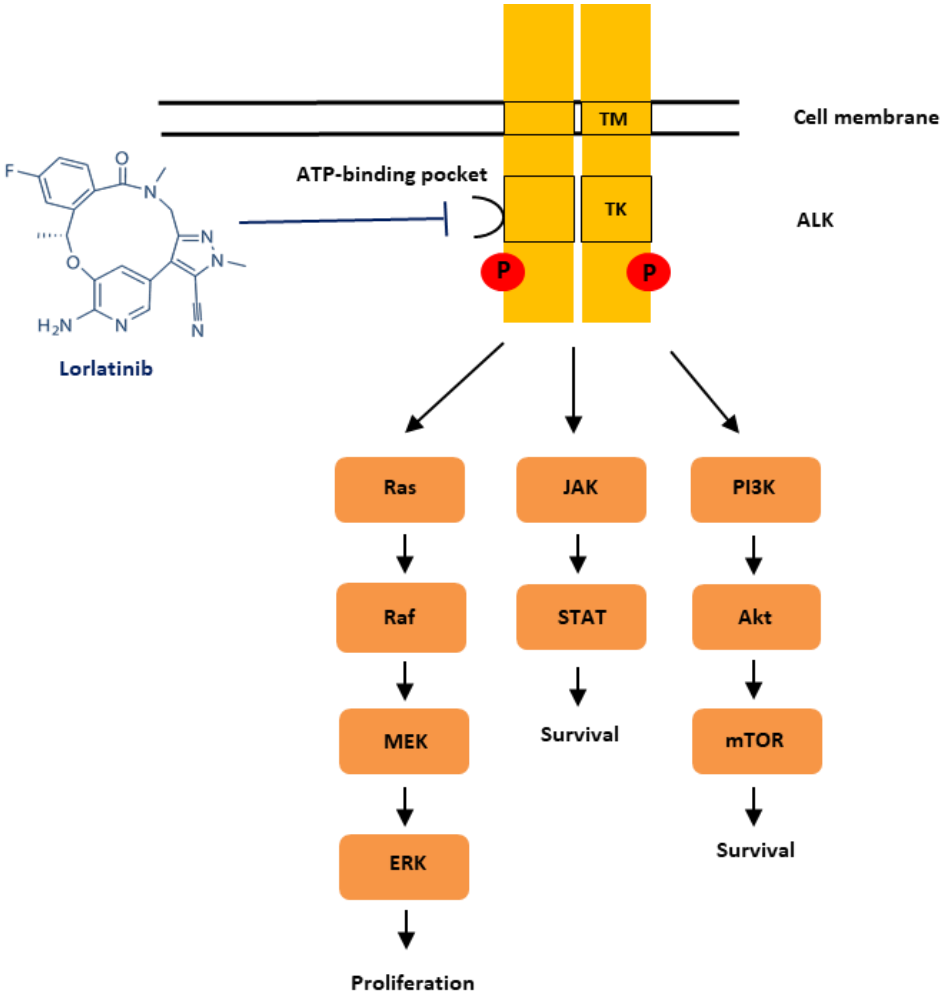

Figure 9. *ALK* receptor signalling pathway and lorlatinib inhibition. Upon receptor activation by growth factors for example, the receptor dimerises and autophosphorylates itself leading to the activation of downstream signalling pathways like MEK, JAK/STAT or mTOR. When lorlatinib is administered, it binds to the ATP binding pocket on the tyrosine kinase domain of the intracellular portion of the ALK receptor, thereby preventing ATP binding and leading to reduced phosphorylation and downstream signalling.

1.6 Preclinical modelling

In vivo models are indispensable in research due to the murine genetic and physiological similarities to the human[158] (90% genome syntheny[159,160]) and the fact that *in vitro* experiments cannot fully replicate the human disease due to e.g. a lack of microenvironmental signalling pathways[161,162]. Upon isolating cells from an organism, not only the gene signatures change[154], but other culture-specific issues arise which result in an ongoing need for *in vivo* models. These include the lack of complex metabolism that is found *in vivo*, the unknown factor of the interaction of cells with other cell types and their microenvironment, the difficulties of long term exposures of drugs in culture medium to recapitulate the situation in humans (including e.g. BBB

penetration) and finally the impossibility to convert doses from *in vitro* system to the human[163] keeping all the above mentioned variables in mind[164]. Therefore, to accompany *in vitro* experiments, *in vivo* analyses are important to get a better idea of the physiological processes in cancers within a complex organism. In particular given the extensive characterisation of murine systems, it is known that the human and mouse CNS are highly preserved across species[165,166] and molecular and cellular mechanisms are well-conserved[159,167-169].

1.6.1 Advantages and disadvantages of different mouse model approaches

With recent technical advances, there are now many different ways to generate mouse models. The pros and cons will be discussed in this section below.

One of the most well-known and frequently used mouse model systems for cancer research is the xenograft model. Xenografts are tissue or cell grafts (mainly tumour cell lines) transplanted from one species to another, mainly from human into immunodeficient mice. One benefit of using xenografts is the reduction of clonal selection in comparison with cell culture studies. Nonetheless, low passages are desired in order to conserve tumour characteristics and keep the tumour closer to the human counterpart. Subcutaneous engraftment is the standard used[170]. With this technique, many cell lines from solid tumours and leukaemias have been transplanted into xenograft models, threby supplying a variety of tumour models for compound testing[171-174]. One step further are orthotopic xenografts, which are implanted into the tissue/organ of origin and not just subcutaneously[175]. That way the microenvironment is thought to reflect the original tumour more accurately. To more reliably predict clinical activity and clinical behaviour of drugs in human tumour tissues, patient-derived xenografts (PDX) have been established. Here, tumour cells from the patients are directly injected[176] into immune-compromised mice with no or only minimal *in vitro* passaging, which is thought to make them genetically more stable[177,178]. The mice used for xenograft experiments however are adult mice, which get injected with cells from an already established tumour. One restriction of this as a model method of choice is therefore the differences in the microenvironment in a paediatric setting compared with adults. Also, more benign tumours such as LGGs have thus far not been successfully grown as xenografts[179,180], with a certain degree of aggressiveness of the primary

tumour seeming to be required for growth in this setting. Furthermore, some studies have found that results from personalised xenograft models have not translated well into the clinic[181,182], i.e. the expected results that were predicted from the mouse studies failed to be recapitulated in patients. The interaction between the tumour cells and the surrounding cells in the microenvironment can also not be optimally studied in xenograft models due to the lack of the immune system, which may give totally different results in response to therapy[183].

In terms of indicating proof-of-concept activity of a compound against one particular driving event, xenografts may also harbour too great a genetic heterogeneity with multiple cooperating alterations[184,185]. To avoid this issue, genetically engineered mouse models (GEMMs) have been developed that harbour a simplified genetic background mimicking what are thought to be the key events in the human tumour. The expression of oncogenes in the germline of the mouse has been shown for many years to reliably result in cancer formation[186]. Unlike xenografts, GEMMs can precisely combine expression of oncogenes and loss of tumour suppressor genes in either a tissue- or whole organism-specific manner[187] through recombinant DNA technologies. The insertion of genes of interest uses a technology whereby the changes are introduced into the mouse genome heritably. Modern GEMMs use inducible systems to have temporal and tissue-specific control over the expression of tumour suppressor genes or oncogenes[170]. Although tumour latency is typically low in GEMMs, the generation of these germline-altered mice was (prior to the CRISPR era) a long process, which could not keep up with the quickly evolving field of tumour sequencing and identification of new candidate genes. Whether this may change once more with the expanding use of genome-editing techniques, remains to be seen.

For generation of tumours in a rapid and flexible way which also have more relevance to the paediatric setting, different mouse models have previously been described[188-191]. The RCAS/*t-va* system, for example, has been used for paediatric[192] and adult[193] glioma mouse models and was originally developed by the Holland lab. It allows for somatic gene transfer of oncogenic genes into the early postnatal brain (p0-p2) into targeted cells expressing the tva receptor. This can further be defined to only be expressed on

certain cells, i.e. neuronal cells, where the tva receptor is under a nestin promoter (n-tva).

The Replication-Competent ASLV long terminal repeat (LTR) with a Splice acceptor (RCAS) vector, which is derived from the SR-A strain of rous sarcoma virus (RSV), a member of the avian sarcoma-leukosis virus (ASLV) family, will only replicate in avian cells[194,195] (for experimental purposes, DF-1 chicken fibroblasts). The gene of interest cloned into the RCAS vector will then transfect chicken cells and lead to virus production. After three days, the virus-producing cells are injected into the mouse brain to infect the target cells – initiating tumour growth if the time point and location of injection is suitable for the oncogenic driver.

If injection post-natally is considered to be too late for the oncogenic gene to exert an effect on the right cell population, then the use of another paediatric-relevant engineered mouse modelling technique can be of value. *In utero* electroporation (EP) is normally carried out between E10.5 and 14.5 of development. The benefits of using *in utero* electroporation are the region-specificity[190] of injection of vectors carrying an oncogenic candidate gene and the possibility that multiple genes can be targeted at once[196] for loss of function and gain of function experiments (Figure 10). The gain of function is induced through a transposon vector (PT2K) carrying the gene of interest. When injected into the mouse together with a transposase, the gene of interest gets excised out of its vector and inserted into an appropriate site in the host DNA sequence depending on the transposon system used. The CRISPR (Clustered Regularly Interspaced Short Palindromic Repeats)/Cas9 system is responsible for inducing loss of function in desired genes, mainly tumour suppressor genes like *p53* or *cdkn2a*. In this case a single guide RNA (gRNA) composed of 20 nucleotides directs the Cas9 nuclease enzyme to a specific target site at the locus that needs to be cut. This double strand break results in either of two repair mechanisms - Non-Homologous End Joining (NHEJ) or Homology-Directed Repair (HDR)[197]. These are error-prone, typically resulting in Indels (Insertions and deletions) that introduce a frameshift and thereby non-functional proteins.

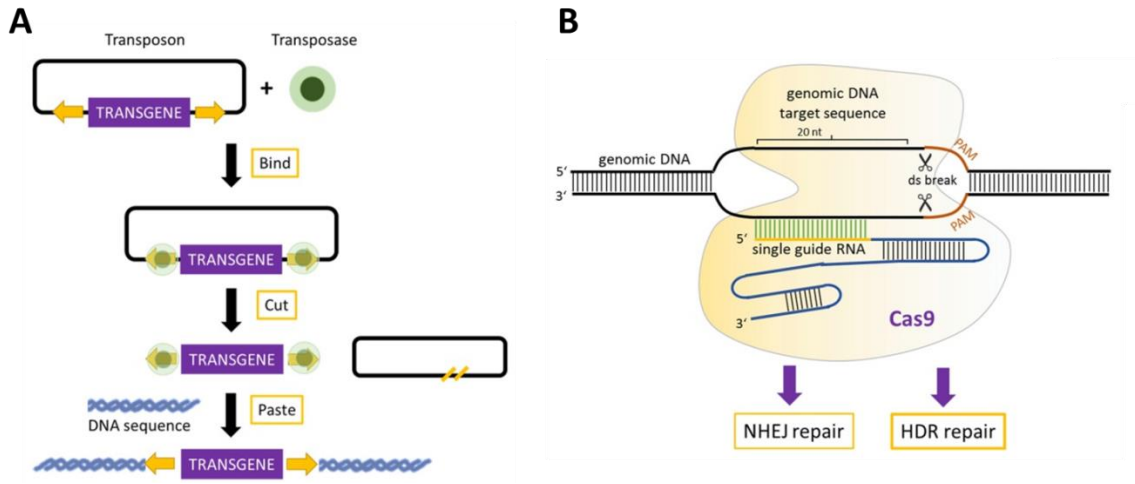

Figure 10. Mechanisms of gain- and loss of function in *in utero* electroporation mouse models. A. When the transposase enzyme and the transposon vector containing a gene of interest come together, the former excises the gene of interest from the vector and inserts it into a suitable DNA sequence leading to gain of function. B. Loss of function is achieved with the CRISPR/Cas9 technology, where a 20 nucleotide single guide RNA guides the Cas9 enzyme to the genomic target sequence leading to a double strand break. This activates either NHEJ or HDR repair mechanisms resulting in Indels and subsequently dysfunctional proteins. Taken from Lampreht Tratar *et al.*[175].

Taking into account the above listed advantages and disadvantages of the described model systems, the RCAS/tv-a and *in utero* EP systems were chosen for this study to try and establish mouse models for the different candidate genes identified. Drug response tests were conducted both *in vitro* and *in vivo,* to firstly see if and how they differ, and secondly to have two independent pieces of evidence for justifying the possible effectiveness of a given drug. Nevertheless, one needs to keep in mind that the mouse is only a model organism and all results should be carefully considered for their predictive value and re-tested in the human situation.

1.7 Future applications and hopes

More, and more precise, clinical trials are urgently needed for children with paediatric gliomas, because the current standard of therapy is either a) largely ineffective (for HGG) or b) associated with significant toxicity (for LGG), and medications are frequently prescribed to children on a trial-and-error basis without specific knowledge about the dosing, efficacy and safety of the drug in children[198-200]. With specific mouse model development and subsequent preclinical testing, the bench-to-bedside process will hopefully decrease in time enabling the patients to get more specific therapy faster based on their genetic alterations. Kolb *et al.*[201] showed that improved MEK inhibitors

have led to not only successful preclinical testing in mouse models, but also initiation of a clinical trial in LGG patients with such an inhibitor, selumetinib (AZD6244; NCT01089101) - discovered by Array BioPharma and licensed to AstraZeneca.

It is hoped that this study may represent an important part of the preclinical pipeline towards lorlatinib approval in children with *ALK*-altered tumours in particular (hopefully with the initiation of a clinical trial in infant patients harbouring an *ALK* alteration), and in general a useful proof-of-concept methodology for accelerating regulatory approval of targeted treatments for childhood cancer.

2. Materials & Methods

2.1 Materials

2.1.1 Solutions, Buffer, Media, Reagents

Solution/Buffer/Media/Reagents	Supplier
Accumax	eBioscience, Karlsruhe, Germany
Albumin fraction V	Carl Roth, Karlsruhe, Germany
ATP solution (25-mM)	Epicentre, Madison, USA
B-27 supplement (50x)	Thermo Fisher Scientific, Karlsruhe, Germany
Biotin-blocking system	Agilent, Santa Clara, USA
Boric acid	Fisher Bioreagents, Pittsburgh, USA
cOmplete™ Mini EDTA-free protease inhibitor cocktail tablets	Roche Diagnostics, Mannheim, Germany
CutSmart® buffer (10x)	New England Biolabs, Ipswich, USA
Dako antibody diluent	Agilent, Santa Clara, USA
DAPI fluoromount-G® mounting medium	Thermo Fisher Scientific, Karlsruhe, Germany
DMEM/F-12 medium	Thermo Fisher Scientific, Karlsruhe, Germany
ECL western blotting reagents	Merck, Darmstadt, Germany
EGF-basic, recombinant human protein	PeproTech, Hamburg, Germany
Eosin G solution 0.5% in water	Carl Roth, Karlsruhe, Germany
Ethanol absolute	Fisher Chemical, Pittsburgh, USA
Eukitt® mounting medium	O. Kindler GmbH, Freiburg, Germany
Fast digest buffer (10x)	Thermo Fisher Scientific, Karlsruhe, Germany
Fast green FCF	Merck, Darmstadt, Germany
FGF-basic, recombinant human protein	PeproTech, Hamburg, Germany
Formalin solution, neutral buffered, 10%	Merck, Darmstadt, Germany

FuGene HD transfection reagent	Promega, Madison, USA
Glycine	Merck, Darmstadt, Germany
Heparin sodium	Merck, Darmstadt, Germany
HotStarTaq plus master mix	Qiagen, Hilden, Germany
Hydrochloric acid puriss. p.a. reag. ph. eur. ≥37%	Merck, Darmstadt, Germany
Hydrochloric acid, 1mol/l (1N)	VWR International, Bruchsal, Germany
Laminin	Merck, Darmstadt, Germany
Luciferin	BioVision, San Francisco, USA
Mayer's haematoxylin solution	AppliChem, Darmstadt, Germany
Methanol	Fisher Chemical, Pittsburgh, USA
Neurobasal-A medium	Thermo Fisher Scientific, Karlsruhe, Germany
Normal donkey serum	Merck Millipore, Darmstadt, Germany
NP-40 lysis buffer	Thermo Fisher Scientific, Karlsruhe, Germany
NuPAGE™ 4-12% Bis-Tris gel	Thermo Fisher Scientific, Karlsruhe, Germany
NuPAGE™ antioxidant	Thermo Fisher Scientific, Karlsruhe, Germany
NuPAGE™ LDS sample buffer (4x)	Thermo Fisher Scientific, Karlsruhe, Germany
NuPAGE™ MES SDS running buffer (20x)	Thermo Fisher Scientific, Karlsruhe, Germany
Opti-MEM	Thermo Fisher Scientific, Karlsruhe, Germany
Paraformaldehyde solution 4% in PBS	Santa Cruz Biotechnology, Dallas, USA
PDGF-AA recombinant human protein	PeproTech, Hamburg, Germany
Plasmid-safe™ ATP-dependent DNase	Epicentre, Madison, USA
Plasmid-Safe™ reaction buffer (10x)	Epicentre, Madison, USA
Poly(ethylene glycol), average Mn300	Merck, Darmstadt, Germany

Poly-L-Ornithine hydrobromide	Merck, Darmstadt, Germany
Protease/Phosphatase inhibitor cocktail (100x)	Cell Signaling Technology, Danvers, USA
Proteinase K	Promega, Madison, USA
RIPA lysis buffer (10x)	Merck, Darmstadt, Germany
SOC medium	Made myself
Sodium chloride	Merck, Darmstadt, Germany
ß-Mercaptoethanol	Merck, Darmstadt, Germany
Synth-a-freeze cryopreservation medium	Thermo Fisher Scientific, Karlsruhe, Germany
T4 DNA ligase reaction buffer	New England Biolabs, Ipswich, USA
TC10 trypan blue dye	BioRad, Hercules, USA
TRANSIT®-LT1 transfection reagent	Mirus Bio, Madison, USA
Trisma base	AppliChem, Darmstadt, Germany
Tri-sodium citrate dehydrate	Merck, Darmstadt, Germany
Triton™ X-100	Merck, Darmstadt, Germany
Trypsin-EDTA (10x)	Merck, Darmstadt, Germany
Tween®20	Merck, Darmstadt, Germany
UltraPure™DNase/RNase-free distilled water	Thermo Fisher Scientific, Karlsruhe, Germany
Water, double-processed, cell culture tested	Merck, Darmstadt, Germany
Xylene	VWR International, Bruchsal, Germany

2.1.2 Antibodies

Antigen	**Clone**	**Primary (P)/ Secondary (S)**	**Dilution**	**Supplier**	**Catalogue number**
Alexa Fluor® 568 donkey anti-rabbit IgG	N/A	S	1:400	Thermo Fisher Scientific, Karlsruhe, Germany	A10042

ALK (Y1278 + Y1282 + Y1283) rabbit	N/A	P	1:200	Bioss, Woburn, USA	bs-3021R
ALK/CD246 rabbit	N/A	P	1:300	Thermo Fisher Scientific, Karlsruhe, Germany	51-3900
Cleaved Caspase-3 (Asp175) rabbit	5A1E	P	1:500	Cell Signaling Technology, Danvers, USA	9664
GAPDH mouse	6C5	P	1:5000	Millipore, Darmstadt, Germany	CB1001
HA-tag rabbit	C29F4	P	1:800 (IHC, IF)/ 1:3000 (WB)	Cell Signaling Technology, Danvers, USA	3724
IgG-HRP goat anti-mouse	N/A	S	1:3000	Cell Signaling Technology, Danvers, USA	7076
IgG-HRP goat anti-rabbit	N/A	S	1:2000	Cell Signaling Technology, Danvers, USA	7074

Ki-67 rabbit	B56	P	1:1000	BD Biosciences, San Jose, USA	550609
Phospho-ALK (Tyr1604) rabbit	Tyr1604	P	1:1000	Cell Signaling Technology, Danvers, USA	3341

2.1.3 Kits

Name	**Supplier**
CellTiter-Glo luminescent cell viability assay	Promega, Madison, USA
CloneJET PCR cloning kit	Thermo Fisher Scientific, Karlsruhe, Germany
Dead cell apoptosis kit with annexin V FITC and PI, for flow cytometry	Life Technologies, Karlsruhe, Germany
DNeasy blood & tissue kit	Qiagen, Hilden, Germany
Endofree plasmid maxi kit	Qiagen, Hilden, Germany
LSAB+ dako real detection systems	Agilent, Santa Clara, USA
PRECISOR high-fidelity DNA polymerase	Biocat, Heidelberg, Germany
Propidium iodide flow cytometry kit	Abcam, Cambridge, United Kingdom
QIAprep spin miniprep kit	Qiagen, Hilden, Germany
QIAquick gel extraction kit	Qiagen, Hilden, Germany
QIAquick PCR purification kit	Qiagen, Hilden, Germany
Quick ligation™ kit	New England Biolabs, Ipswich, USA
SuperScript™ II reverse transcriptase	Thermo Fisher Scientific, Karlsruhe, Germany

2.1.4 Mouse Line

Strain	Supplier	Genotype
CD1	Central Animal Facility of the DKFZ Heidelberg / Envigo	Wild-type
NSG	Central Animal Facility of the DKFZ Heidelberg	*Prkdc*^{scid}*IL2rg*^{null}
N-tva	Central Animal Facility of the DKFZ Heidelberg/ Jackson Laboratory	Wild-type; Nestin promoter-driven tva receptor
XFM	Central Animal Facility of the DKFZ Heidelberg/ Jackson Laboratory	Cdkn2a-KO; Pten$^{fl/fl}$, Nestin promoter-driven tva receptor

2.1.5 Pharmaceutical drugs and inhibitors

Drug	Effect	Supplier
Alectinib	ALK inhibitor	Selleck Chemicals, Munich, Germany
AZD4547	FGFR inhibitor	Selleck Chemicals, Munich, Germany
Ceritinib	ALK inhibitor	Selleck Chemicals, Munich, Germany
Crizotinib	ALK/c-MET inhibitor	Selleck Chemicals, Munich, Germany
Dovitinib	Multitargeted RTK inhibitor	Selleck Chemicals, Munich, Germany
Entrectinib	pan-TrkA/B/C, ROS1 and ALK inhibitor	Selleck Chemicals, Munich, Germany
Infigratinib	FGFR inhibitor	Selleck Chemicals, Munich, Germany

Larotrectinib	TRK inhibitor	Selleck Chemicals, Munich, Germany
Lorlatinib	ALK/Ros1 inhibitor	Selleck Chemicals, Munich, Germany
Merestinib	MET tyrosine kinase inhibitor	Selleck Chemicals, Munich, Germany
Metamizol	Analgetica	WDT, Garbsen, Germany
PD173074	FGFR1 inhibitor	Selleck Chemicals, Munich, Germany
Ponatinib	Abl, PDGFRα, VEGFR2, FGFR1 and Src inhibitor	Selleck Chemicals, Munich, Germany
Rimadyl® (Carprofen)	NSAID	Zoetis, Berlin, Germany
Temozolomide (TMZ)	SN-1 alkylating agent	Selleck Chemicals, Munich, Germany

2.1.6 Cells

Name	**Cell type**	**Supplier**	**Biological Source**
BI#169	*PPP1CB:ALK*-positive	Generated through *in utero* EP	Mouse brain
BI#190	*PPP1CB:ALK*-positive	Generated through *in utero* EP	Mouse brain
BI#191	*PPP1CB:ALK*-positive	Generated through *in utero* EP	Mouse brain
BI#238	*QKI:NTRK2*-positive	Generated through *in utero* EP	Mouse brain
BI#239	*QKI:NTRK2*-positive	Generated through *in utero* EP	Mouse brain
BI#271	*PPP1CB:ALK*-positive	Generated through *in utero* EP	Mouse brain
BI#283	*PPP1CB:ALK*-positive	Generated through *in utero* EP	Mouse brain

BI#298	*QKI:NTRK2*-positive	Generated through *in utero* EP	Mouse brain
BI#299	*QKI:NTRK2*-positive	Generated through *in utero* EP	Mouse brain
BI#300	*QKI:NTRK2*-positive	Generated through *in utero* EP	Mouse brain
BI#301	*QKI:NTRK2*-positive	Generated through *in utero* EP	Mouse brain
BI#386	*PPP1CB:ALK*-positive	Generated through *in utero* EP	Mouse brain
HEK-293	Human Embryonic kidney	ATCC, Wesel, Germany	Human Embryonic kidney
UMNSAH/DF-1	Chicken fibroblasts spontaneously transformed	ATCC, Wesel, Germany	Gallus gallus embryo

2.1.7 Oligonucleotides

Primer	**Sequence 5‘ to 3‘**
4/5_PJET_rev (pJET)	GCATCTCGAGGAGACGTCAAGCGTAATCTGGAACATCGTATGGGTAGCGGCGTTTGAGTCCGC
BI_alkfusion_EP_for	ACGTGAATTCACCATGGCGGACGGGGAGCT
BI_alkfusion_EP_rev	ACGTCTCGAGTCAAGCGTAATCTGGAACATCGTATGGGTAGGGCCCAGGCTGGTTCAT
BI_alkfusion_HAtag_for	ACGTGCGGCCGCACCATGGCGGACGGGGAGCT
BI_alkfusion_HAtag_rev	ACGTATCGATTCAAGCGTAATCTGGAACATCGTATGGGTAGGGCCCAGGCTGGTTCAT
BI_alkfusion_inthemiddle	CGACTACAACCCCAACTACTG
BI_alkfusion_theend	GGTACCTCTGTTCAGGCTAC
BI_alkfusion_thestart	CAGCGGTGCTTCCAATTCC
Crispr_seq_2	ACTATCATATGCTTACCGTAAC
CRISPRseq3	CATATGCTTACCGTAACTTGAAAG

FGFR1_mut_EP_for	ACGTCGTCTCGAATTCACCATGTGGAGCTGGAAGTGCC
FGFR1_mut_inthemiddle1	CTTCACTTAAGAAATGTCTCCTTTG
FGFR1_mut_inthemiddle2	GGAGGCCCCCAGGGCT
FGFR1_mut_startofmiddle	ATGTGTAAGGTGTACAGTGACC
FGFR1_mut_thestart	CCGCAGCCGACAGCGAA
FGFR1-mutation_for (pJET)	ACGTCGTCTCGCTAGCACCATGTGGAGCTGGAAGTGCC
FRFR1_mut_theend	TGTCCATGCCCCTGGACC
MYB:QKI_end	ATGAGTACCCCTACACATTGG
MYB:QKI_fusion_for	CTCACGTCTCATTCTGCAGAAGGAGAAGACAGCCT
MYB:QKI_fusion_rev	CTCACGTCTCAAGAATCTATAAATTGGAGTGTTTCTG
New_1_EP_rev (pJET)	GCATCTCGAGGAGACGCTAAGCGTAATCTGGAACATCGTATG GGTAGCCTAGAATGTCCAGGTAGAC
New_4/5_EP_rev	CATGCTCGAGTCAAGCGTAATCTGGAACATCGTATGGGTAGC GGCGTTTGAGTCCGC
NEW_MYB:QKI_rev (pJET)	ACGTCTCGAGCTAAGCGTAATCTGGAACATCGTATGGGTAGT TGCCGGTGGCGGCTC
pCAGGS_seq_for	TCCATCTCCAGCCTCGGGGC
PT2K_forward_seq	GCTCTAGCTAGAGCCTCTGCTAACC
PT2K_MYB:PCDHGA1/QKI_ for	ACGTCGTCTCGAATTCACCATGGCCCGAAGACCCCGG
PT2K_MYB:QKI_rev	ACGTCTCGAGTTAAGCGTAATCTGGAACATCGTATGGGTAGT TGCCGGTGGCGGCTCG
PT2K_reverse_seq	TAAACCAAATACTCATTCTG
px330_insert_rev_further	GTCAATAGGGGGCGTACTT
px330_seq_for	CCTTTTGCTGGCCTTTTGCTC
pX330_seq_rev_new	CAGCCAGGCGGGCCATTTA
QKI:NTRK2_EP_for	ACGTGAATTC ACCATGGTCGGGGAAATGGAAACG
QKI:NTRK2_for	ACGTCGTCTCGCTAGCACCATGGTCGGGGAAATGGAAACG
QKI:NTRK2_theend	GGCCGAGTCCTGCAGCG
QKI:NTRK2_thestart	GTGTCATTGTACATGTCTTTCCG
RCAS_FGFR1dupl/mut_for	ACGTGCGGCCGCACCATGTGGAGCTGGAAGTGCCTC

RCAS_FGFR1dupl/mut_rev	ACGTATCGATTCAAGCGTAATCTGGAACATCGTATGGGTAGC GGCGTTTGAGTCCGCC
RCAS_MYB:PCDHGA1/QKI_ for	ACGTGCGGCCGCACCATGGCCCGAAGACCCCGGCA
RCAS_MYB:QKI_rev	ACGTATCGATTTAAGCGTAATCTGGAACATCGTATGGGTAGT TGCCGGTGGCGGCTCG
RCAS_NACC2:NTRK2/QKI: NTRK2_rev_new	TCGAATCGATCTAAGCGTAATCTGGAACATCGTATGGGTAGC CTAGAATGTCCAGGTAGAC
RCAS_QKI:NTRK2_for_new	ACGTGCGGCCGCACCATGGTCGGGGAAATGGAAACG

2.1.8 Plastics

Designation	**Supplier**
8-well nunc™ lab-tek™ II chamber slides™	Thermo Fisher Scientific, Karlsruhe, Germany
Cell strainer 40µm	NeoLab Migge, Heidelberg, Germany
Centrifuge tube, 15ml	TPP, Klettgau, Germany
Centrifuge tube, 50ml	TPP, Klettgau, Germany
Corning® Costar® Stripette® serological pipette, 10ml	Merck, Darmstadt, Germany
Corning® Costar® Stripette® serological pipette, 25ml	Merck, Darmstadt, Germany
Corning® costar® stripette® serological pipette, 50ml	Merck, Darmstadt, Germany
Corning® costar® stripette® serological pipette, 5ml	Merck, Darmstadt, Germany
Electroporation cuvettes 1mm	Biozym, Hessisch Oldendorf, Germany
Eppendorf tube® 1,5ml	Eppendorf, Hamburg, Germany
Eppendorf tube® 2,0ml	Eppendorf, Hamburg, Germany
Millex®-GS filter unit, 0.22 µm	Merck Millipore, Darmstadt, Germany
Millex®-GS filter unit, 0.45 µm	Merck Millipore, Darmstadt, Germany

Millipore express® PLUS membrane 500ml funnel, 0.22µm GP	Merck Millipore, Darmstadt, Germany
PCR tubes	Biozym, Hessisch Oldendorf, Germany
Petri dishes, Ø 100mm	VWR International, Bruchsal, Germany
SafeSeal-tips® professional, 10µl	Biozym, Hessisch Oldendorf, Germany
SafeSeal-tips® professional, 1000µl	Biozym, Hessisch Oldendorf, Germany
SafeSeal-tips® professional, 20µl	Biozym, Hessisch Oldendorf, Germany
SafeSeal-tips® professional, 200µl	Biozym, Hessisch Oldendorf, Germany
Stericup® receiver Bottle, 500ml	Merck Millipore, Darmstadt, Germany
SurPhob® Tips, 10µl	Biozym, Hessisch Oldendorf, Germany
SurPhob® Tips, 1000µl	Biozym, Hessisch Oldendorf, Germany
SurPhob® Tips, 200µl	Biozym, Hessisch Oldendorf, Germany
SW41 ultracentrifuge tubes	Beckman Coulter, Krefeld, Germany
Tissue culture dish, Ø 100mm	TPP, Klettgau, Germany
Tissue culture flask 25cm^2	TPP, Klettgau, Germany
Tissue culture flask 75cm^2	TPP, Klettgau, Germany
Tissue culture flask 150cm^2	TPP, Klettgau, Germany

2.1.9 Electrical equipment

Description	**Specification**	**Company**
Automated cell counter	TC20™	BioRad, Hercules, USA
Cell analyser	FACSCanto™ II	BD Biosciences, San Jose, USA
Centrifuge	Varifuge 3.0R	Heraeus, Hanau, Germany
Centrifuge	Multifuge 3s	Heraeus, Hanau, Germany
Chemiluminescence imager	ECL Chemostar	Intas, Göttingen, Germany
CO_2 incubator	Heracell™ 150i	Thermo Fisher Scientific, Karlsruhe, Germany
CO_2 incubator	Innova® CO-48	New Brunswick Scientific,

		Edison, USA
Cold plate for cooling paraffin blocks	EG1130	Leica, Wetzlar, Germany
Electrophoresis power supply	Consort EV231	Merck, Darmstadt, Germany
Electroporation apparatus	MicroPulser™	BioRad, Hercules, USA
Embedding workstation	HistoStar™	Thermo Fisher Scientific, Karlsruhe, Germany
Epi-fluorescence illuminator	Intensilight C-HGFI	Nikon Instruments, Amsterdam, The Netherlands
Fast Real-Time PCR system	7900HT	Thermo Fisher Scientific, Karlsruhe, Germany
Flaming/Brown micropipette puller	P-97	Sutter Instrument, Novato, Germany
Fluorescent microscope	Axio Imager.M2	Zeiss, Oberkochen, Germany
Gel electrophoresis	Mini-PROTEAN® Tetra System	BioRad, Hercules, USA
Horizontal mixer	RM5-30 V	CAT M. Zipperer GmbH, Ballrechten-Dottingen, Germany
In vivo pre-clinical imaging system	IVIS® Lumina LT Series III	PerkinElmer, Waltham, USA
Incubation hood	Certomat® HK	Sartorius Group, Göttingen, Germany
Inverted microscope	Eclipse TS100	Nikon Instruments, Amsterdam, The Netherlands
Mastercycler	Epgradient S	Eppendorf, Hamburg, Germany
Microcentrifuge	Fresco™ 17	Thermo Fisher Scientific, Karlsruhe, Germany

Microgrinder	EG-45	Narishige, Tokyo, Japan
Microplate reader	Mithras LB 940	Berthold Technologies, Bad Wildbach, Germany
Mini centrifuge	Spectrafuge	NeoLab Migge, Heidelberg, Germany
Mini-Cell electrophoresis system	XCell SureLock™	Thermo Fisher Scientific, Karlsruhe, Germany
Orbital shaker	Seastar™	Thermo Fisher Scientific, Karlsruhe, Germany
Precision scales	1200-3A	Kern PLJ, Balingen, Germany
Rotary disc microtome	DSC1	Leica, Wetzlar, Germany
Slide scanner	PrimeHisto XE	NeoLab Migge, Heidelberg, Germany
Spectrophotometer	NanoDrop® ND-1000	Thermo Fisher Scientific, Karlsruhe, Germany
Spin tissue processor	Microm STP 120	Thermo Fisher Scientific, Karlsruhe, Germany
Thermal cycler	GeneAmp® PCR System 9700	Thermo Fisher Scientific, Karlsruhe, Germany
Thermal cycler	DNA Engine Dyad®	BioRad, Hercules, USA
Thermo shaker	PHMT-PSC24	Grant Instruments™, Shepreth, United Kingdom
Ultrasonic bath		Arrayit®, Sunnyvale, USA
Ultraviolet transilluminator system	Gel Doc 2000	BioRad, Hercules, USA
Water bath	1002	GFL, Burgwedel, Germany
Water bath	HI1210	Leica, Wetzlar, Germany

2.1.10 Enzymes

Enzyme	Supplier
ClaI	New England Biolabs, Ipswich, USA
FastDigest EcoRI	Thermo Fisher Scientific, Karlsruhe, Germany
FastDigest Esp3I	Thermo Fisher Scientific, Karlsruhe, Germany
FastDigest PstI	Thermo Fisher Scientific, Karlsruhe, Germany
FastDigest SalI	Thermo Fisher Scientific, Karlsruhe, Germany
FastDigest XhoI	Thermo Fisher Scientific, Karlsruhe, Germany
KpnI-HF®	New England Biolabs, Ipswich, USA
NheI	Thermo Fisher Scientific, Karlsruhe, Germany
NotI-HF®	New England Biolabs, Ipswich, USA
PciI	New England Biolabs, Ipswich, USA
Xba1	Thermo Fisher Scientific, Karlsruhe, Germany

2.1.11 Plasmids

Plasmid	Source
Lentiguide-puro	Marc Zuckermann, DKFZ, Heidelberg, Germany
pCAGGS	Sato Y. *et al.*[202]
pCW-Cas9	Marc Zuckermann, DKFZ, Heidelberg, Germany
pJET1.2 blunt vector	Thermo Fisher Scientific, Karlsruhe, Germany
pMD2.G	Kathrin Schramm, DKFZ, Heidelberg,

	Germany
psPAX2	Kathrin Schramm, DKFZ, Heidelberg, Germany
PT2K IRES-Luciferase	Sato Y. *et al.*[203]
pX330	Feng Zhang, MIT, Cambridge, USA
RCAS	Kathrin Schramm, DKFZ, Heidelberg, Germany
Transposase	Marc Zuckermann, DKFZ, Heidelberg, Germany

2.1.12 Software

Software	**Source**
EndNote X7	Thomson Reuters, Carlsbad, USA
FACS Diva	BD Biosciences, San Jose, USA
FlowJo™ v10	BD Biosciences, San Jose, USA
Living Image®	PerkinElmer, Waltham, USA
Microsoft Excel 2010	Microsoft, Redmond, USA
Microsoft PowerPoint 2010	Microsoft, Redmond, USA
Microsoft Word 2010	Microsoft, Redmond, USA
Multiple Sequence Alignment (MUSCLE)	EMBL-EBI, Hinxton, United Kingdom
NCBI Align Sequences Nucleotide BLAST	NCBI, Bethesda, USA
NEBioCalculator	New England Biolabs, Ipswich, USA
Prism 5.04 GraphPad	GraphPad Software Inc., La Jolla, USA
Sequence Scanner v1.0	Thermo Fisher Scientific, Karlsruhe, Germany

2.1.13 Miscellaneous

Material	Company
1 kb DNA ladder	Thermo Fisher Scientific, Karlsruhe, Germany
100 bp DNA ladder	Thermo Fisher Scientific, Karlsruhe, Germany
Borosilicate glass capillaries	World Precision Instruments, Sarasota, USA
Cover slips, menzel-gläser	VWR International, Bruchsal, Germany
Dako pen	Agilent, Santa Clara, USA
Disposable scalpel No.10	pfm medical, Cologne, Germany
E.cloni 10G ELITE electrocompetent cells	Biocat, Heidelberg, Germany
Histoacryl® tissue glue	B.Braun Surgical, Melsungen, Germany
Isoflo®	Zoetis, Berlin, Germany
NEB 10-ß competent E.coli	New England Biolabs, Ipswich, USA
One shot Stbl3 chemically competent E.coli	Thermo Fisher Scientific, Karlsruhe, Germany
One shot TOP10 chemically competent E.coli	Thermo Fisher Scientific, Karlsruhe, Germany
Platinium tweezer electrode, 3mm diameter	BTX, Holliston, USA
PVDF transfer membrane	Thermo Fisher Scientific, Karlsruhe, Germany
Spectra™ multicolor broad range protein ladder	Thermo Fisher Scientific, Karlsruhe, Germany
Superfrost plus microscope slides, menzel-gläser	VWR International, Bruchsal, Germany
Whatman® cellulose chromatography paper	Merck, Darmstadt, Germany

2.2 Methods

2.2.1 Molecular analysis

Methylation data were obtained using the Illumina Infinium HumanMethylation 450 (450k) and Illumina Infinium MethylationEPIC arrays according to manufacturer's instructions. The analyses were conducted by the Genomics and Proteomics Core Facility of the DKFZ, Heidelberg. Copy-number variation plots were generated from the Bioconductor package 'conumee' version 1.12.0.

2.2.2 cDNA synthesis

The following tumour IDs were used as starting material for cDNA synthesis of the respective candidate gene fusion: GBM1297 (*PPP1CB:ALK*), ICGC_PA82 (*QKI:NTRK2*). 1µl of RNA was mixed with 1 µl Oligo(dT) primers (500µg/ml) and 1µl dNTPs (10mM) from the SuperScript II reverse transcriptase kit and filled up with 9µl of nuclease-free water. This mixture was heated to 65°C for 5 minutes and briefly chilled on ice before adding 4µl 5x First-Strand Buffer, 2µl 0.1M DTT and 1µl RNase OUT. This was then incubated at 42°C for 2 minutes before adding 1µl SuperScript RT and two further incubation steps first at 42°C for 50 minutes and then at 70°C for 15 minutes. This served as a DNA template for the following polymerase chain reaction (PCR) in 2.2.4.

For both *FGFR1* (*Fibroblast Growth Factor Receptor 1*) mutations, no cDNA synthesis was required, because both were already present in the pcDNA3.1 vector, which was used as a DNA template for the PCR in the next step.

2.2.3 ASAP cloning

For the *QKI:MYB* fusion, no corresponding RNA was available from the patient, so therefore the most commonly found fusion sequence was taken from Bandopadhayay *et al.*[204] and cloned using ASAP (Adaptable System for Assembly of multiplex Plasmids) cloning (Zuckermann *et al. in preparation*) with pre-prepared *MYB* and *QKI* clones from Dharmacon and the DKFZ Genomics & Proteomics Core Facility, respectively. A single cell smear from the glycerol stocks were plated onto LB-Ampicillin (*MYB*) and LB-Kanamycin (*QKI*) agar plates and colonies were picked on the next day, which were incubated in LB-Ampicillin and LB-Kanamycin medium overnight at 37°C. DNA was isolated using QIAprep® Spin Miniprep kit according to manufacturer's protocol. This was then used for a PCR reaction to amplify the DNA using the following setup:

2. Materials & Methods

PCR reaction:

1µl DNA (~10ng)

1µl dNTPs

5µl GC Buffer

2µl Primer mix (450µl H_2O, 25µl forward and reverse primer each (100µM)

0.5µl Precisor DNA polymerase

14.5µl H_2O

PCR setup:

98°C - 5 min

98°C - 30 sec

57° - 30 sec

72°C - 45 sec (*QKI*)/ 1 min (*MYB*)

x40 cycles

72°C - 10 min

4°C - hold

PCR purification was performed using QIAquick PCR purification kit before the following digestion and ligation reaction was set up as follows:

1µl XbaI

1µl NheI

1µl BsmBI

1µl Quick Ligase

1µl Fast Digest Buffer

1µl Quick Ligase Buffer

1µl 1:5 px330 (200ng)

xµl insert in 2:1 molar insert:vector ratio

xµl H_2O

37°C - 20 sec
37°C - 3 min
16° - 4 min
x26 cycles
50°C - 5 min
80°C - 5 min
4°C - hold

To cut non-circular DNA, a Plasmid Safe reaction was performed as follows and incubated at 37°C for 30 minutes:

Plasmid Safe reaction:

11µl GGB product
1µl Plasmid safe Nuclease
1.5µl ATP
1.5µl Plasmid Safe Buffer

2.2.4 Amplification of cDNA and digestion

1µl of DNA from steps 2.2.2 and 2.2.3 DNA was used as a template for gene amplification in the following PCR reaction and setup:

PCR reaction:

1µl DNA (~10ng)
1µl dNTPs
5µl GC Buffer
2µl Primer mix (450µl H_2O, 25µl forward primer, 25µl reverse primer)
0.5µl Precisor DNA polymerase
14.5µl H_2O

PCR purification was performed according to manufacturer's instructions using the QIAquick PCR purification kit. For the RCAS cloning, the PCR product was then digested with the restriction enzymes NotI and ClaI in Cut Smart Buffer at 37°C for 1 hour, after which the cut product was run on a 1% Agarose gel at 120V for 50 minutes. The correct band size for the respective candidate gene was then cut out and the DNA was extracted using the QIAquick Gel Extraction kit according to manufacturer's instructions. For the PT2K cloning, the purified PCR product was digested with EcoRI and XhoI in Fast Digest

Buffer at 37°C for 15 minutes and applied to a 1% Agarose gel, which was run for 50 minutes at 120V. The correct band of the candidate gene's corresponding size was also cut out here using the QIAquick Gel Extraction kit according to manufacturer's instructions. The DNA concentrations of the extracted products were measured.

2.2.5 Cloning into the RCAS vector

The gel extracted insert with the NotI and ClaI overhangs was then ligated into the in-gel RCAS vector (preheated to 60°C) using the Takara ligation mixture. For that, 10µl of a 3:1 molar ratio of insert to vector was added to 10µl Takara DNA ligation mix and incubated at 16°C for 30 minutes. 5µl of this ligation mix was then added to 25µl of One Shot TOP10 Chemically Competent E.coli bacterial solution and incubated on ice for 30 minutes. This was followed by a heat shock step for 40 seconds in a 42°C warm water bath and 2 minutes on ice. 250µl of SOC medium was added to the transformation mixture, and 140µl of this was plated onto a pre-warmed Agar plate containing Ampicillin. Due to the vector containing an Ampicillin resistance gene, only bacteria containing the vector-DNA ligation will grow on the plate. The plate was incubated at 37°C overnight and bacterial colonies were picked the next day and inoculated in 3ml LB-Amp medium and again incubated overnight at 37°C on a rocking platform. 2ml of the bacterial solution was then used for isolation of the plasmid using the QIAprep® Spin Miniprep kit according to manufacturer's protocol. A control digestion with ClaI and NotI was performed for 1 hour at 37°C in CutSmart Buffer and run on a 1% Agarose gel at 120V for 30-60 minutes to check if both the RCAS vector (~11.7kB) and the insert are present. For the isolated DNA, which showed the correct bands on the gel, 80ng/µl in 20µl was send to GATC Biotech (Konstanz, Germany) for Sanger sequencing. The resulting sequence was then checked with the sequence of the inserted DNA fragment using the Sequence Scanner software. If no or only silent mutations were present in the insert, 100µl of the remaining bacterial solution of the corresponding isolated DNA were inoculated in 200ml LB-Amp Medium and incubated overnight at 37°C on a rocking platform. The next morning, the plasmid was isolated using the Endofree Plasmid Maxi kit according to the manufacturer's instructions.

2.2.6 Cloning into the PT2K vector

50ng of the PT2K vector were combined with a 3-fold molar excess of the cut DNA insert with XhoI and EcoRI overhangs using 2x Ligation Buffer, as well as the T4 DNA Ligase and mixed thoroughly. This mixture was incubated at room temperature for 5 minutes before bacterial transformation was performed as described in 2.2.5. The remaining steps are the same as in 2.2.5, apart from the control digestion, which was performed with EcoRI and XhoI.

2.2.7 Transfection of DF-1 cells and p0 injection

Ntv-a or XFM pairings were set up and the vaginal plug-positive date was recorded. Two weeks before the p0 injection, DF-1 cells were thawed and kept in DMEM + 10% FCS + 1% Penicillin/Streptomycin (P/S) + 1% Glutamax at 5% CO_2 at 39°C. Cells were split twice a week with Trypsin-EDTA in a 1:10 ratio. Four days before the calculated birth date, DF-1 cells were plated at 2-3x10^5 cells/ T25 flask in 5ml DMEM as described above. The day after, the cells were transfected with the RCAS virus as follows: 4µg of the RCAS plasmid was incubated in 200µl of room-temperature Optimem and 10µl FuGene transfection reagent. After a 15-minute incubation time, this mixture was slowly added to the settled DF-1 cells, mixed well by gently moving the flask and placed back in the incubator. An RCAS-GFP plasmid was always run in parallel in a separate flask to check for transfection success. If these DF-1 cells express GFP on the day of injection, it can be assumed that the transfection also worked for the other plasmids assuming all steps were done the same way.

On the day of birth, the transfected DF-1 cells were harvested using 10x Trypsin-EDTA and counted using the automated cell counter TC20™. 4x10^5 cells in 1µl were used for the p0 injection. The required amount of cells, depending on the size of the litter, was eluated in DMEM culture medium. The pups were taken out of the cage in a sterile hood and injected into the striatum with 1µl of the DF-1 cell solution using a 10µl Hamilton syringe (ga26s/51mm/pst2; Figure 11).

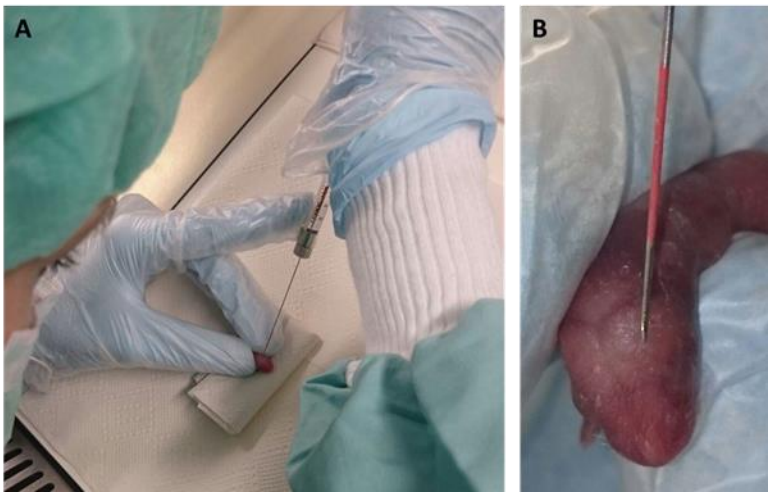

Figure 11. p0 injection into the striatum of a neonatal XFM mouse. A. Handling of the pup with correct positioning of the Hamilton syringe. The insertion angle should be 45° with an insertion depth of 2-3mm into the left hemisphere, B. The tip of the Hamilton syringe shows the point of injection. The red paint on the tip aids in judging the insertion depth, a third of the needle below the red mark was inserted into the mouse brain.

After injection, the needle was very slowly drawn out of the head. No analgetics or anesthesia are needed, due to an absence of pain perception of the pups at this stage of life. After, the pups were placed back into the cage and covered by nesting material to override any foreign smell. Animals were observed until the mother took care of them again and weaned at 3 weeks after birth. Animals were separated according to sex and observed daily for symptoms of tumour growth. These experiments were carried out under the registered and approved animal protocols G-212/16 and G-238/12.

2.2.8 *In utero* electroporation

Before surgery, the injection needle and the plasmid solution had to be prepared. For the former, Borosilicate Glass Capillaries were pulled on the Micropipette Puller (Heat=560, Pull=150, Velocity=75, Time=250) and ground at a 30° angle to produce a sharp angled tip enabling injections into the embryonic brain without further harming it. The plasmid solution was prepared as follows:

0.5µl Fast Green, 10x Phosphate Buffered Saline (PBS) was diluted to 1x PBS according to the final volume, 1mg/µl of PT2K-IRES-Luciferase containing the human influenza hemagglutinin (HA)-tagged gene of interest, the transposase vector and optionally, a guide RNA (gRNA) vector of either *cdkn2a* or *p53*. This was then made up to the total volume of ~10µl/pregnant mouse with water. Pregnant CD1 animals were generated at the Central Animal Facility of the DKFZ Heidelberg and the VP date was recorded. One

day before the *in utero* electroporation surgery, the animals were given the pain killer Metamizol in the drinking water at a concentration of 800mg/kg/day. At E14.5, the pregnant animals were anesthetized with 2% isoflurane p.i. and placed on a heating mat, on which they stayed for the whole duration of the surgical procedure. A small skin incision was made on the ventral side of the mouse followed by an incision of the peritoneum. The whole uterine horn was gently retrieved and placed onto the female's belly (Figure 12A). Approximately 2µl of the plasmid solution was injected into the lateral ventricle of the embryos (Figure 12B) and subsequently electroporated with forceps-like electrodes at 33V for 5 pulses for 50ms (Figure 12C). After all embryos had been injected and electroporated, the uterine horn was placed back into the mother and both incisions were sewed back together (Figure 12D). The mouse was then placed back into the cage onto a heating mat and closely observed for the next 24 hours. Up to 48 hours after surgery, animals received Metamizol in the drinking water at the same concentration mentioned above.

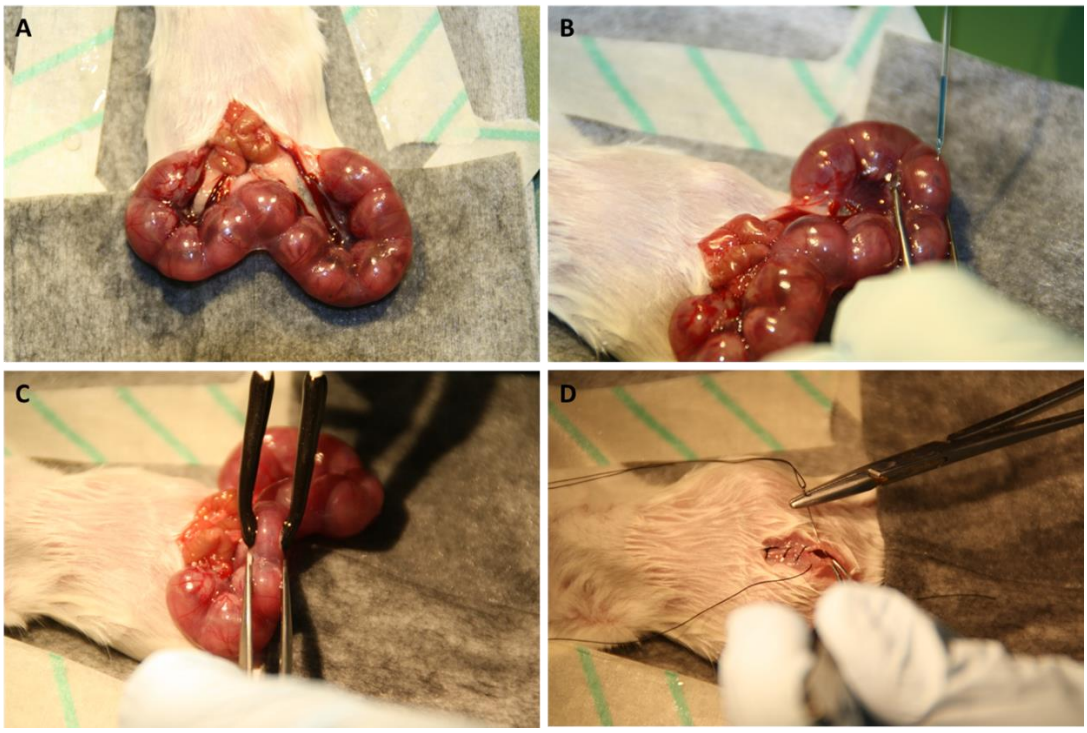

Figure 12. *In utero* electroporation at E14.5; A. A skin and peritoneum incision are made after which the whole uterine horn is placed outside the belly. B. The prepared injection solution containing the PT2K-IRES-Luciferase vector with HA-tagged candidate gene and Transposase vector and (where desired) a guide RNA is injected into the ventricle. C. The brain of the embryo is exposed to five, 50ms electric pulses of 33V each so that the injection solution penetrates the ventricular wall and can be taken up by the stem cells lining the ventricle. D. At the end of the surgery, the peritoneum and the skin incision are sewed back together and the mouse is monitored closely.

2.2.9 Luciferase imaging

The luciferase gene on the PT2K vector serves the purpose to evaluate successful incorporation of the plasmid into the embryos' brain, and to subsequently observe tumour growth *in vivo*. The animals, which successfully incorporated the plasmids, will show a positive luminescence signal when imaging around three days after birth. For that, the pups were placed into a 2% isoflurane chamber until asleep and injected with 15mg/ml Luciferin at a volume of 10µl/1g of body weight. Seven minutes later, the pups were placed into the IVIS® Lumina LT Series III (PerkinElmer) and measured for three minutes. All positive pups were placed back into the cage with the mother, whereas all pups showing no luminescence signal were sacrificed by decapitation.

2.2.10 FFPE tissue & Histological stainings

After mouse brains were taken from the animal, they were placed in 10% formalin solution and kept at 4°C until further processing. For that, the brains were placed into formalin in the dehydration machine and underwent the following dehydrating steps over a period of 60 hours: 70% EtOH, 80% EtOH, 80% EtOH, 100% EtOH, 100% EtOH, xylene, xylene and finally two paraffin baths. The dehydrated mouse brain was then paraffin embedded into an embedding cassette.

The blocks were cut at 3µm thickness, sections placed into a 42° C water bath, then onto microscope slides and dried overnight in a 37°C incubator.

Haematoxylin & Eosin (H&E) staining was performed according to standard protocols. Slides were placed into two xylene baths of 15 minutes each followed by two 100% EtOH baths, one 95% EtOH, one 70% EtOH bath and one deionised water bath for 5 minutes each. Slides were stained in Haematoxylin for 1.5 minutes, cleared in tap water for up to 5 minutes and rinsed in deionised water. All acidic and negatively charged substances (DNA/RNA) are now stained violet. The 1-minute Eosin bath that followed binds to positively charged amino acid chains and displays them in pink. The slide is then rinsed in deionised water and 70% EtOH followed by 5 minutes each in 95% EtOH and two 100% EtOH baths and finally two xylene baths of 15 minutes each. The stained slides were covered with Eukitt mounting medium and a cover slip, and dried overnight.

Immunohistochemistry (IHC) staining was performed with the LSAB+ Dako Real Detection kit with two prior steps of deparaffinisation and antigen retrieval. For the deparaffinisation and rehydration, the 3µm sections were placed into two xylene baths of 15 minutes each followed by 5 minutes each in 100% EtOH twice, 95% EtOH, 70% EtOH and distilled water. At the same time 10mM citrate buffer (pH6.0) is preheated in a steamer for 30 minutes into which the deparaffinised and rehydrated slides were placed for 40 minutes. The cuvette with the slides and citrate buffer was then taken out and cooled down at room-temperature for 20 minutes before washing the slides in distilled water for 1 minute and twice in TBS-T for 5 minutes. A 3% H_2O_2 solution (in TBS-T) was prepared and slides were incubated for 10 minutes to block endogenous peroxidase. This was followed by two washes in TBS-T, blocking with avidin, two more washes, blocking with biotin and two more washes before slides were covered with the primary antibody and incubated overnight in the dark at 4°C. Rabbit monoclonal anti-HA-tag (Cell Signaling Technology) was diluted 1:800 in antibody diluent from the kit. The antibody diluent alone served as a negative control.

On the second day, the primary antibody was washed off in TBS-T three times for 5 minutes, and slides were incubated in the DakoREAL biotinylated secondary antibody at room temperature for 15 minutes. Following this were two further washes in TBS-T for 5 minutes each, an incubation of DakoREAL streptavidin peroxidase for 20 minutes at room temperature in the dark and two further washes in TBS-T for 5 minutes each. Detection of the secondary antibody was by a 1:50 dilution of DAB+Chromogen in HRP substrate buffer for 1 minute before placing the slides into deionised water. The nuclei were stained in Haematoxylin for 1 minute and excessive staining was washed off in tap water until clear. Slides were dehydrated again in increasing alcohol concentration baths of 70% for 15 seconds and 95% EtOH followed by two 100% EtOH baths for 5 minutes each and two xylene baths of 15 minutes each. Slides were covered in Eukitt mounting medium and a cover slip and dried overnight.

2.2.11 Primary tumour cell culture

After taking out the tumour bulk from the brain of the mouse, the tissue was mechanically dissociated into single cells immediately, filtered through a 40µm strainer, then cells were counted and seeded onto 10cm culture dishes. The cells were plated in

Neurobasal-A and DMEM/F-12 media containing 1% 1M HEPES Buffer Solution, 1% 100mM Sodium Pyruvate MEM, 1% 10mM MEM Non-Essential Amino Acids Solution, 1% GlutaMAX and 1% Antibiotic-Antimycotic (now termed Base medium) supplemented with 2% B27, 2µg/ml Heparin Solution, 10ng/ml H-PDGF-AA, 20ng/ml Recombinant Human FGF-basic and 20ng/ml Recombinant Human EGF (now growth factor (GF) medium). Cells were grown as sphere cultures. For splitting, cells were dissociated with Accumax at 37°C for 5 minutes.

2.2.12. Sequencing of the *cdkn2a* and *p53* loci

In order to verify that the CRISPR nuclease successfully and correctly cut at the gRNA site of the *p53* and *cdkn2a* loci, DNA was isolated from tumour cell pellets and the respective loci were amplified in a PCR reaction. The product was then run on a 1.5% agarose gel from which it was isolated using the QIAquick Gel Extraction kit according to manufacturer's instructions. 27.5ng of that was added to 1µl blunt pJET vector, 10µl reaction buffer and 1µl T4 DNA ligase and made up to 20µl with water. The vector was ligated to the PCR product for 5 minutes at room temperature and then transformed into electrocompetent E.coli according to standard protocol. The bacterial plates were incubated overnight at 37°C, from which colonies were picked the next day and amplified DNA was extracted the next day using QIAprep Spin Miniprep Kit according to manufacturer's instructions. The product was then sent for sequencing at GATC Biotech and compared against the *cdkn2a* and *p53* locus using Blast to check for Indels.

2.2.13 Protein detection on Western blot

For the phospho blots, $1x10^6$ cells were plated on 10cm dishes and compounds (lorlatinib and crizotinib, with DMSO and GF medium as a negative control) were added to the dishes the next day and harvested 24 hours later. The harvest and following steps were all done on ice or at 4°C. Cell spheres were pelleted, washed in PBS + 1% protease/phosphatase inhibitor cocktail, pelleted again and snap frozen in liquid nitrogen first and then kept at -80°C. The cell pellet was dissolved in 1x NP-40 lysis buffer (2x NP-40 lysis buffer Tris HCl, NaCl and ddH_2O) containing the same inhibitor cocktail mentioned above and incubated on ice for 45 minutes (vortexed from time to time). The cell pellet-lysis buffer mixture was then centrifuged at 13,000rpm for 10 minutes at 4°C before the supernatant was transferred to a new tube. A Bicinchoninic Acid (BCA) assay

was performed according to standard protocol to determine the protein concentration of each sample before denaturing in a NuPage sample buffer, ß-Mercaptoethanol and 1x lysis buffer mixture at 95°C for 5 minutes. 30 µg of the denatured samples were applied to 4-12% gradient NuPage Bis-Tris precast gels for protein electrophoresis and run at 60V for 30 minutes and then for 1.5 hours at 130V. The split protein was then transferred to a PVDF membrane using the following setup:

10 min	100mA
10 min	200mA
10 min	300mA
10 min	400mA
20 min	500mA
10-60 min	50mA

The membranes were then placed into a 5% BSA (Albumin Fraction V) or 5% milk blocking solution for 1 hour at room temperature and cut at ~35kDa and ~50kDa before the membranes were incubated with the primary antibodies at 4°C for 48 hours. The following primary antibodies were used: rabbit monoclonal anti-HA-tag (Cell Signaling Technology) 1:3000 in 5% BSA, rabbit polyclonal anti-ALK (Thermo Fisher Scientific) 1:300 in 5% BSA, rabbit polyclonal anti-phospho-ALK (Cell Signalling Technologies) 1:1000 in 5% BSA, rabbit polyclonal anti-cleaved Caspase-3 (Cell Signalling Technology) 1:500 in 5% milk and mouse monoclonal anti-GAPDH (Millipore) 1:5000 in 5% BSA.

48 hours later, the primary antibody was washed off in 1xTBS-T before the secondary antibody, goat polyclonal anti-Rabbit IgG-HRP or goat polyclonal anti-Mouse IgG-HRP were applied to the membrane in 1:2000 and 1:3000 dilutions, respectively in 5% BSA or 5% milk depending on the primary antibody and incubated overnight at 4°C. Membranes were washed in TBS-T again, after which the proteins were detected using ECL Prime (p-ALK) or ECL (all others) reagents for 1-15 minutes on a chemiluminescence imager (Intas) depending on the strength of their signal.

For the non-phospho Western blots, cells were not treated with any phosphatase inhibitor compounds and were lysed using 1x lysis buffer (10x lysis buffer made from RIPA buffer and cOmplete™ Mini EDTA-free protease inhibitor cocktail tablets). Primary

antibody incubation was only overnight at 4°C and secondary antibody incubation for 1 hour at room temperature. Another difference was that only 30µg of protein were loaded. The rest of the procedure stayed the same.

2.2.14 Immunofluorescence cyto staining

Immunofluorescence (IF) staining was performed to validate the purity of the tumour cells taken in culture to confirm that these cells really originate from the tumour initiated by *in utero* electroporation through the detection of the HA-tag with a fluorescent signal. Tumour cells were plated onto Lab-Tek II chamber slides at $2x10^4$ cells per well in GF medium with 4% FCS and either left in culture for 72-96 hours depending on confluency or treated the next day with 400nM of lorlatinib.

After incubation time, the medium was taken off and slides were washed with PBS and subsequently fixed in 1% PFA (in PBS) solution at room temperature for 10 minutes. Slides were washed twice with PBS before cells were permeabilised with 0.1% Triton-X-100 in PBS for 10 minutes at room temperature. Three washes in PBS followed as well as antigen retrieval in hot citrate buffer for 20 minutes. Afterwards, slides were left in the buffer for 20 minutes to cool down before being washed in PBS again twice. Slides were then blocked in 10% normal donkey serum in PBS-T for one hour at room temperature. After blocking, cells were incubated in a 1:800 dilution of Rabbit anti-HA-tag antibody in PBS-T + 10% normal donkey serum overnight at 4°C. The negative control did not contain the antibody.

On the next day, slides were washed in PBS three times before the secondary antibody Alexa Fluor® 568 donkey anti-rabbit IgG was added in a 1:400 dilution in PBS-T for 1 hour at room temperature. Slides were then washed for 10 minutes each in TBS-T three times, in PBS once and in water once. DAPI Fluoromount-G® mounting medium was added onto the slide, which was then covered with a cover slip and dried overnight in the dark before representative images were taken on the fluorescent microscope.

2.2.15 *In vitro* inhibitor testing

All drugs were purchased from Selleck Chemicals and diluted in DMSO to either a 10mM or 1mM stock, which were stored at -80°C. Primary sphere culture cells were plated at $1x10^4$ cells/well in 80µl GF medium medium/well in 96-well plates. Triplicates per drug

concentration were added 24 hours after seeding the cells in 20µl. The drug concentrations ranged between 30µM and 0.01nM depending on the drug. Corresponding DMSO concentrations were plated to which the treated wells were normalized. ALK-specific inhibitors included: crizotinib, ceritinib, alectinib and lorlatinib. Entrectinib was used as an NTRK inhibitor, and has been shown to function as a TrkA, TrkB, TrkC, ROS1 and ALK inhibitor. Infigratinib (BGJ398) is a FGFR1/2/3-specific inhibitor and was used as a negative control for the specificity of the ALK and NTRK inhibitors on *PPP1CB:ALK*-fused and *QKI:NTRK*-fused cells, respectively.

The CellTiter-Glo readout was conducted 72 hours after drugs were added to the cells. For that 50µl of CellTiter-Glo substrate were added to each well using a multichannel pipette, plates were incubated for 15 minutes whilst shaking in the dark. After that time, the viability of the cells was measured in the microplate reader Mithras LB940. The respective DMSO control value was subtracted from the drug's value to normalize the readout. The IC50 curves show the mean ± SD of the triplicates per condition measured.

2.2.16 Annexin V flow cytometry analysis

PPP1CB:ALK tumour spheres were plated at $3x10^5$ cells in 3 ml per well in 6-well suspension plates and incubated overnight. The next day, three wells each were treated with the following substances: non-treated (GF medium), DMSO control, crizotinib and lorlatinib at an end concentration of 400nM (or 0.004% for the DMSO control). 72 hours later, cells were harvested by pipetting up and down, centrifuged and washed in cold PBS. Staining with FITC annexin V and Propidium Iodide (PI) was performed according to manufacturer's instructions (Dead Cell Apoptosis Kit, Life Technologies). Flow cytometry analysis was perfomed on the FACS Canto, where 100,000 events were counted and recorded and subsequently analysed on the FACS Diva software.

2.2.17 Cell cycle analysis

Cell cycle analysis was performed using the Propidium Iodide Flow Cytometry kit from abcam. *PPP1CB:ALK* tumour spheres were plated at $3x10^5$ cells in 3 ml per well in 6-well suspension plates and incubated overnight. The next day, three wells each were treated with the following substances: non-treated (GF medium), DMSO control, crizotinib and lorlatinib at an end concentration of 400nM (or 0.004% for the DMSO control). 72 hours later, cells were harvested by pipetting up and down, centrifuged at 500 x g for 5

minutes and washed in 1x PBS before being centrifuged again. The supernatant was discarded and cells were fixed in 66% EtOH for 2 hours at 4°C. Cells were equilibrated to room temperature before being pelleted, washed in 1x PBS and pelleted again. Pellets were resuspended in 200µl 1x Propidium Iodide + RNase staining solution and incubated in the dark at 37°C for 20-30 minutes. Cells were then placed on ice and ready for flow cytometry analysis. This was performed on the FACS Canto, where 100,000 events were counted and recorded and subsequently analysed on the FACS Diva software.

2.2.18 Intracranial injection

To test the effectiveness of ALK inhibition *in vivo*, intracranial injection of 6 week old CD1 mice with mouse *PPP1CB:ALK* tumour cells was performed. For that, mice were given 800mg/kg/day Metamizol in the drinking water 24 hours before the surgery. On the day of injection, mice were anesthetised by inhalation with 2% isoflurane and placed onto a heat mat and into the stereotactic frame. Bepanthen was put onto the eyes to avoid blindness, as well as onto the head to make the hairs sticky so that they do not enter the open wound. A small incision was made, followed by a hole slowly drilled into the skull at the point indicated in Figure 13. 4µl of the tumour cells were drawn up in a Hamilton syringe, which was placed into the stereotactic frame. The needle was then inserted into the hole made and the tumour cells were slowly injected over two minutes. The Hamilton needle was then slowly pulled out of the hole to avoid negative pressure and the cut was glued together with tissue glue. The mouse was placed back into the cage and observed closely for the next 24 hours.

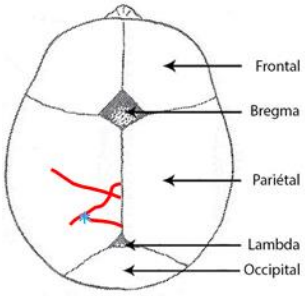

Figure 13. Dorsal view onto mouse skull with blood vessels and injection area for injections into the striatum indicated.

2.2.19 *In vivo* inhibitor testing

The animal protocol under which the inhibitor testing was conducted (G-168/17) was approved by the Regierungspräsidium Karlsruhe before starting the experiment. The chosen inhibitor was lorlatinib based on the *in vitro* results, as well as HCl and Temozolomide as vehicle control and standard-of-care, respectively. The doses and treatment regime of the first two drugs were adapted from Infarinato *et al*.[205] and Temozolomide was administered according to the suggested dose on the suppliers website (http://www.selleckchem.com/products/Methazolastone.html). Animals were weighed three times a week and any abnormal behaviour or symptoms were recorded and the animals were sacrificed when they reached a critical status. Half of the mouse brain was then formalin-fixed and paraffin embedded and the other half was snap frozen in liquid nitrogen and frozen at -80°C for further analysis.

3. Results

3.1 Proof of concept animal model

Before testing drugs or specific targeted inhibitors in clinical trials in humans, their effectiveness and safety needs to be pre-clinically tested *in vivo*. In order to do that, respective animal models of recurrent somatic mutations found in the paediatric patients' tumours need to be established and validated. Here, I used the techniques of *in utero* electroporation and p0 injection using the RCAS/t-va system to generate tumour bearing mouse models aiming to recapitulate the appearance of the paediatric tumours as close to the human situation as possible. The main focus of this work was on the *PPP1CB:ALK* fusion, however other candidate genes were also tested to support the more general applicability of the pre-clinical pipeline outlined here.

3.1.1 Successful cloning of recurrent paediatric candidate genes

After extraction of RNA, synthesis of cDNA and cloning of the fusion gene cDNA into the RCAS and PT2K vectors, the plasmids were sequenced using Sanger sequencing at GATC Biotech. The *PPP1CB:ALK* fusion was correctly cloned into the vectors with three known SNPs at protein positions 1461, 1491 and 1529 compared with the reference sequence (data not shown). To test if the RCAS vector is working sufficiently and expressing the correct fusion/mutation proteins, DF-1 chicken cells were transfected with 4µg of the plasmid. During cloning of the human *PPP1CB:ALK* sequence, the sequence for the human influenza hemagglutinin (HA) glycoprotein was added to the C-terminus of the fusion gene. This enables easy detection of the desired fusion gene by staining against the HA-tag in immunohistochemistry or immunofluorescence staining or by Western blotting. After three days, pellets of the cells were harvested and run on a Western blot against the HA-tag to confirm that the tagged protein of interest is present (Figure 14). The harvested DF-1 cells expressed the respective protein of the transfected plasmids for all HA-tagged samples. The red arrows indicate the detected band of the desired proteins, which were as follows: PPP1CB:ALK- 85kDa, QKI:NTRK2- 76kDa, MYB:QKI- 64kDa and FGFR1mut- 93kDa. All proteins ran at ~10-15kDa higher than expected based

on calculated molecular weight. RCAS_GFP, which does not contain a HA-tag, serves as a negative control and was therefore not detected on the blot.

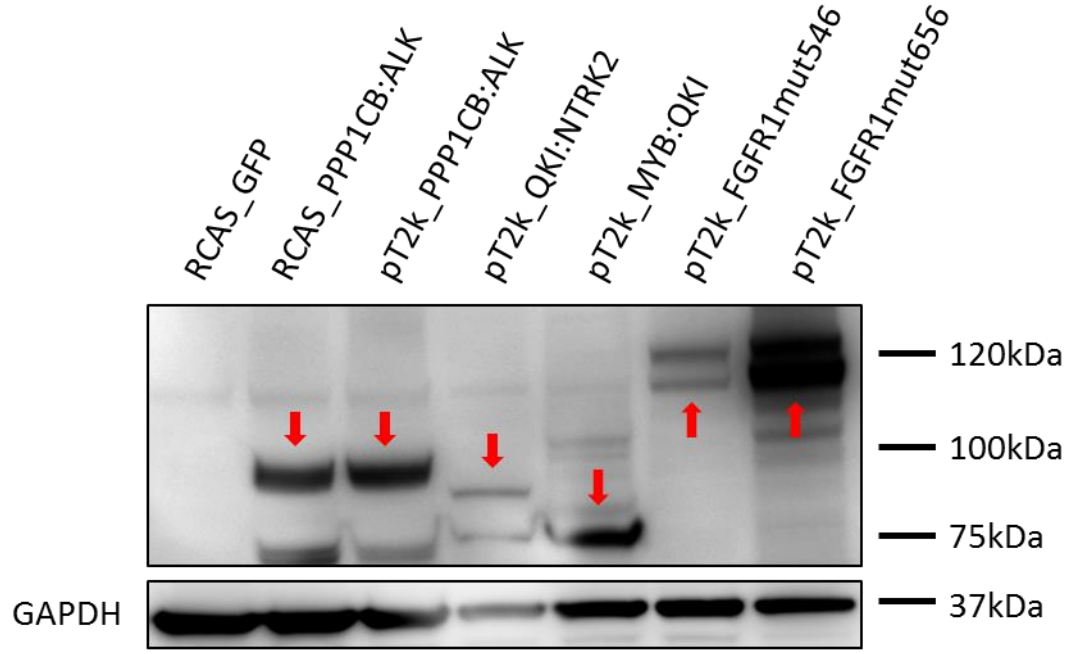

Figure 14. Western blot against HA detecting cloned constructs of candidate genes. DF-1 cells were transfected with the cloned constructs using FuGene. This Western blot was performed as described in 2.2.13 and stained against HA-tag and GAPDH as a loading control (~37kDa). The membrane was exposed to ECL detection reagent for 30 seconds. The RCAS_GFP vector serves as a negative control, because it does not have the HA-tag fused to it unlike all the other constructs, which all show a positive signal. This means that all vectors were successfully cloned and express the desired protein.

3.1.2 *ALK* fusion-containing mice successfully develop tumours from 29 days after *in utero* electroporation

To generate tumours bearing the desired *PPP1CB:ALK* fusion, one prenatal and one neonatal method of somatic gene transfer were applied to test the oncogenicity of this fusion *in vivo*. The two experimental methods of inducing *PPP1CB:ALK*-positive tumours *in vivo* gave different results. The p0 injected XFM animals did not develop any tumours, but rather died from other symptoms at an average age of 195 days (n=19) due to the constitutive *Cdkn2a* (cyclin-dependent kinase inhibitor 2A) knock-out of the mice (Figure 15B).

Therefore, all of the following results are based on tumours derived from *in utero* electroporated CD1 mice (Figure 15A). On average about 30% of all electroporated animals survive the *in utero* electroporation procedure, out of which half contain the inserted transgene, shown by a positive luciferase signal detected through the IVIS device three days after birth. Tumours arose in almost 100% of positive luciferase signal pups. Tumours harbouring *PPP1CB:ALK* in combination with either *sgp53* or *sgcdkn2a* developed quicker than tumours just containing the fusion gene. On average, they survived 137 (wt; n=2), 55 (*sgcdkn2a*; n=4) and 35 (*sgp53*; n=10) days after birth until tumour-related symptoms developed (Figure 15, Table 3). Symptoms included reduced locomotion, hunched back and rounded skull.

This high penetrance and fast tumour development of the *sgcdkn2a* and *sgp53* combination with *PPP1CB:ALK* makes *in utero* electroporation a good method for mouse model development in this setting.

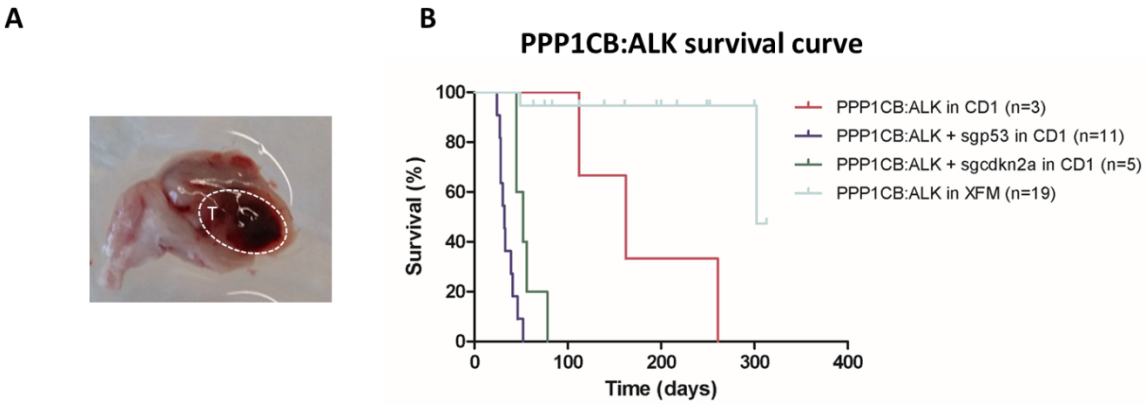

Figure 15. *PPP1CB:ALK* tumours from *in utero* electroporation. A. CD1 mouse brain showing a *PPP1CB:ALK* + *sgp53* bearing tumour within the striatum at 39 days after birth. This mouse was sacrificed, because it developed symptoms due to the tumour growth. B. Kaplan-Meier survival curve of animals injected with *PPP1CB:ALK* at either E14.5 or p0. The latter did not develop tumours, whereas animals from *in utero* electroporation did. These developed quicker when combined with a sgRNA against either *cdkn2a* or *p53*. Only two of 19 XFM mice harboured a tumour and the others all died on non-brain tumour related symptoms indicated by the small vertical lines across the horizontal one.

Table 3 is an overview of all *PPP1CB:ALK* tumours generated from *in utero* electroporation either alone or in combination with a second hit against the tumour suppressors *cdkn2a* or *p53*. Tumour cells were not taken into culture from all of these

tumours, but the ones from which cells are available in culture and further validation experiments were obtained are marked with an asterisk.

Table 3. Listing of tumour-bearing mice by their ID and the corresponding genetic aberration and latency.
* indicates that the tumour cells were taken into culture and further analyses were done

ID	Candidate gene	Second hit	Latency (days)
BI#169*	*PPP1CB:ALK*	*sgcdkn2a*	45
BI#386*	*PPP1CB:ALK*	*sgcdkn2a*	45
BI#292	*PPP1CB:ALK*	*sgcdkn2a*	52
BI#305	*PPP1CB:ALK*	*sgcdkn2a*	78
BI#357	*PPP1CB:ALK*	*sgp53*	24
BI#361	*PPP1CB:ALK*	*sgp53*	28
BI#362	*PPP1CB:ALK*	*sgp53*	28
BI#190*	*PPP1CB:ALK*	*sgp53*	30
BI#191*	*PPP1CB:ALK*	*sgp53*	32
BI#272	*PPP1CB:ALK*	*sgp53*	33
BI#363	*PPP1CB:ALK*	*sgp53*	39
BI#365	*PPP1CB:ALK*	*sgp53*	41
BI#281	*PPP1CB:ALK*	*sgp53*	46
BI#283*	*PPP1CB:ALK*	*sgp53*	52
BI#207	*PPP1CB:ALK*	-	112
BI#271*	*PPP1CB:ALK*	-	162

3.1.3 Tumour cells *in vitro*

Table 3 lists the mice, which successfully developed a tumour from *in utero* electroporation with the *PPP1CB:ALK* fusion alone or in combination with a suppressor knock-out of *p53* or *cdkn2a.* The asterisk indicates the cases from which cells from the tumour bulk were taken into culture. The tumour tissue was dissociated into single cells mechanically and then filtered before cells were plated into 10cm dishes. Cells were kept as sphere cultures in non-attachment dishes where they formed spheres nicely

(Figure 16). Spheres had to be split and dissociated into single cells every 3-4 days. Cells maintained their sphere forming ability for at least 20 passages.

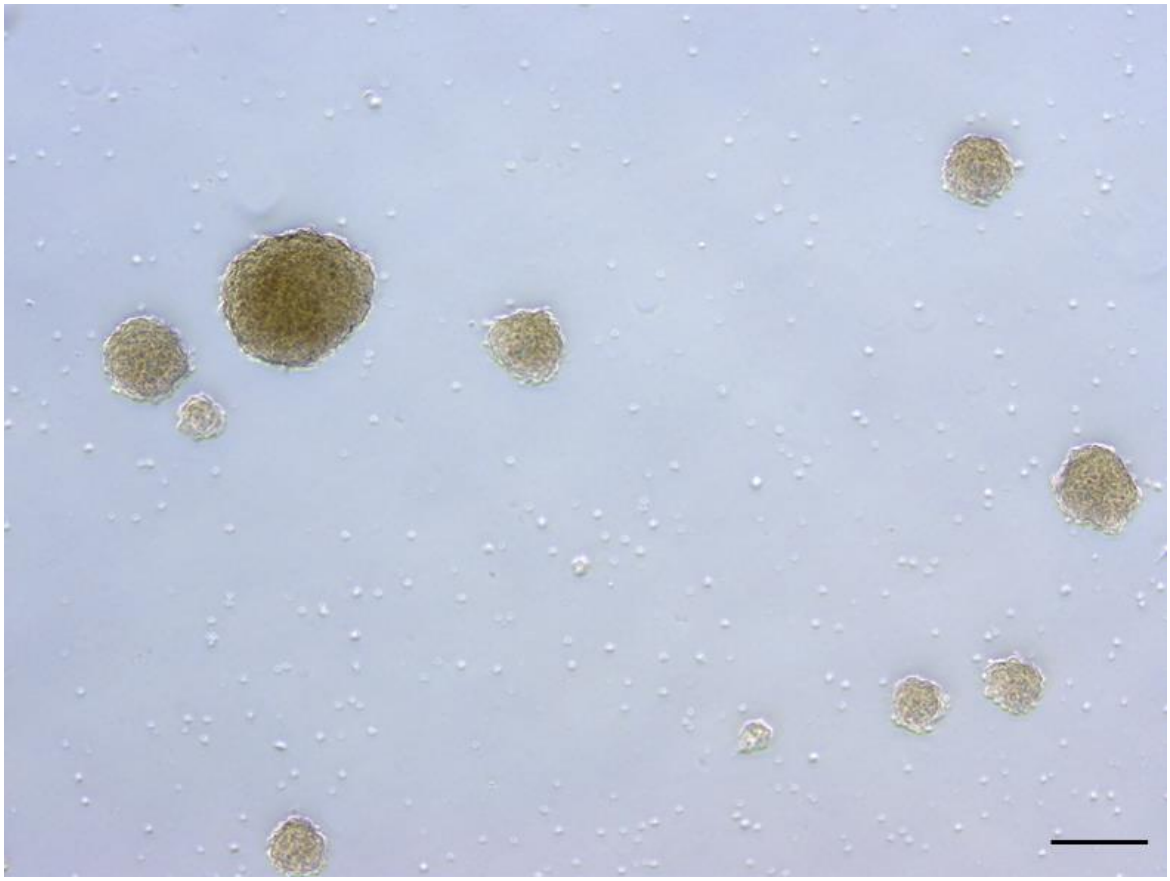

Figure 16. BI#283 spheres in culture. Cells are kept in non-attachment dishes at 37°C with 5% CO_2 in growth factor medium. Scale bar: 200µm.

3.1.4 *PPP1CB:ALK* model characteristics

The presence of the HA-tag is a valuable tool to detect the fusion protein not only on Western blot, as already seen in Figure 14, but also in IHC and IF staining. This characteristic was utilised to show that the tumours in the mice are a direct result from the *in utero* electroporated oncogenic plasmids.

Figure 17 shows the formalin-fixed paraffin-embedded (FFPE) mouse brains stained for H&E and the corresponding IHC staining against the HA-tag. In all of the tumours, the observed tumour mass in the H&E staining unambiguously corresponds to the positive staining of the IHC (Figure 17A). IHC staining of the mouse brains recapitulates the ALK-positive human tumours by morphology nicely as assessed by two independent

experienced neuropathologists (Prof. Dr. David Capper and Prof. Dr. David Ellison). The fusion was not only detectable in the tissue sections, but also in the tumour cells taken into culture. This Western blot (Figure 17B) was an important step in defining the origin of the tumour and confirming that the sphere-forming cells cultured from the tumours are truly *PPP1CB:ALK* fused tumour cells developed from *in utero* electroporation, making them suitable for further experiments. 30µg of protein were loaded onto the protein gel to be able to compare relative expression of the fusion protein between the different primary cell cultures. Looking at Figure 17, BI#169 and BI#271 seem to have a lower protein expression of the HA-tag, but when taking the intensity of the GAPDH band in consideration, this is only true for BI#271 after all. This shows lower expression of the *PPP1CB:ALK* fusion protein compared to the other five primary cell cultures. However, the exposure time in this Western blot figure is relatively short (60 seconds), indicating that the absolute expression of the protein is high in all of these primary cells. Cells from HD-MB03 served as a negative control not expressing the HA-tag to make sure that the primary antibody is specifically only detecting the HA-tag.

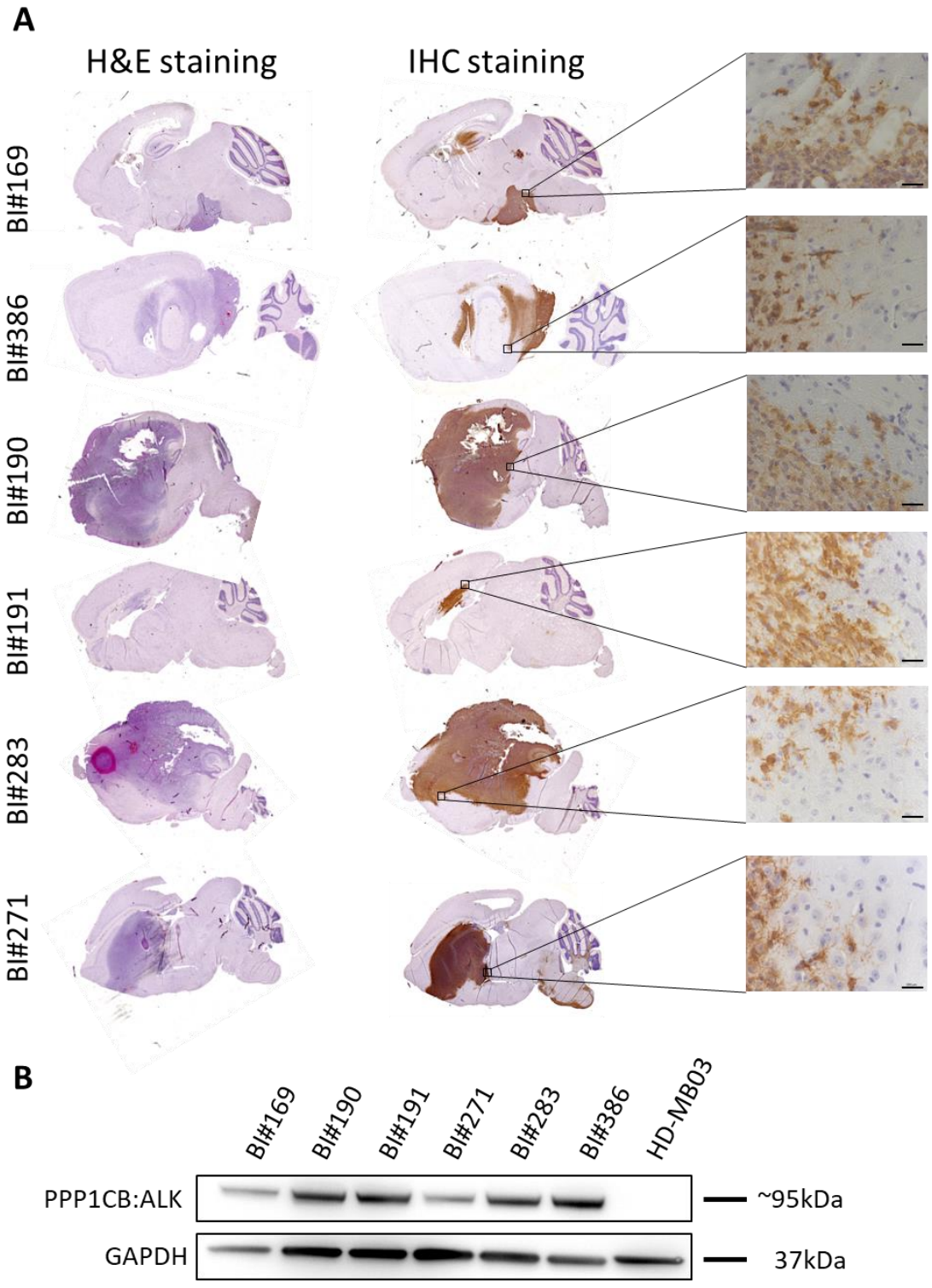

Figure 17. Detection of the fusion protein by H&E and IHC staining on FFPE mouse tissue and Western blot from *in vitro* tumour cells. A. H&E staining and the corresponding IHC staining against the HA-tag clearly show that the observed tumour mass in the former, nicely correspond to the brown staining in the latter. The close up images are of 40x magnification and the scale bar is 100µm. B. Detection of 30µg of the fusion-HA-tag protein on Western blot. The detected bands all ran at ~95kDa, which is about 10kDa bigger than the theoretical protein size calculated. The protein was detected using ECL detection reagents.

The next step was to test if the tumour cells not only express the HA-tag and therefore the *PPP1CB:ALK* fusion, but also contain a dysfunctional second hit of either *p53* or *cdkn2a* as expected (Figure 18). For this purpose, DNA was extracted from the primary cell cultures, a PCR of the *cdkn2a* or *p53* locus was performed and that product was then cloned into the pJET vector, which then underwent Sanger sequencing. Figure 18 depicts the results of the sequenced bacterial colonies. As expected, BI#271 cells (electroporated with the *PPP1CB:ALK* fusion alone) show intact *p53* and *cdkn2a* loci, confirming that no gRNA was electroporated in addition to the fusion gene. Both of the *PPP1CB:ALK* + *sgcdkn2a* primary cell cultures (BI#169 and BI#386) and BI#283 (*PPP1CB:ALK* + *sgp53*) only showed one inserted base (Adenine or Thymine) in all sequenced colonies at the position where the CRISPR nuclease is supposed to cut, thereby inducing a frame shift mutation resulting in a non-functional protein. BI#191 contains a one base insertion in most of the colonies sequenced, however it also shows a 245 base deletion after the site where the nuclease is supposed to cut in three cases. BI#190 is the most varied of all primary cell cultures, because it shows one (n=3) or two (n=1) base insertions, a 169 base deletion (n=1) or no cut (n=4) at the CRISPR target site.

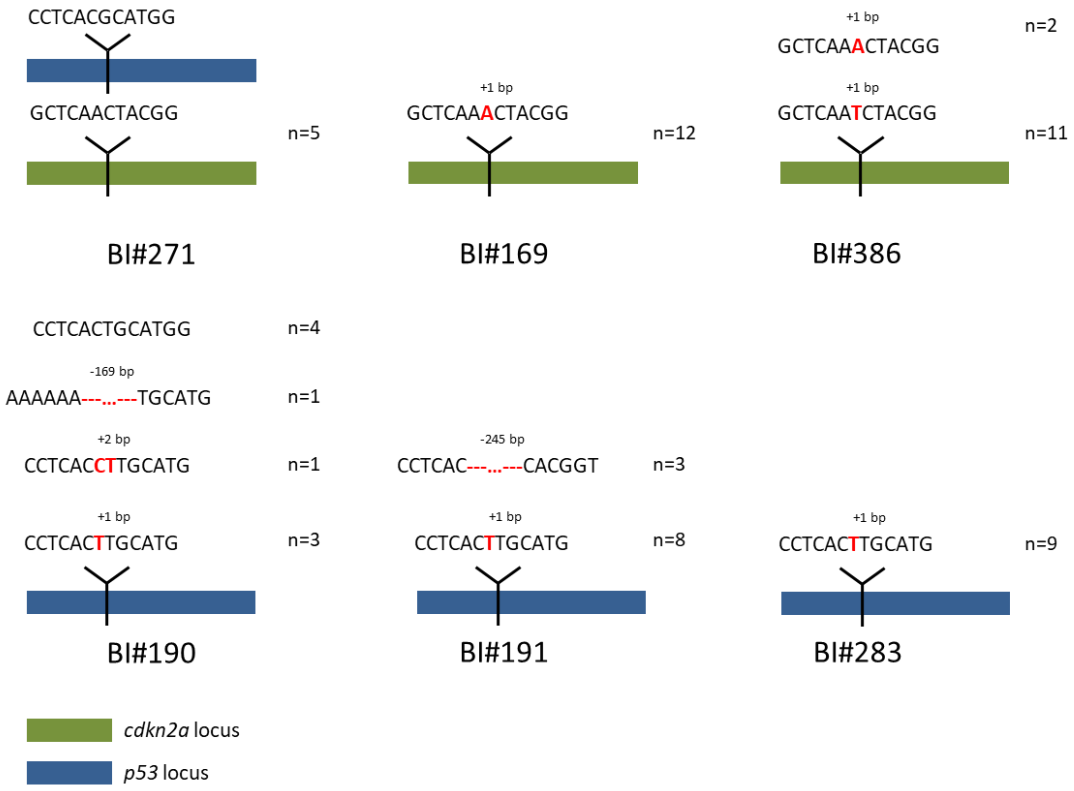

Figure 18. Testing the effectiveness of the gRNA in the primary tumour cell cultures. BI#271, which are cells from a mouse not electroporated with a gRNA, show intact *p53* and *cdkn2a* loci. Both *PPP1CB:ALK* fusion + *sgcdkn2a* primary tumour cell cultures show an insertion of an Adenine or Thymine base at the position where the DNA was supposed to be cut. This frame shift mutation results in a non-functional *cdkn2a* loci, which contributes to the tumourgenicity of the cells resulting in a faster tumour growth than just the *PPP1CB:ALK* fused cells as seen in Figure 15. The gRNA against *p53* seems to result in more heterogenous tumour cells with one or two base pairs inserted, or a series of bases being deleted. In four colonies of BI#190, no cut was detected. The green bar represents the *cdkn2a* locus and the blue one the *p53* locus. bp = base pair

Furthermore, the cells in culture were also immunofluorescently stained against the HA-tag to define the percentage of *PPP1CB:ALK*-positive cells in culture. This analysis confirmed that nearly 100% of cells in culture are *ALK* fusion positive tumour cells (Figure 19). This remained true for the surviving cells after treatment with lorlatinib (concentrations according to Figure 20 shows that the first line inhibitor crizotinib performs worst of all tested ALK inhibitors *in vitro* in the *PPP1CB:ALK-fused* cells with either of the CRISPR gRNAs against cdkn2a and p53 (BI#169, BI#190, BI#191, BI#283, BI#386). Cells show a better response to second line ALK inhibitors ceritinib and alectinib, as well as the combined NTRK and ALK inhibitor entrectinib, all developed later than crizotinib and therefore showing more specific targeting. Nevertheless, the latest

developed inhibitor, lorlatinib, performs best in terms of the dose response with low IC50 values ranging from 0.35-1.24nM. These values correspond to achievable concentrations that can be administered in patients in the clinic206. The FGFR1 inhibitor, BGJ398 (infigratinib) is ineffective against *ALK-positive* cells, showing the specificity of the ALK inhibitors against cells harbouring this aberration. It also becomes clear that for essentially none of the tumour cell cultures do any of the drugs give a 100% viability drop in response to treatment. This may be due either to a small proportion of the cells being resistant to treatment, which are therefore still metabolically active (which the CellTiter-Glo assay is detecting), or it could indicate that a proportion of the cells respond rather with a stop of proliferation (cytostatic) than by undergoing cell death (cytotoxic). This response however might shift upon s shorter or longer exposure time, which will need to be tested.

Looking at Figure 20, it also becomes clear that the drug response curves of the primary cell culture from the tumour of just the *PPP1CB:ALK* fusion (BI#271) all show (nearly) 100% response at the 2mM or 30µM concentration. Lorlatinib, however, does not seem to have an effect on these tumour cells with a high mean IC50 value of 11nM from the two replicates. This shows that the ALK inhibitors are potent to ALK-positive cells in combination with a tumour suppressor knock-out.

After having determined the mean IC50 values of the three different primary tumour cell culture combinations, further tests were conducted to investigate what the ALK inhibitors are actually doing to the cells to explain the decreased viability of tumour cells being treated and the IC50 curves not reaching 0% in the majority of primary cell cultures in Figure 20.

The mean of the IC50 values from the duplicates of the experiment were calculated and used as the basis for the drug concentrations for the flow cytometric and Western blot analysis. Table 4 indicates the IC50 values used for lorlatinib and crizotinib. The DMSO control concentrations are based on the lorlatinib concentrations. All lorlatinib concentrations are below 1.4nM (mean 0.76nM), which none of the other inhibitors come close to. The second best ALK inhibitor is alectinib with a mean IC50 of 3.3nM.

Table 4; data not shown), indicating no enrichment for e.g. drug-resistant stromal cells accounting for this surviving population. DAPI is stained in blue and the HA-tagged cells are shown in red. Images of the cells after treatment are not shown, since they were essentially identical to those displayed in Figure 19. The negative controls all just show DAPI staining and no specific staining of the Alexa Fluor dye, which is why they are not shown here.

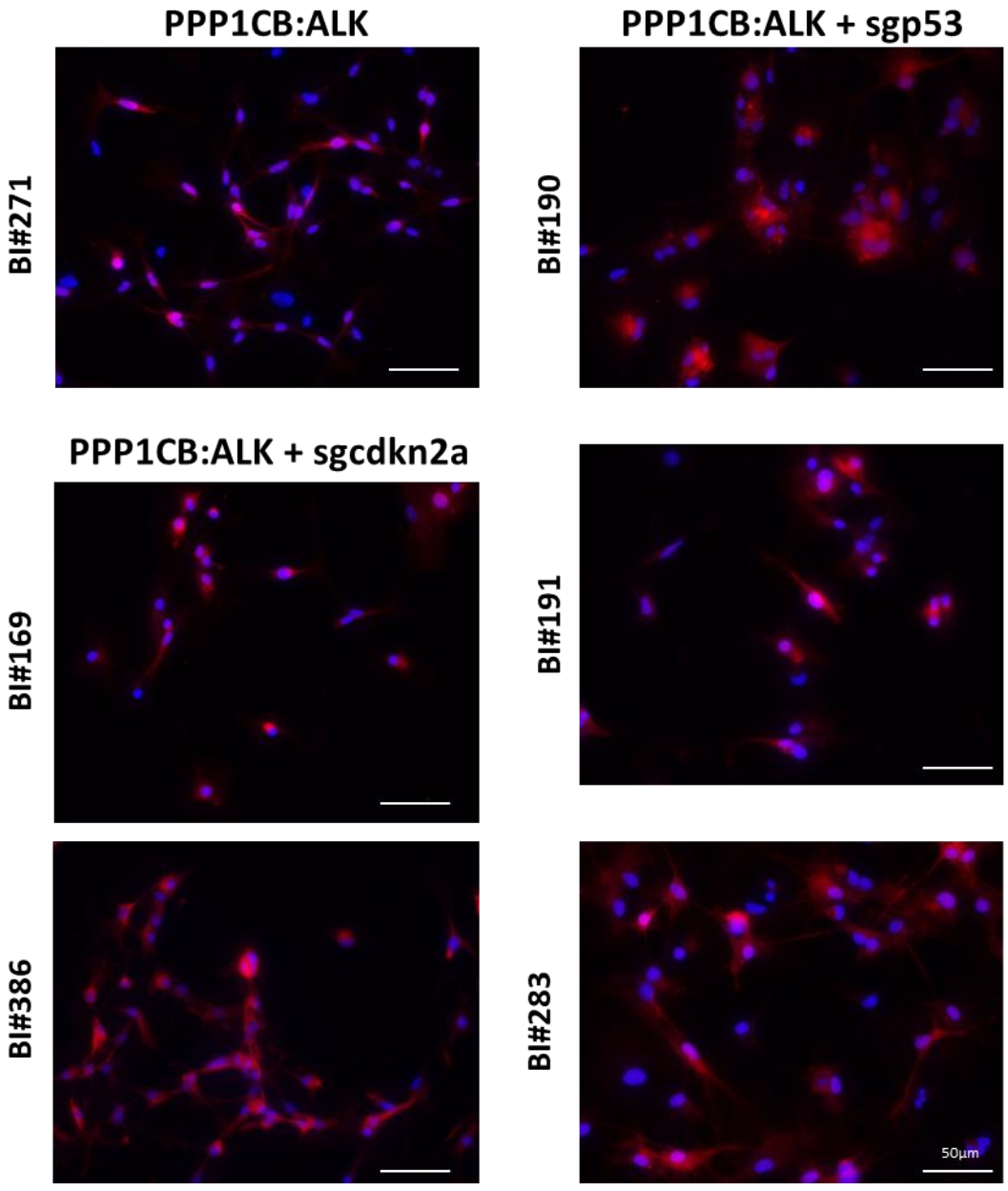

Figure 19. Representative immunofluorescence images of mouse extracted tumour cells *in vitro* stained against HA-tag bound to Alexa Fluor® 568. The top left image (BI#271) shows primary tumour cells from a *PPP1CB:ALK* fused only tumour, whereas the two images below that (BI#169 and BI#386) and the

complete right column images (BI190, BI#191 and BI#283) show *ALK* fused cells with *sgcdkn2a* and *sgp53*, respectively. In all representative images, almost 100% of cells are positive for the HA-tag indicating that the tumour cell culture is of high purity. Scale bar: 50µm.

3.2 Comparison of different ALK-specific inhibitors

After having tested the identity and purity of the cells taken into culture from the murine tumours, the next logical step was to test commercially available ALK-specific inhibitors on these *ALK*-fused cells to comment on their effectiveness and mechanism of action. In recent years, ALK inhibitor development has made great progress. From crizotinib, a first line ALK inhibitor, through alectinib and ceritinib showing effectiveness against crizotinib-resistant tumours to lorlatinib being an even more potent third line inhibitor. I therefore hypothesised that the latter inhibitor would give the most effective results in inhibiting ALK-positive tumour cells *in vitro*.

3.2.1 Lorlatinib inhibits growth of *ALK*-fused primary cell cultures on average at 56-fold lower concentrations than crizotinib

After confirming the true *PPP1CB:ALK* identity of the tumour cells and that the models recapitulate features of their human counterparts, the next step was to initiate pre-clinical drug testing *in vitro* prior to going back into the mouse to do the same therefor *in vivo* confirmation.

CellTiter-Glo is a luminescence-based viability assay measuring ATP to determine the number of viable cells in culture after treatment with chemotherapeutic agents, for example. It is based on the amount of ATP present, only found in live cells. Dead cells lose their membrane integrity and with this the ability to produce ATP. The luminescence signal intensity is therefore proportional to the number of metabolically active cells.

Figure 20 shows one representative IC50 graph (experiment performed in duplicate) of each of the primary cell culture derived from the murine tumours marked with an asterisk listed in Table 3. Cells were plated at a density of $1x10^4$ cells/well in a 96-well, white, clear bottom plate and after 24 hours, four different ALK-specific inhibitors (ceritinib, crizotinib, lorlatinib and alectinib) together with an FGFR1-specific inhibitor (BGJ398) and an NTRK/ALK inhibitor (entrectinib) were added in eight different

concentrations ranging from 0.01nm-30µM together with the corresponding DMSO concentrations. After a further 72 hours, CellTiter-Glo substrate was added and the luminescence of the treated cells was measured using a Mithras plate reader. From the generated data, the IC50 curves below were calculated using the GraphPad Prism software.

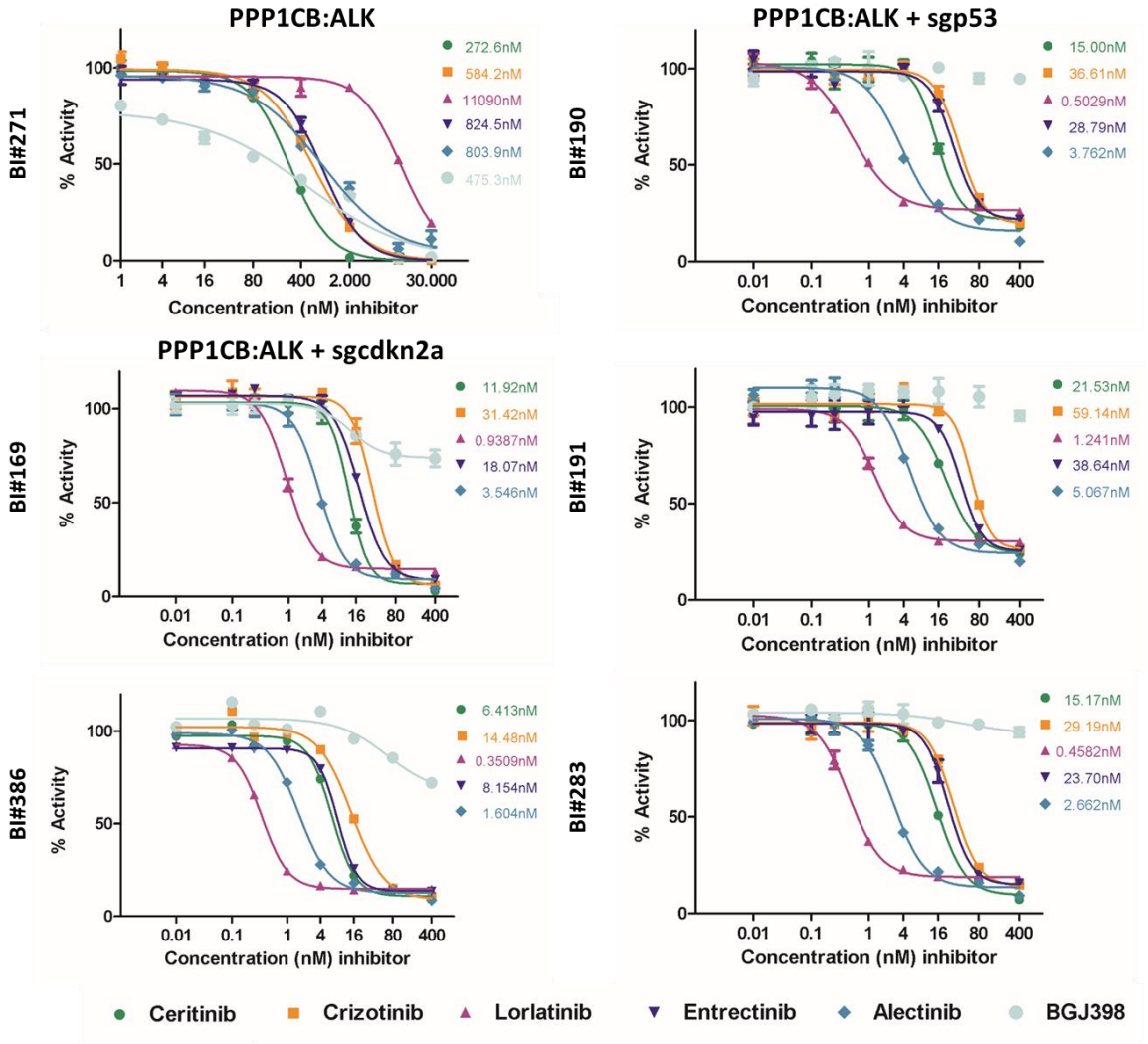

Figure 20. IC50 curves of *ALK*-fusion cells treated with first, second and third line inhibitors, as well as NTRK- and FGFR1-specific inhibitors. The concentrations indicated next to the graphs, resemble the IC50 value of that compound on those cells. In all but one primary cell culture (BI#271), lorlatinib performs best with IC50 values between 0.35 and 1.24nM. Cells were treated with the drugs for 72 hours.

Figure 20 shows that the first line inhibitor crizotinib performs worst of all tested ALK inhibitors *in vitro* in the *PPP1CB:ALK*-fused cells with either of the CRISPR gRNAs against cdkn2a and p53 (BI#169, BI#190, BI#191, BI#283, BI#386). Cells show a better response

to second line ALK inhibitors ceritinib and alectinib, as well as the combined NTRK and ALK inhibitor entrectinib, all developed later than crizotinib and therefore showing more specific targeting. Nevertheless, the latest developed inhibitor, lorlatinib, performs best in terms of the dose response with low IC50 values ranging from 0.35-1.24nM. These values correspond to achievable concentrations that can be administered in patients in the clinic[206]. The FGFR1 inhibitor, BGJ398 (infigratinib) is ineffective against *ALK*-positive cells, showing the specificity of the ALK inhibitors against cells harbouring this aberration. It also becomes clear that for essentially none of the tumour cell cultures do any of the drugs give a 100% viability drop in response to treatment. This may be due either to a small proportion of the cells being resistant to treatment, which are therefore still metabolically active (which the CellTiter-Glo assay is detecting), or it could indicate that a proportion of the cells respond rather with a stop of proliferation (cytostatic) than by undergoing cell death (cytotoxic). This response however might shift upon s shorter or longer exposure time, which will need to be tested.

Looking at Figure 20, it also becomes clear that the drug response curves of the primary cell culture from the tumour of just the *PPP1CB:ALK* fusion (BI#271) all show (nearly) 100% response at the 2mM or 30µM concentration. Lorlatinib, however, does not seem to have an effect on these tumour cells with a high mean IC50 value of 11nM from the two replicates. This shows that the ALK inhibitors are potent to ALK-positive cells in combination with a tumour suppressor knock-out.

After having determined the mean IC50 values of the three different primary tumour cell culture combinations, further tests were conducted to investigate what the ALK inhibitors are actually doing to the cells to explain the decreased viability of tumour cells being treated and the IC50 curves not reaching 0% in the majority of primary cell cultures in Figure 20.

The mean of the IC50 values from the duplicates of the experiment were calculated and used as the basis for the drug concentrations for the flow cytometric and Western blot analysis. Table 4 indicates the IC50 values used for lorlatinib and crizotinib. The DMSO control concentrations are based on the lorlatinib concentrations. All lorlatinib

concentrations are below 1.4nM (mean 0.76nM), which none of the other inhibitors come close to. The second best ALK inhibitor is alectinib with a mean IC50 of 3.3nM.

Table 4. Mean IC50 concentrations of lorlatinib and crizotinib as assessed by CellTiter-Glo analysis used for the drug treatment of cells for Western blot, Immunofluorescence and Annexin V staining, and cell cycle analysis.

Primary cells	Lorlatinib concentration	Crizotinib concentration
BI#169	0.9nM	28nM
BI#190	0.6nM	32nM
BI#191	1.3nM	66nM
BI#283	0.5nM	48nM
BI#386	0.5nM	24nM

3.2.2 ALK inhibitors effectively diminish pALK signal *in vitro*

Using the IC50 concentrations calculated in Table 4, BI#169 and BI#283 cells (harbouring PPP1CB:ALK with sgcdkn2a or sgp53, respectively) were treated with either normal GF medium as a negative control, DMSO, crizotinib or lorlatinib to evaluate the abilities of the ALK inhibitors to decrease excessive downstream signalling via the ALK receptor (indicated by receptor phosphorylation).

Six-hour treatment of BI#169 and BI#283 with 28/48nM crizotinib and 0.9/0.5nM lorlatinib decreased the p-ALK signal and thus likely also downstream signalling. There is no difference seen in total ALK protein. Figure 21 shows that the apoptosis pathway is activated upon ALK inhibitor treatment by increased cleaved Caspase 3 signal compared to the non-treated and DMSO controls. High centrifugation of the treated cells was used in order to also pellet dead cells, which can then be detected on the Western blot.

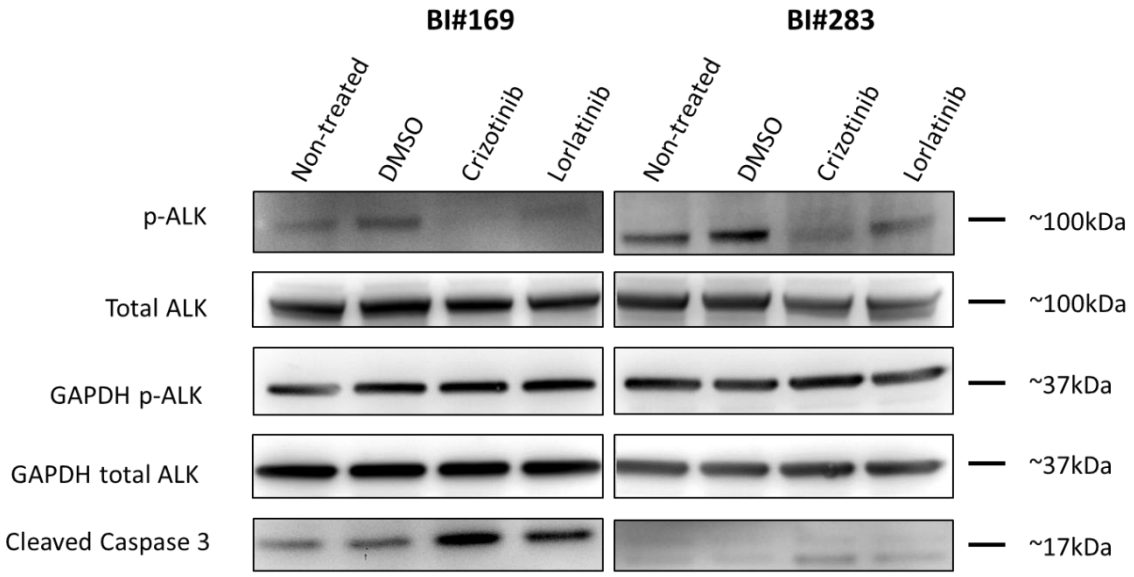

Figure 21. Western blot of BI#169 and BI#283 treated cells *in vitro* stained against p-ALK, total ALK and cleaved Caspase 3. Upon ALK inhibitor treatment, p-ALK reduces in signal strength and cleaved Caspase 3 increases in both primary cell cultures (BI#169 and BI#283). Total ALK signal stays the same. 60µg of protein was loaded. For the detection, ECL prime (for p-ALK and cleaved Caspase 3) or ECL (for total ALK and GAPDH) detection reagents were used. The membranes were developed for 30 seconds each.

3.2.3 ALK inhibitors lead to DNA fragmentation

Knowing that tumour cells show a decreased viability after ALK inhibitor treatment, it was of interest to see how this links to the stage of the cell cycle the treated and control cells are in. For that, flow cytometric analysis was performed using propidium iodide (PI) as a staining agent on tumour cells treated with crizotinib and lorlatinib at the calculated mean IC50 concentrations. PI is a stoichiometric dye, meaning it will bind to the proportion of DNA present in a cell. That way the cell cycle stages can be differentiated based on the premise that cells in G1 have half the amount of DNA than cells in G2, whereas cells currently in S-phase show an intermediate DNA amount. Cells residing in the sub G1 stage were also expected, because the CellTiter-Glo analysis revealed dying/dead cells after inhibitor treatment. The Sub G1 stage shows DNA fragmentation, a sign of apoptosis or necrosis. The number of cells in this stage increased upon treatment with crizotinib and lorlatinib, with more crizotinib-treated cells showing DNA fragmentation compared with lorlatinib-treated cells (Figure 22).

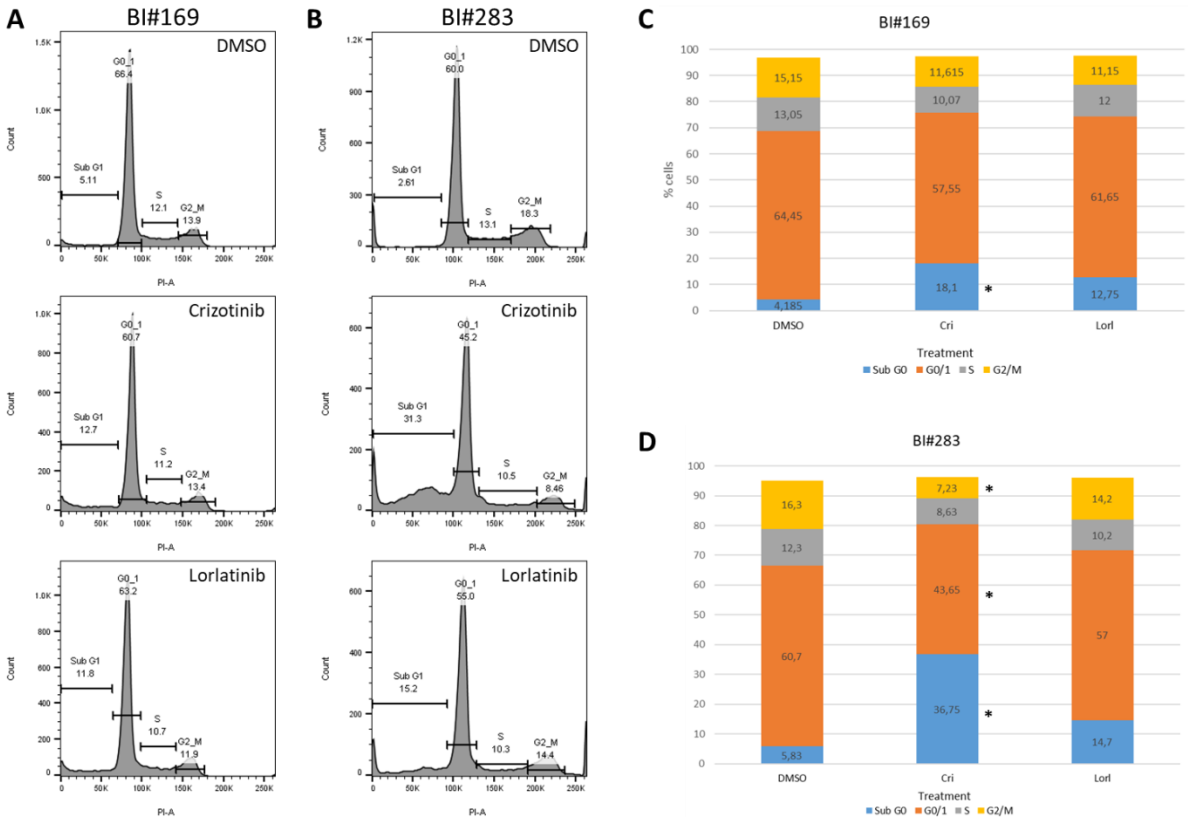

Figure 22. Cell cycle analysis of treated tumour cells *in vitro*. A. Representative flow cytometric cell cycle graph of BI#169 cells treated with DMSO, crizotinib and lorlatinib. B. Representative flow cytometric cell cycle graph of BI#283 cells treated with DMSO, crizotinib and lorlatinib. Drug treatment increases the fraction of cells in the Sub G1 phase, and decreases cells residing in G0/1 and G2/M. C. Graphical representation of the cell cycle stages in BI#169 cells based on the mean of the duplicated experiment. D. Graphical representation of the cell cycle stages in BI#283 cells based on the mean of the duplicated experiment. The asterisk (*) shows a significant difference of <0.05 between treatment with the ALK inhibitor crizotinib compared to the DMSO control. The numbers indicated within the bars indicate the mean percentage of cells in that phase taken from the duplicated experiment.

BI#283 cells show a smaller proportion of cells in G0/1 phase after treatment compared to BI#169 cells, this might be due to differential effects of the deletion of *p53* in the former cells compared with *cdkn2a* loss in the latter.

3.2.4 ALK-specific inhibitor treatment drives cells into apoptosis and necrosis

Knowing that the inhibitors result in fragmented DNA, it was important to evaluate further what effects crizotinib and lorlatinib have on the ALK-positive tumour cells *in vitro*. Therefore, an apoptosis assay was performed to distinguish between early and late apoptosis, and necrosis. Programmed cell death (apoptosis) is a naturally occurring process in living organisms to remove unwanted cells[207] and can easily be analysed with flow cytometry with the use of fluorochrome-labeled Annexin V. Annexin V is a Ca^{2+}-

dependent phospholipid-binding protein with a high affinity for phosphatidylserine (PS). PS is translocated from the inner side of the plasma membrane to the surface as one of the earlier events of apoptosis. This exposes PS to the external cellular environment ready to be detected by Annexin V[208-210], which is bound to the fluorochrome FITC responsible for the fluorescence signal detected on the flow cytometer.

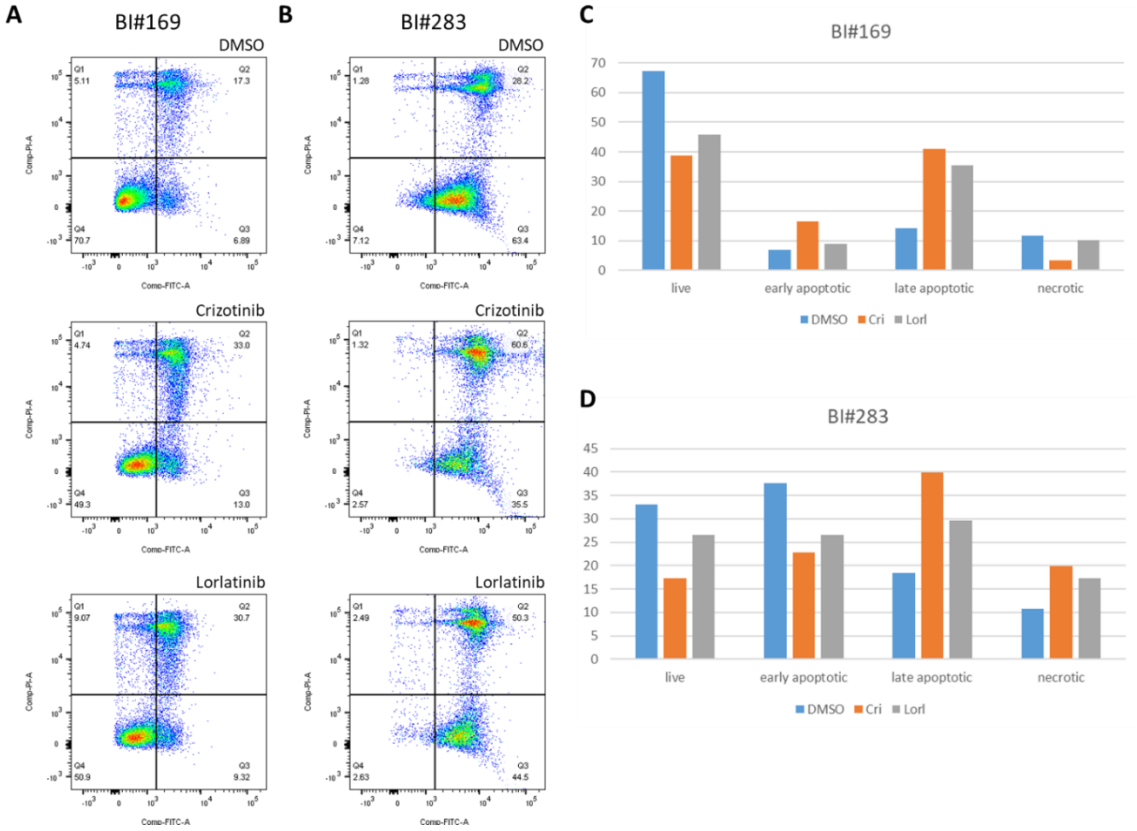

Figure 23. Flow cytometric Annexin V assay. A. FACS plot of BI#169 (*PPP1CB:ALK* + *sgcdkn2a*) cells treated with DMSO, crizotinib and lorlatinib (from top to bottom). B. FACS plot of BI#283 (*PPP1CB:ALK* + *sgp53*) cells treated with DMSO, crizotinib and lorlatinib (from top to bottom).C. and D. Graphical depiction of A and B. Error bars are not shown, since the experiment was repeated only twice with three pooled samples each.

When looking at Figure 23 above, a difference in live/apoptotic status of the differently treated cells can be seen. The bar charts in Figure 23C and D graphically present what is seen in A and B. The colour code at the bottom shows DMSO bars in blue, crizotinib in orange and lorlatinib in grey.

Upon crizotinib treatment, cells mostly move from the fourth quadrant (live cells) to the third and second quadrant (early apoptotic and late apoptotic cells, respectively).

Crizotinib-treated BI#169 cells reside mostly in early and late apopotosis compared with lorlatinib-treated cells, which are mostly late apoptotic and necrotic. Lorlatinib treatment drives a higher proportion of BI#169 cells into necrosis compared to cells under crizotinib treatment.

BI#283 cells seem to have a higher proportion of cells (for both ALK inhibitors) in the early apoptosis and necrosis stages compared to BI#169 cells, which is most likely due to the missing *p53* tumour suppressor gene. With *p53* being disrupted in BI#283 cells, they likely go into necrosis faster and in greater quantities, with a relative 'bypass' of apoptosis.

These results can give the impression that crizotinib has a stronger and better apoptotic effect on the cells, however one needs to keep in mind that for both drugs, the IC50 values calculated in Table 4 from Figure 20 were used in order to make a mechanistic comparison. Thus, a much lower overall concentration of lorlatinib is able to achieve approximately the same effect as crizotinib. Judging from the IC50 curves, one can predict that lorlatinib will have a stronger effect on the cell cycle and apoptosis than crizotinib if both are applied at the same concentration.

Overall, one can conclude that both ALK inhibitors successfully drive cells into apoptosis, with a portion of cells being necrotic, after 72 hours of treatment.

3.3 Effectiveness of third line ALK inhibitor *in vivo*

After having evaluated lorlatinib's potential *in vitro*, the next logical step was to see if this ALK inhibitor has the same promising effect *in vivo* at reducing tumour growth. Going into the mouse to confirm *in vitro* results is an imporant process in the preclinical pipeline before an inhibitor is allowed to be tested in clinical trials in humans. For drug testing, there are certain aspects which cannot be modeled *in vitro*, which is why *in vivo* tests are a necessity to evaluate factors such as BBB penetrance, pharmacokinetics, drug metabolism and microenvironment. All these aspects need to be considered to assess the activity and toxicity of a compound before testing it in humans.

3.3.1 Lorlatinib successfully decreases tumour growth signal

To test *in vivo* efficacy, BI#190 cells were intracranially injected at $5x10^5$ cells into the striatum of 6-8 week old CD1 female mice. The tumours were allowed to develop for two weeks before animals were stratified into three treatment groups based on their luciferase signal (rank 1, 4, 7 etc. being assigned to lorlatinib, rank 2, 5, 8 etc. to temozolomide, and rank 3, 6, 9 etc. to vehicle control). The animals‘ signal was monitored every week in the IVIS® Lumina and normalized to a photon signal intensity of $4.00x10^5$, which is shown in Figure 24A. It can be clearly seen that the tumour decreases in size for the lorlatinib-treated animals, whereas it keeps increasing for the TMZ- and vehicle control-treated animals over time until their endpoint. No animal in the latter two groups survived longer than 51 days and 37 days after tumour injection and start of treatment, respectively. In contrast, all lorlatinib-treated animals, except for two non-tumour related deaths (hardly any tumour tissue visible histologically), survived the four weeks of treatment with the luciferase signal constantly decreasing. However, after the end of the four-week treatment period these animals started to develop symptoms due to recurring tumour growth (Figure 24A). Nevertheless, macroscopically the tumours from the lorlatinib-treated animals were not as vascularised as tumours from the other two groups when examined after sacrificing.

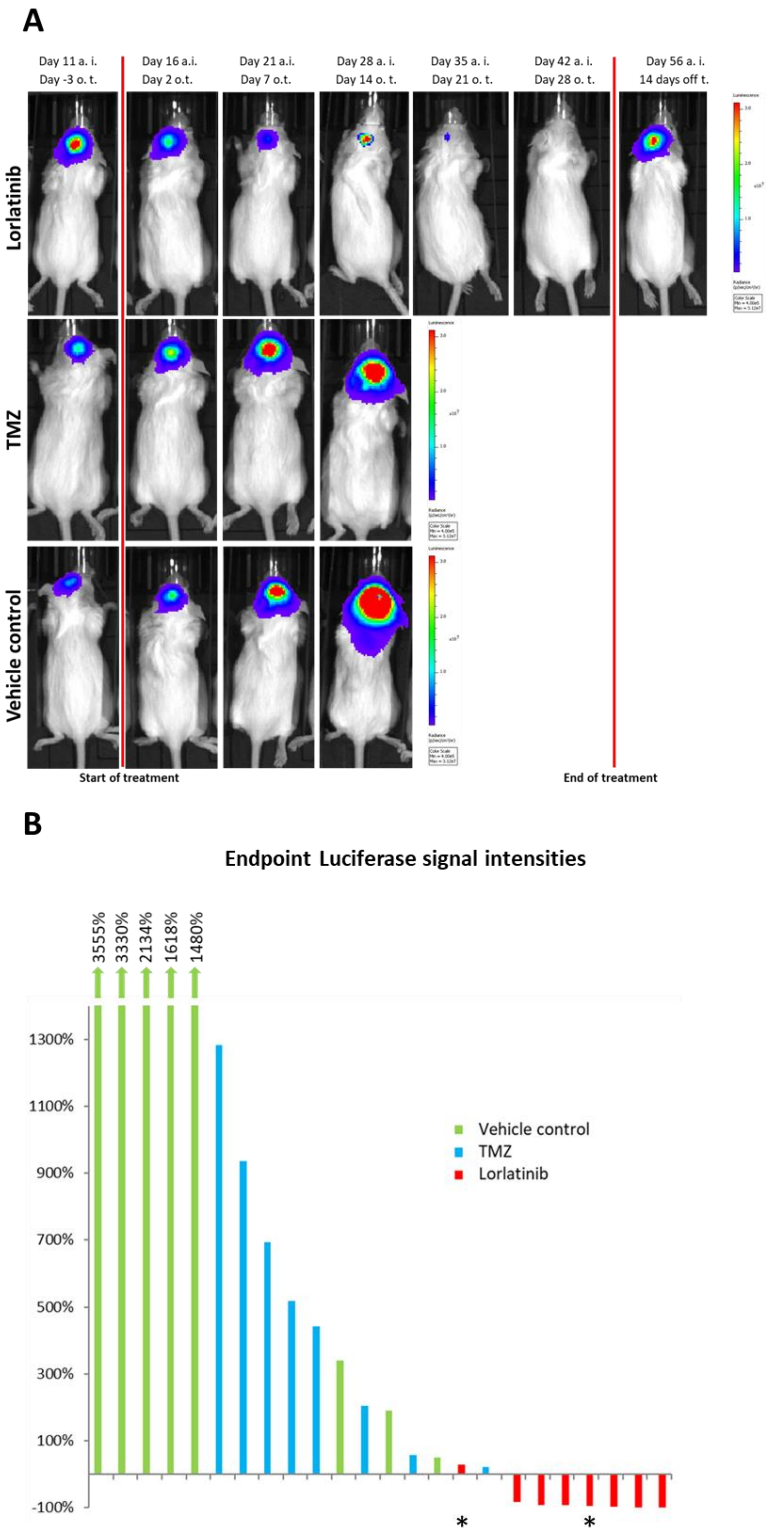

Figure 24. Reduction in tumour mass under Lorlatinib treatment. A. IVIS images of the tumour growth of representative animals under lorlatinib, TMZ and vehicle control treatment normalized to a photon signal intensity of 4.00 x 10^5. a.i. = after injection, o.t = of treatment. B. The percentage growth or reduction of luciferase signal detected in the IVIS Imaging system. The asterisks (*) indicate the two animals which died from a non-tumour related cause.

3.3.2 ALK inhibition *in vivo* significantly prolongs survival

The positive effect on tumour volume of lorlatinib treatment was also mirrored in the survival of the treated mice (Figure 25). The mean survival of the lorlatinib-, TMZ- and vehicle control-treated animals were 49.4 days (range from 19-62 days; mean 57.7 days without the two non-tumour-related deaths), 29.1 days (range from 22-37 days) and 27.9 days (range from 22-37 days), respectively. Lorlatinib treatment therefore significantly increases survival compared to TMZ or vehicle control treatment ($p<0.0001$).

Not only overall survival, but also potential toxicities should be considered in the evaluation of successful treatments *in vivo*. Weight loss is one of the negative side effects of treatment (others include gastrointestinal problems or lethargy) and should therefore be avoided if possible. The good response to lorlatinib treatment was not accompanied by any such negative side effects. The weight change of all mice in the three different treatment groups is illustrated in in Figure 25B. The mean weight of the three treatment groups is not significantly different. In addition, the lorlatinib-treated group also did not show any other adverse side effects when being treated, which is a positive sign for translation of this compound into the clinic.

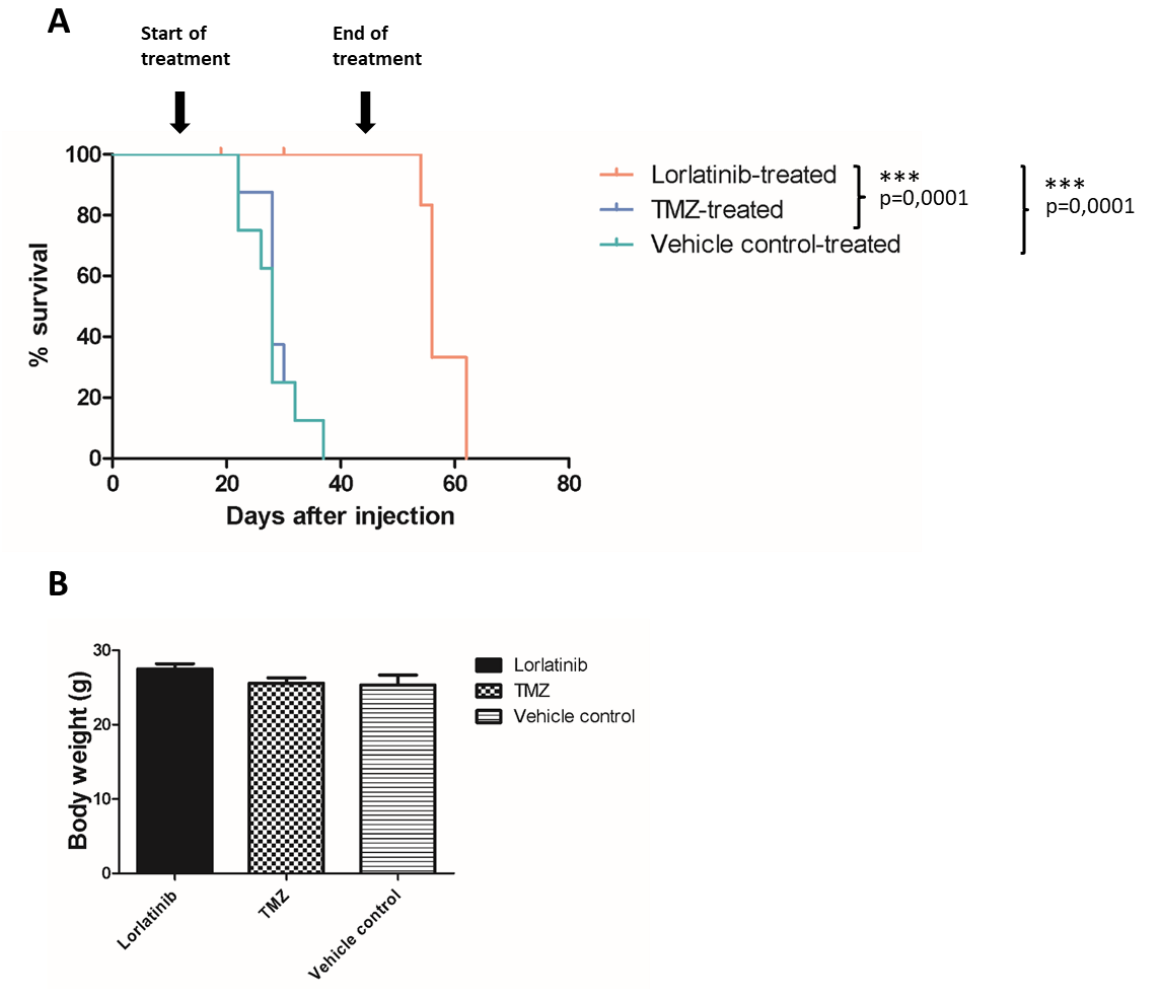

Figure 25. Kaplan-Meier survival curve of CD1 tumour-bearing mice on treatment of either the ALK inhibitor Lorlatinib, it's vehicle control and the standard-of-care in the clinic, Temozolomide and the mean body weight whilst under treatment. A. Kaplan-Meier survival curve with indications of start and end of treatment at 14 days post intracranial injection for four weeks. Lorlatinib treatment significantly increased the survival of *PPP1CB:ALK* tumour bearing mice. The significance test of choice was the Log-rank (Mantel-Cox) test with p-values of 0.0001 for lorlatinib vs. TMZ survival and lorlatinib vs. vehicle control survival. B. Mean body weight with s.d. bars shown for the three treatment groups, which all lie within the normal body weight for wild-type CD1 mice.

3.3.3 Lorlatinib effectively diminishes pALK signal and reduces proliferation *in vivo*

To test the dephosphorylation properties of lorlatinib on the ALK-positive tumour cells as well as seeing if it is efficient at reducing cell proliferation, it was planned to investigate tumours from lorlatinib- and vehicle control-treated animals using Western blot and IHC stain against Ki67, respectively. Keeping in mind that lorlatinib is supposed to block the ATP site of the ALK receptor, a reduction in phosphorylation was expected in these samples compared to the vehicle control brains similar to the *in vitro* results shown in Figure 21. However, the tumours had reduced drastically in size after three

days of treatment (Figure 26), which made it not possible to extract any tumour tissue for protein extraction and subsequent Western blot against p-ALK. When repeating this experiment, the drug concentrations should be measured in the animals' brains and compare to the drug plasma levels

Nevertheless, I would like to hypothesise what was expected from this *in vivo* Western blot. With similar total ALK signals, p-ALK signal would only have been detectable from the vehicle control-treated brains with lorlatinib-treated brains showing a significant decrease in such signal, similar to the *in vitro* results. Cleaved Caspase 3 would only have been detected in the vehicle control brains showing activation of Caspase 3 and therewith marking the apoptotic process. A possible explanation why lorlatinib-treated brains show no Caspase activation although *in vitro* results have shown that tumour cells enter apoptosis upon ALK inhibitor treatment might be the size of the tumour. The tumours had reduced drastically in size after three days of treatment (Figure 26) so that the dead cell clearance from within the tumour was more effective due to better penetration and shorter distance from within the tumour to the outside. It is more difficult to drain apoptotic or dead cells from the tumour mass when the tumour is more compact and bigger in size. The reason for dead cells being detected in *in vitro* samples is due to high centrifugation of the harvested treated cells in this artificial setting compared to *in vivo* where the microenvironment also plays a major role.

Ki67 is a proliferation marker commonly used to detect dividing cells, therefore a decrease in Ki67 staining in the lorlatinib-treated brain is expected due to the compound blocking tumour growth.

Figure 26 shows the H&E stainings of three brains each from the lorlatinib and vehicle control group, where the animals were only treated for three days and then sacrificed one hour after the last dose. The H&E stainings already show the drastic effect lorlatinib has on the tumour even after such a short period of time. In two of these tumours, one cannot even see tumour tissue anymore and the tumour that is still visible in the third animal is very small. The tumours from the control animals are bigger and show a stronger H&E staining. The same applies to the Ki67 staining. The Ki67 staining for the

vehicle control-treated animals is much stronger than for BI#336 (lorlatinib-treated). For two of the ALK inhibitor treated animals, no Ki67 staining was possible, because there is no tumour visible anymore in the H&E staining. From this, one can conclude that lorlatinib acts extremely rapidly to decrease the proliferation of the tumour cells and induce cell death, which makes the lorlatinib-treated tumours smaller than the vehicle control-treated ones already after three days of treatment twice daily.

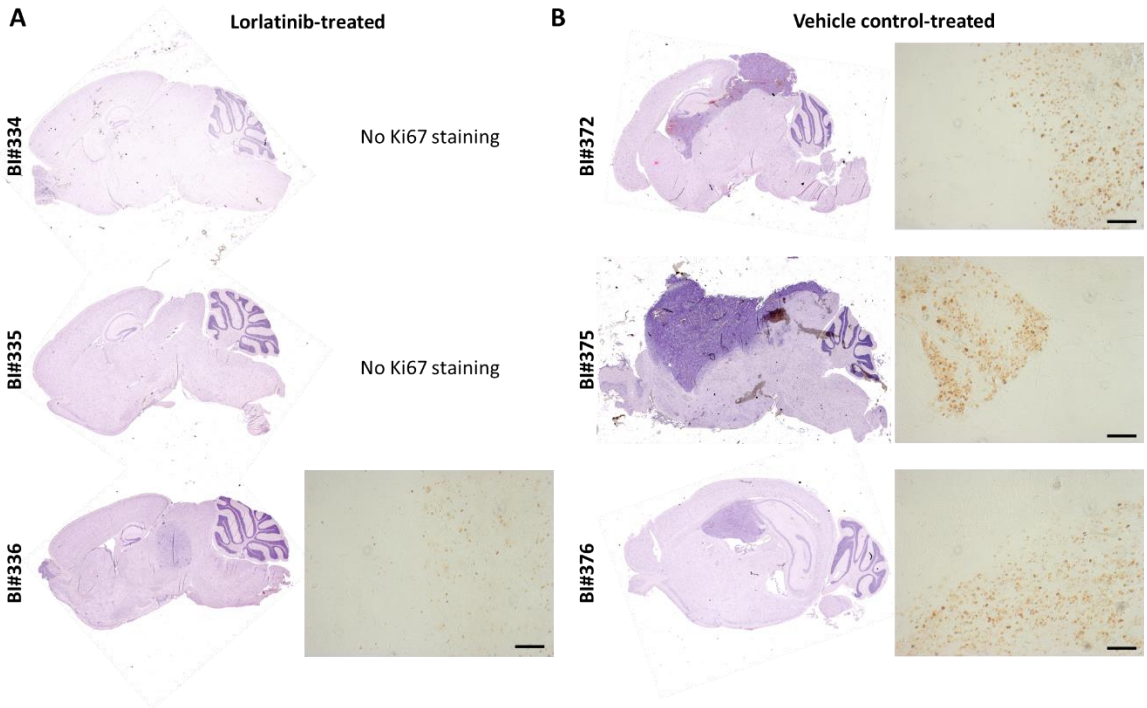

Figure 26. H&E staining and IHC staining against Ki67 of three exemplary lorlatinib- and vehicle control-treated animals. A. H&E and close-up IHC images against Ki67 of lorlatinib-treated animals. B. H&E and close-up IHC images against Ki67 of vehicle control-treated animals. The tumours seen in B are bigger and stain much more strongly for the proliferation marker Ki67 compared with lorlatinib-treated animals in A. Scale bar: 200µm.

3.4 Further applications of the mouse model development pipeline

Another recurring event that came to our attention through tumour profiling programs such as the INFORM and ICGC PedBrain projects was the fusion of *NTRK*-family oncogenes (*NTRK1/2/3*) through chromosomal translocation. These gene fusions were found in different biological entities, including pilocytic astrocytoma, infant hemispheric gliomas (with a typical age at diagnosis under 24 months) and a group of adult IDH wildtype tumours termed ‘anaplastic neuroepithelial tumour with condensed nuclei’

(ANTCN). To date, the original histological and radiological diagnoses of the latter two groups of patients is highly varied, since they have not been formally recognised as distinct subgroups. This therefore has an impact on treatment planning, with some patients receiving a low-grade glioma or even embryonal tumour therapy, and those diagnosed as HGG receiving TMZ chemotherapy and (for older patients) radiotherapy. There is no clear NTRK-targeted standard of care treatment available yet, and in many cases this alteration would not be tested for because of a lack of appreciation that this defines a biologically distinct entity, which at least in the case of the adult tumours seems to hold true (Ismer *et al.*, *in preparation*). *NTRK* fusion was therefore considered as a good candidate to further support our statement about *in utero* electroporation being a good method for somatic gene transfer for tumour model development. A *QKI:NTRK2* fusion gene (first identified in a PA) was injected and electroporated *in utero* into pregnant CD1 mice at E14.5. Figure 27 below shows that also with this candidate gene, tumours develop almost exclusively when in combination with a guide RNA against *cdkn2a* or *p53*. No tumours developed from just the fusion alone indicating that a second hit of a knock-out of a tumour suppressor gene is needed for oncogenic transformation. Indeed, around half of the human patients with a putative ANTCN tumour also showed deletion of *cdkn2a/b*

Finally, two hotspot *FGFR1* mutations at positions 546 and 656 also gave tumours, through p0 injection or *in utero* electroporation, respectively (Figure 27). These alterations are found in paediatric LGGs including PA and, more frequently, dysembryoplastic neuroepithelial tumour (DNET), and also represent a promising drug target. On the other hand, another promising gene fusion found mostly in paediatric LGGs was *MYB:QKI*, which when electroporated alone or in combination with *sgcdkn2a* did not develop a single tumour after one year on observation.

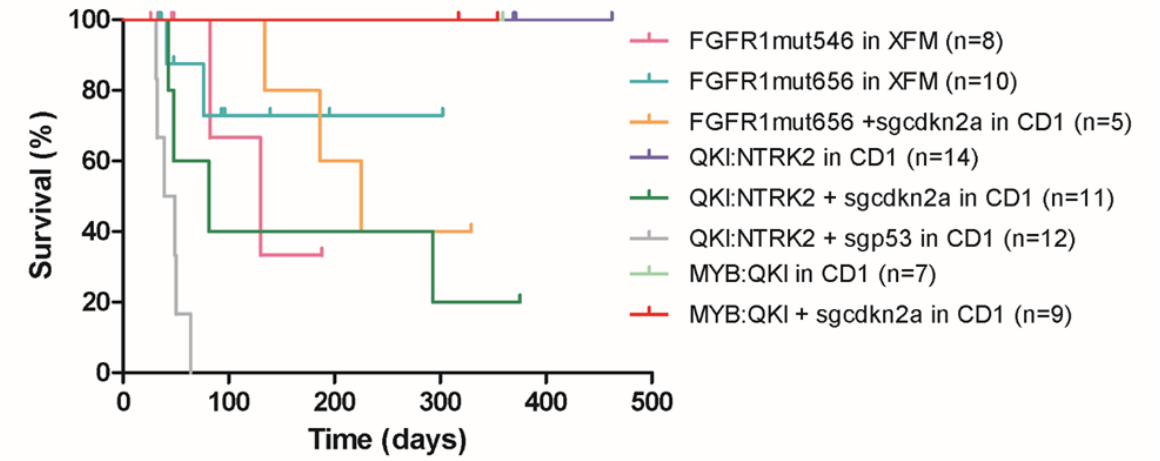

Figure 27. Kaplan-Meier survival curve of other candidate genes p0 injected or *in utero* electroporated. No tumours developed in CD1 mice electroporated with the *MYB:QKI* fusion (alone or in combination with *sgcdkn2a*) or the *QKI:NTRK2* fusion alone. However, when combining the latter fusion with *sgp53* or *sgcdkn2a*, the mice develop tumours at 43 days and 75 days on average. The *FGFR1* mutation at amino acid 546 can most likely be modelled using the RCAS/T-va system at p0, whereas the FGFR1 mutation at amino acid 656 more efficiently gave tumours when delivered via *in utero* electroporation.

The mean latency of *QKI:NTRK2* tumours in combination with *sgcdkn2a* and *sgp53* are 75 (50 days without the latest outlier at 293 days; n=9/10) and 43 (n=12) days, respectively. These time points are only a few days higher than the ones for the *PPP1CB:ALK* fusion. In both cases, however, the fusion in combination with *sgp53* gives the lowest latency, suggesting that this may have the highest tumourigenic potential when used in combination as a second hit. No tumours developed from just the *QKI:NTRK2* fusion from *in utero* electroporation.

The histological stainings of the *QKI:NTRK2* fused tumours (Figure 28A) also here clearly show that the tumour seen in the H&E staining matches the positive signal of the HA-tag in the IHC staining, meaning that the tumour arose from the somatic gene transfer of the *in utero* electroporation. Figure 28B shows that the cells taken into culture from these mice brains, express the *QKI:NTRK2* fusion by staining against the HA-tag on Western blot, further supporting the IHC staining results.

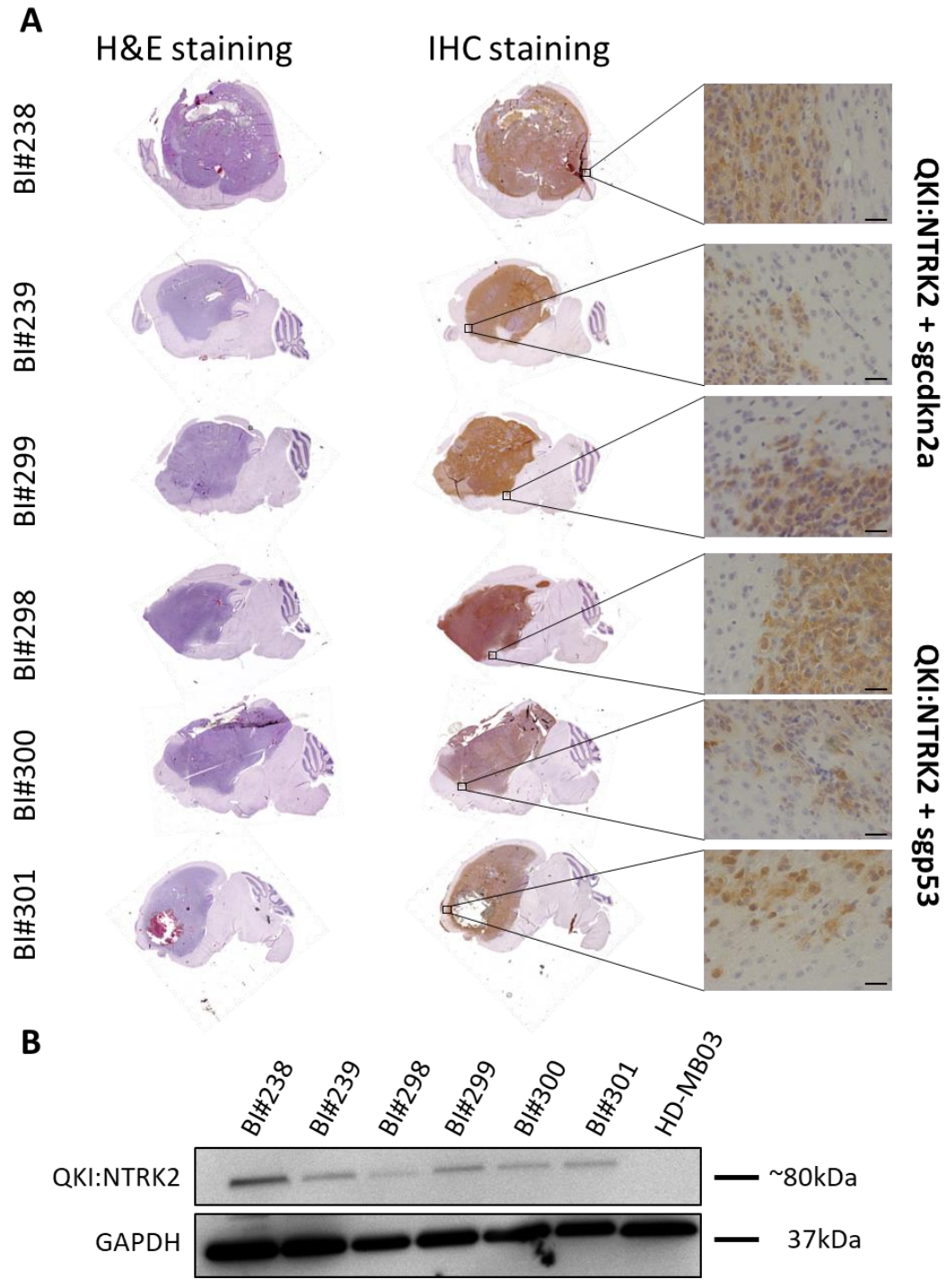

Figure 28. Proof of *QKI:NTRK2* identity by histological stainings and Western blot. A. H&E and the respective IHC staining against HA-tag. The positive IHC stainings clearly correlate with the tumour seen in the H&E staining. The magnified images show a close up of the positive HA-tag staining with the scale bar of 100µm. B. The tumour cells taken into culture from the other hemisphere of these brains were evaluated and stained for HA-tag. All derived tumour cell cultures express the HA-tag and therefore the *QKI:NTRK2* fusion protein.

4. Discussion

A key aspect in translational oncology is the identification of novel tumour-driving gene alterations in patients followed by the generation of representative mouse models in order to test specific, more tailored therapies on them. This is exactly the pipeline that was described in this work using *in utero* electroporation as the delivery method of different somatic gene alterations to generate a variety of mouse models of relevance to paediatric gliomas. The necessity of mouse models has long been recognised, because *in vitro* systems lack the tumour complexity normally found *in vivo* and do not recapitulate the tumour microenvironment[211].

The electroporation method used here overcomes hurdles of some other murine model systems in cancer biology. For example, generating GEMMs is a lengthy process, which cannot keep up with the speed of new alterations being identified in tumour-sequencing projects. PDX models on the other hand always depend on fresh human tumour tissue being available (which is sadly still not collected as standard in most centres, and is always subject to competing demands from diagnosticians and researchers); they lack some levels of tumour complexity that needs to be accounted for in drug tests, e.g. tumour microenvironment, and many tumour types will not grow as a PDX[187,212-214]. *In utero* electroporation allows for somatic overexpression as well as gene knock-outs to be modelled at the same time within a very short time frame. It was shown that the timing of the manipulation of the developing mouse brain is critical and the outcome varies drastically between two different paediatric time points. The mouse models described here nicely recapitulate the human counterpart histologically and molecularly. The cloning of such constructs can be performed in a reasonably timeframe, and tumour development driven by the *PPP1CB:ALK* or *QKI:NTRK2* fusions had a reasonably short latency, which means that preclinical results can be generated quickly and translated into the clinic. The results obtained above will be systematically evaluated and discussed below.

4.1 Efficiency of *in utero* electroporation

One point for discussion is clearly the efficiency of the *in utero* electroporation- only 15% of all electroporated pups were found to carry the transgene from which tumours arise. When initially trying the surgery at E13.5 like other groups have published[215,216], the observed efficiency was even lower. Multiple adjustments were then made to the surgery technique, post-surgical care, needle preparation and other parameters in order to try to improve this. As such, the 15% efficiency rate represents an improvement on previous attempts with this approach, and can be accepted as a method to be further used for the development of paediatric brain tumour-relevant mouse models. Allografting of derived tumour cells, as for the *in vivo* preclinical testing presented here, was more efficient for tumour development due to syngeneity of isolated and cultures tumour cells and can therefore help to reduce the total number of animals required. As seen in the comparison of the *in utero* electroporation and RCAS-p0 injection method, the time of gene manipulation in the embryonic/neonatal mouse brain is crucial, and the former method seems to better recapitulate the time point of development in humans for certain genetic alterations. Given the challenges of manipulation at this age, the success rate is always likely to be somewhat reduced. Given the value of these models for their preclinical utility in a devastating childhood disease, it is felt that the harm/benefit ratio can be accepted here.

4.2 Murine vs. Human *PPP1CB:ALK* tumours

The tumours developed from *in utero* electroporated animals recapitulate the human situation, where both develop in a paediatric setting where it is very unlikely that environmental factors could have played a major role. Interestingly, *ALK*-positive NSCLC is associated with patients of younger age with a non-smoking history and no *EGFR* mutations[126,127], suggesting that this is another setting in which *ALK* fusion can serve as a strong oncogenic inducer with relatively few co-mutations. Knowing that the tumour-inducing genetic aberrations happen early in development (*ALK* fusion-positive patients are typically less than 2 years old) without any external influences, two different methods for the mouse model generation were initially tested. This showed how important the time of gene manipulation is when attempting to model paediatric

tumours. *PPP1CB:ALK*-positive tumours developed within a few weeks after *in utero* electroporation at E14.5, whereas mice from the p0 injection - injected only seven days later - did not develop tumours. The reason why the p0 injected animals did not develop any *ALK*-positive tumours is most likely due to the absence of the correct cell population at this stage of development. Whilst it could be the case that Nestin+ cells (the driver of the tva receptor) are not the right population to be targeted by *ALK* fusions, this system generally covers multiple stem and precursor lineages, and has been previously used successfully for brain tumour development. Thus, it is thought more likely that by p0 there is no longer a sufficient population of the right target cells, which are susceptible to oncogenic transformation. The cells of origin of paediatric tumours are difficult to define due to the highly dynamic environment during early development[203,217-219]. Therefore, it is difficult to predict in advance precisely the right target population – further rationale for taking a multi-pronged approach similar to that used here. It is not believed that a simple lack of oncogenic potential of the *PPP1CB:ALK* fusion could be the reason for the lack of RCAS tumours, given the success of the EP model and the well-established driving role of ALK in several other tumour types[220-226].

Although the murine tumours histologically recapitulate the human tumours well, one needs to keep in mind that all of the post-characterisation was done on *ALK* fusion tumour cells with a second hit of either *cdkn2a* or *p53*, of which neither are normally found in the clinical situation. For a preclinical model, a mean latency of 137 days (as seen with the *ALK* fusion alone) is too long when one has the opportunity to use a faster mouse model, which also recapitulates the human tumour in terms of histological morphology. However, it was of interest to assess how oncogenic the BI#271 cells, i.e. *ALK* fusion cells without a second hit, are when allografted into CD1 mice and compare that to the allografted BI#190 cells used for the inhibitor testing. For that, BI#271 cells were reinjected into five CD1 mice (Figure 29), which were monitored for tumour-related symptoms. Four of the five allografted mice developed a tumour, giving these cells a penetrance of 80%. The fifth mouse was sacrificed 79 days after tumour cell injection, because of the lack of luciferase signal throughout the experiment.

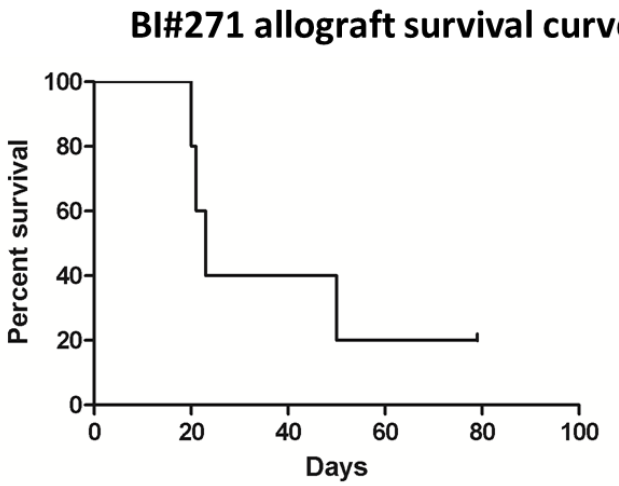

Figure 29. Kaplan-Meier survival curve of BI#271 allografted CD1 mice. The mean latency of the four mice that developed a tumour was 28.5 days. The fifth mouse was sacrificed after 79 days due to lack of luminescence signal being detected, meaning that the tumour cells did not engraft.

The mean survival of the four tumour-bearing mice injected with *ALK* fusion-only cells was 28.5 days and shows that even without a knock-out of *cdkn2a* or *p53,* these cells are oncogenic enough to form tumours again. Therefore, the next step to make this model recapitulate the human situation more closely, would be to repeat the inhibitor testing on BI#271-injected mice to see if the positive effect on survival of lorlatinib-treated animals can be replicated in these mice. This would make the preclinical pipeline in general more representative. These results also give further support to the strategy of using allografts of initially generated tumours for further expansion, both to increase efficiency of tumour development over *in utero* EP alone and to reduce latency.

Another interesting point that should be tested is a potential resistance mechanism of tumour cells against lorlatinib. It was shown that NSCLC cells developed resistance against the first line ALK inhibitor crizotinib, leading to the development of alectinib and ceritinib targeting the mutations that arose from crizotinib treatment. Testing for a resistance mechanism caused by lorlatinib could be done in various ways. For example, the *in vivo* testing with lorlatinib could be repeated to the point where the tumours start to grow back after initial stop of treatment. After that, the mice could be treated with lorlatinib again to see if the initial response on treatment can be recapitulated a second time. If this is the case, it would reassure that a 'drug holiday' alone would be unlikely to induce lorlatinib resistance in *ALK* positive cells. Subsequently, the initial treatment

could be extended until the tumours recur while still under therapy, at which point they could be molecularly profiled to look for possible secondary hits accounting for the resistance. No signs of resistance were observed during the (admittedly relatively short) period of drug administration used here.

4.3 Differences in drug responses to ALK inhibitors *in vitro*

Another aspect to be considered is the different drug response *in vitro* of BI#271 cells compared to the other primary tumour cell cultures. This is another reason for doing the *in vivo* test of reinjected BI#271 cells into CD1 mice to see if the lorlatinib treatment shows a similar significant benefit in survival. This would be much faster with BI#271 reinjected tumour cells because of the decreased latency of 28.5 days (Figure 29). As seen in Figure 20, the continuous development of specific small molecule inhibitors is crucial. The third line ALK inhibitor, lorlatinib, shows the best results in terms of lowest concentration at which 50% of tumour cells die (IC50), whereas the first line ALK inhibitor, crizotinib, the worst. The tumour cells also respond better to alectinib, a second line ALK inhibitor, developed after *ALK*-positive tumours showed resistance to crizotionib, than to crizotinib. This shows that continuous work needs to be conducted on possible resistance mechanisms and on further exploring more potent compounds, even after one drug in a given class has already been approved for clinical use. Indeed, the generations of ALK inhibitors are a good example of this, whereby NSCLC patients being treated with crizotinib developed resistance which could be overcome by subsequent compounds[123,227,228].

4.4 Drug's mechanism of action

Before discussing the results of the *in vivo* study of lorlatinib compared to its vehicle control and the standard of care temozolomide, the underlying mechanism of ALK inhibitors needs to be evaluated to understand what the drug is doing to the tumour cells.

The cell cycle analysis in Figure 22 shows that *ALK* fusion cells upon treatment with crizotinib or lorlatinib show fragmented DNA, meaning they have either gone into apoptosis or necrosis upon treatment. BI#283 cells show a smaller proportion of cells in

G0/1 phase after treatment compared to BI#169 cells. This might be due to the deletion of *p53* in the former cells. P53 for example governs the G1/S phase checkpoint through induction of the Cdk inhibitor p21[229] and when *p53* is missing, gives the cells less time to repair DNA, i.e. less time in the G1 phase of the cell cycle[230,231]. Lukin *et al*.[232] have shown that p53 wild type cells go into reversible cell cycle arrest upon chemosensitisation to promote cell survival, possibly explaining the higher number of BI#169 cells in the G0/1 phase upon treatment. A significant difference in the number of cells spent in each cell cycle stage was only detected in crizotinib-treated cells and not lorlatinib-treated cells. This is most likely due to the difference in IC50 concentrations with IC50 values of crizotinib being 31-fold and 96-fold higher than IC50 values of lorlatinib in BI#169 and BI#283 cells, respectively. Thus, a much lower overall concentration of lorlatinib is able to achieve approximately the same effect as crizotinib. Judging from the IC50 curves, one can predict that lorlatinib will have a stronger effect on the cell cycle and apoptosis than crizotinib if both are applied at the same concentration.

The Annexin V staining that followed was conducted to evaluate in which stage of cell death these tumour cells are after treatment. The results revealed that a higher percentage of cells after three days of lorlatinib treatment are in necrosis, which is described as an "irreversible disturbance of cellular homeostatic mechanisms"[207]. As necrosis is only a state describing the presence of dead tissue[233-235], one can only assume which cell death pathway these cells underwent to become necrotic. For that, the flow cytometric analysis would need to be repeated in a time course experiment to safely say that cells went into apoptosis first and then ended up in apoptotic necrosis[236]. Another necessary experiment to confirm this hypothesis is to use a different IF staining protocol and stain the treated cells without washing away potentially apoptotic or necrotic cells and look at their morphology and/or stain for necrotic and apoptotic factors. Understanding the potential underlying mechanism of action of both tested ALK inhibitors, the results obtained from the *in vivo* drug treatment should be discussed.

4.5 Significant survival advantage of lorlatinib-treated animals and lack of efficacy of TMZ

Another somewhat surprising observation made from this experiment is the similarity in survival and tumour growth rate of the TMZ-treated animals compared to the vehicle control animals (Figure 24 and Figure 25). While lorlatinib shows significant tumour regression *in vivo* and increases survival, TMZ shows almost the same results as the vehicle control, although it is used as standard of care in the clinic for different gliomas[237-241]. TMZ is used in the clinic as a standard of care for patients with high-grade glioma at the moment, because no ALK inhibitor is approved in paediatrics yet and *ALK* has not yet been formally described as a distinct entity in paediatric brain tumours to suggest ALK inhibitors as a better choice for the 5% of patients carrying an *ALK* fusion. Based on the preclinical results shown here, choosing TMZ for the treatment of *ALK* fusion brain tumours does not seem ideal, because TMZ is neither prolonging survival nor inhibiting tumour growth in any way *in vivo*. In addition, many groups have reported resistance mechanisms against TMZ and recurrence of tumours during or after TMZ treatment[241,242]. It has also been shown by others that TMZ fails to improve the outcome[243] in children with high-grade astrocytomas for example[34], but yet, it is still used in many patients, because no other more specific or effective treatment is available.

It is therefore important to accelerate the clinical trial pipeline of lorlatinib (and other rationally-targeted compounds) in paediatric brain tumour patients to enable them to receive the best possible treatment strategy based on promising results from this study and others.

4.6 Not all candidate genes are suitable for *in vivo* modelling

Whilst multiple driver genes successfully generated tumour models during the course of this study, it should be noted that the methodologies described are not 100% efficient when applied with any gene alteration found in the sequencing of the patient's tumour. There are potential oncogenic driver mutations found in the clinic that do not develop into tumours in the mouse using the somatic gene transfer method of *in utero* electroporation. One example for that is the *MYB:QKI* fusion, which does not lead to

tumour development and growth *in vivo* within one year of surgery either in combination with *sgcdkn2a* (n=9) or alone (n=7). Potential reasons for this could be that the wrong cells are hit, i.e. too early or late in development where the introduction of this oncogenic fusion at E14.5 does not have a strong enough effect on the cells anymore to transform into tumour cells, similar to the *PPP1CB:ALK* fusion at the p0 time point. Another possible explanation could be that the *MYB:QKI* fusion itself is not oncogenic enough to form tumours at the injected concentration, or that other intracellular stimuli are needed in addition to make this fusion oncogenic.

4.7 Future directions for *NTRK2*-fused cells

None of the points mentioned in 4.6 apply to the *QKI:NTRK2* fusion mouse model, which successfully developed tumours with a mean survival of 75 and 43 days in combination with *cdkn2a* and *p53* knock-out, respectively. The next step for this project would be to follow the preclinical pipeline established for the *ALK* fusion tumours, after further characterisations of the tumour to prove that the tumours truly recapitulate their human counterparts as closely as possible. The most promising NTRK inhibitor in development at present, and used in paediatric clinical trials already, is larotrectinib (LOXO-101). Many clinical case reports have shown that this drug, taken once daily orally, can give tremendously positive results with treated tumours often not visible on MRI anymore after a given period. To further enhance the possible benefits of this compound, more supporting preclinical trials are needed to better understand the functional consequences of inhibition; biomarkers of sensitivity or primary resistance, and possible mechanisms of acquired resistance. Additional models will help to achieve this goal, which will hopefully help paediatric HGG patients whose tumour harbours an *NTRK* gene aberration.

4.8 Conclusion

Finally, the work of this thesis touches on the importance of developing better clinical trials for paediatric cancer patients, and with that, the crucial role for analysis of individual tumour tissue on a molecular level. The MNP2.0 study has shown that histological diagnosis can be discrepant to the molecular one in up to 15-20% of cases

due to overlapping and hard to distinguish histological features of the tumours, especially in the interface/overlap between paediatric low-grade gliomas and high-grade gliomas. Such discrepancies can have serious adverse effects for patient management. In general, the approach of treating with non-specific "one-size-fits-all" chemotherapeutics, like TMZ leading to serious side effects and no significant reduction in tumour growth, also needs major rethinking. This development of changing from purely histological to a combination diagnosis of histological and molecular analysis requires more efforts in terms of discovery, education, and access to testing, but several examples have shown that molecular diagnoses have the potential to improve patient management and provide better prognostic value.

Studies like INFORM and MNP2.0 enable us to identify driver mutations on a case by case basis and pick up on novel targets, such as *ALK,* that may not have previously been recognised. The work in this thesis mostly addresses the next step, moving from identifying tumour-causing mutations to developing and pre-clinically treating respective mouse models and translating the findings back to the clinic; potentially advising clinicians on the best treatment strategy for each novel gene aberration. Targeted inhibition in paediatric patients is only just starting to become more widespread, so therefore clinical results as to how progression-free survival changes with these targeted therapies can only be expected in the next few years. Nevertheless, this is why preclinical data is so important to accelerate this process of starting clinical trials and ultimately approving new treatments for children.

With continued efforts to keep molecularly analysing patients' tumours and developing the analytical methods further, we can ensure that the patients will receive the best possible therapy based on their personally identified mutational burden. The above described pipeline allows for faithful recapitulation of key driver events (i.e. recurrent gene alterations in a number of patients) in a relatively rapid manner. This is particularly promising for oligo mutated tumours, i.e. paediatric tumours, where the one tumour driving alteration can be targeted, hopefully ensuring that the tumour does not use one of the other pathways affected to evade treatment action. That is different and more difficult in adult tumours due to their tumours heterogeneity and genetic complexity.

4. Discussion

This work will hopefully contribute to a faster bench to bedside workflow of tailored therapy and accelerated approval of new compounds for paediatric low- and high-grade gliomas, thereby assisting in the goals of minimising toxicity for patients and improving progression-free and overall survival.

5. References

1 Alexandrov, L. B. *et al.* Signatures of mutational processes in human cancer. *Nature* **500**, 415-421, doi:10.1038/nature12477 (2013).

2 Davidoff, A. M. Pediatric oncology. *Seminars in pediatric surgery* **19**, 225-233, doi:10.1053/j.sempedsurg.2010.03.007 (2010).

3 Jones, D. T. *et al.* Dissecting the genomic complexity underlying medulloblastoma. *Nature* **488**, 100-105, doi:10.1038/nature11284 (2012).

4 Parsons, D. W. *et al.* The genetic landscape of the childhood cancer medulloblastoma. *Science (New York, N.Y.)* **331**, 435-439, doi:10.1126/science.1198056 (2011).

5 Barrow, J. *et al.* Homozygous loss of ADAM3A revealed by genome-wide analysis of pediatric high-grade glioma and diffuse intrinsic pontine gliomas. *Neuro-oncology* **13**, 212-222, doi:10.1093/neuonc/noq158 (2011).

6 Paugh, B. S. *et al.* Integrated molecular genetic profiling of pediatric high-grade gliomas reveals key differences with the adult disease. *Journal of clinical oncology : official journal of the American Society of Clinical Oncology* **28**, 3061-3068, doi:10.1200/jco.2009.26.7252 (2010).

7 Bax, D. A. *et al.* A distinct spectrum of copy number aberrations in pediatric high-grade gliomas. *Clinical cancer research : an official journal of the American Association for Cancer Research* **16**, 3368-3377, doi:10.1158/1078-0432.ccr-10-0438 (2010).

8 Qu, H. Q. *et al.* Genome-wide profiling using single-nucleotide polymorphism arrays identifies novel chromosomal imbalances in pediatric glioblastomas. *Neuro-oncology* **12**, 153-163, doi:10.1093/neuonc/nop001 (2010).

9 Schiffman, J. D. *et al.* Oncogenic BRAF mutation with CDKN2A inactivation is characteristic of a subset of pediatric malignant astrocytomas. *Cancer research* **70**, 512-519, doi:10.1158/0008-5472.can-09-1851 (2010).

10 Wong, K. K. *et al.* Genome-wide allelic imbalance analysis of pediatric gliomas by single nucleotide polymorphic allele array. *Cancer research* **66**, 11172-11178, doi:10.1158/0008-5472.can-06-2438 (2006).

11 Schwartzentruber, J. *et al.* Driver mutations in histone H3.3 and chromatin remodelling genes in paediatric glioblastoma. *Nature* **482**, 226-231, doi:10.1038/nature10833 (2012).

12 Mueller, S. & Chang, S. Pediatric brain tumors: current treatment strategies and future therapeutic approaches. *Neurotherapeutics : the journal of the American Society for Experimental NeuroTherapeutics* **6**, 570-586, doi:10.1016/j.nurt.2009.04.006 (2009).

13 Ostrom, Q. T. *et al.* Alex's Lemonade Stand Foundation Infant and Childhood Primary Brain and Central Nervous System Tumors Diagnosed in the United States in 2007-2011. *Neuro-oncology* **16 Suppl 10**, x1-x36, doi:10.1093/neuonc/nou327 (2015).

14 Jones, D. T., Gronych, J., Lichter, P., Witt, O. & Pfister, S. M. MAPK pathway activation in pilocytic astrocytoma. *Cellular and molecular life sciences : CMLS* **69**, 1799-1811, doi:10.1007/s00018-011-0898-9 (2012).

15 Sturm, D., Pfister, S. M. & Jones, D. T. W. Pediatric Gliomas: Current Concepts on Diagnosis, Biology, and Clinical Management. *Journal of clinical oncology : official*

journal of the American Society of Clinical Oncology **35**, 2370-2377, doi:10.1200/jco.2017.73.0242 (2017).

16 Ostrom, Q. T. *et al.* CBTRUS Statistical Report: Primary Brain and Central Nervous System Tumors Diagnosed in the United States in 2008-2012. *Neuro-oncology* **17 Suppl 4**, iv1-iv62, doi:10.1093/neuonc/nov189 (2015).

17 Schwartzbaum, J. A., Fisher, J. L., Aldape, K. D. & Wrensch, M. Epidemiology and molecular pathology of glioma. *Nature clinical practice. Neurology* **2**, 494-503; quiz 491 p following 516, doi:10.1038/ncpneuro0289 (2006).

18 Ostrom, Q. T. *et al.* The epidemiology of glioma in adults: a "state of the science" review. *Neuro-oncology* **16**, 896-913, doi:10.1093/neuonc/nou087 (2014).

19 Kleihues, P. *et al.* The WHO classification of tumors of the nervous system. *Journal of neuropathology and experimental neurology* **61**, 215-225; discussion 226-219 (2002).

20 States, C. B. T. R. o. t. U. <http://www.cbtrus.org/index.html>

21 Ertosun, M. G. & Rubin, D. L. Automated Grading of Gliomas using Deep Learning in Digital Pathology Images: A modular approach with ensemble of convolutional neural networks. *AMIA ... Annual Symposium proceedings. AMIA Symposium* **2015**, 1899-1908 (2015).

22 Kleihues, P., Burger, P. C. & Scheithauer, B. W. The new WHO classification of brain tumours. *Brain pathology (Zurich, Switzerland)* **3**, 255-268 (1993).

23 Louis, D. N. *et al.* The 2007 WHO classification of tumours of the central nervous system. *Acta neuropathologica* **114**, 97-109, doi:10.1007/s00401-007-0243-4 (2007).

24 Gilles, F. H. *et al.* Pathologist interobserver variability of histologic features in childhood brain tumors: results from the CCG-945 study. *Pediatric and developmental pathology : the official journal of the Society for Pediatric Pathology and the Paediatric Pathology Society* **11**, 108-117, doi:10.2350/07-06-0303.1 (2008).

25 Jones, C. & Baker, S. J. Unique genetic and epigenetic mechanisms driving paediatric diffuse high-grade glioma. *Nature reviews. Cancer* **14**, doi:10.1038/nrc3811 (2014).

26 Mackay, A. *et al.* Integrated Molecular Meta-Analysis of 1,000 Pediatric High-Grade and Diffuse Intrinsic Pontine Glioma. *Cancer cell* **32**, 520-537.e525, doi:10.1016/j.ccell.2017.08.017 (2017).

27 Kramm, C. M. *et al.* Thalamic high-grade gliomas in children: a distinct clinical subset? *Neuro-oncology* **13**, 680-689, doi:10.1093/neuonc/nor045 (2011).

28 Soffietti, R. *et al.* Guidelines on management of low-grade gliomas: report of an EFNS-EANO Task Force. *European journal of neurology* **17**, 1124-1133, doi:10.1111/j.1468-1331.2010.03151.x (2010).

29 Broniscer, A. *et al.* Clinical and molecular characteristics of malignant transformation of low-grade glioma in children. *Journal of clinical oncology : official journal of the American Society of Clinical Oncology* **25**, 682-689, doi:10.1200/jco.2006.06.8213 (2007).

30 Fangusaro, J. Pediatric high grade glioma: a review and update on tumor clinical characteristics and biology. *Frontiers in oncology* **2**, 105, doi:10.3389/fonc.2012.00105 (2012).

31 Jones, C., Perryman, L. & Hargrave, D. Paediatric and adult malignant glioma: close relatives or distant cousins? *Nature reviews. Clinical oncology* **9**, 400-413, doi:10.1038/nrclinonc.2012.87 (2012).

32 Broniscer, A. & Gajjar, A. Supratentorial high-grade astrocytoma and diffuse brainstem glioma: two challenges for the pediatric oncologist. *The oncologist* **9**, 197-206 (2004).

33 Broniscer, A. Past, present, and future strategies in the treatment of high-grade glioma in children. *Cancer investigation* **24**, 77-81, doi:10.1080/07357900500449702 (2006).

34 Cohen, K. J. *et al.* Temozolomide in the treatment of high-grade gliomas in children: a report from the Children's Oncology Group. *Neuro-oncology* **13**, 317-323, doi:10.1093/neuonc/noq191 (2011).

35 Finlay, J. L. & Zacharoulis, S. The treatment of high grade gliomas and diffuse intrinsic pontine tumors of childhood and adolescence: a historical - and futuristic - perspective. *Journal of neuro-oncology* **75**, 253-266, doi:10.1007/s11060-005-6747-7 (2005).

36 Cancer incidence in five continents. Volume VIII. *IARC scientific publications*, 1-781 (2002).

37 Bondy, M. L. *et al.* Brain tumor epidemiology: consensus from the Brain Tumor Epidemiology Consortium. *Cancer* **113**, 1953-1968, doi:10.1002/cncr.23741 (2008).

38 Ostrom, Q. T. *et al.* CBTRUS Statistical Report: Primary Brain and Other Central Nervous System Tumors Diagnosed in the United States in 2009-2013. *Neuro-oncology* **18**, v1-v75, doi:10.1093/neuonc/now207 (2016).

39 Selt, F. *et al.* Establishment and application of a novel patient-derived KIAA1549:BRAF-driven pediatric pilocytic astrocytoma model for preclinical drug testing. *Oncotarget* **8**, 11460-11479, doi:10.18632/oncotarget.14004 (2017).

40 Pollack, I. F. The role of surgery in pediatric gliomas. *Journal of neuro-oncology* **42**, 271-288 (1999).

41 Freeman, C. R., Farmer, J. P. & Montes, J. Low-grade astrocytomas in children: evolving management strategies. *International journal of radiation oncology, biology, physics* **41**, 979-987 (1998).

42 Blaney SM, K. L., Hunter J, et al. *Tumors of the Central Nervous System*. Vol. 5th 786–864 (Lippincott Williams & Wilkins, 2006).

43 Terashima, K. *et al.* Long-term outcome of centrally located low-grade glioma in children. *Cancer* **119**, 2630-2638, doi:10.1002/cncr.28110 (2013).

44 Nishikawa, R. Pediatric and adult gliomas: how different are they? *Neuro-oncology* **12**, 1203-1204, doi:10.1093/neuonc/noq175 (2010).

45 Cella, M., Knibbe, C., Danhof, M. & Della Pasqua, O. What is the right dose for children? *British journal of clinical pharmacology* **70**, 597-603, doi:10.1111/j.1365-2125.2009.03591.x (2010).

46 Ostrom, Q. T. *et al.* CBTRUS Statistical Report: Primary brain and other central nervous system tumors diagnosed in the United States in 2010-2014. *Neuro-oncology* **19**, v1-v88, doi:10.1093/neuonc/nox158 (2017).

47 Raabe, E., Kieran, M. W. & Cohen, K. J. New strategies in pediatric gliomas: molecular advances in pediatric low-grade gliomas as a model. *Clinical cancer*

research : an official journal of the American Association for Cancer Research **19**, 4553-4558, doi:10.1158/1078-0432.ccr-13-0662 (2013).

48 Sievert, A. J. & Fisher, M. J. Pediatric low-grade gliomas. *Journal of child neurology* **24**, 1397-1408, doi:10.1177/0883073809342005 (2009).

49 Kandil, A. *et al.* Low-grade astrocytoma--a retrospective analysis of 102 patients. *Acta oncologica (Stockholm, Sweden)* **38**, 1051-1056 (1999).

50 Laws, E. R., Jr., Taylor, W. F., Clifton, M. B. & Okazaki, H. Neurosurgical management of low-grade astrocytoma of the cerebral hemispheres. *Journal of neurosurgery* **61**, 665-673, doi:10.3171/jns.1984.61.4.0665 (1984).

51 North, C. A., North, R. B., Epstein, J. A., Piantadosi, S. & Wharam, M. D. Low-grade cerebral astrocytomas. Survival and quality of life after radiation therapy. *Cancer* **66**, 6-14 (1990).

52 Lote, K. *et al.* Survival, prognostic factors, and therapeutic efficacy in low-grade glioma: a retrospective study in 379 patients. *Journal of clinical oncology : official journal of the American Society of Clinical Oncology* **15**, 3129-3140, doi:10.1200/jco.1997.15.9.3129 (1997).

53 Aibaidula, A. *et al.* Adult IDH wild-type lower-grade gliomas should be further stratified. *Neuro-oncology* **19**, 1327-1337, doi:10.1093/neuonc/nox078 (2017).

54 Sun, H. *et al.* Prognostic significance of IDH mutation in adult low-grade gliomas: a meta-analysis. *Journal of neuro-oncology* **113**, 277-284, doi:10.1007/s11060-013-1107-5 (2013).

55 Sepulveda-Sanchez, J. M. *et al.* SEOM clinical guideline of diagnosis and management of low-grade glioma (2017). *Clinical & translational oncology : official publication of the Federation of Spanish Oncology Societies and of the National Cancer Institute of Mexico* **20**, 3-15, doi:10.1007/s12094-017-1790-3 (2018).

56 Kong, J. *et al.* In silico analysis of nuclei in glioblastoma using large-scale microscopy images improves prediction of treatment response. *Conference proceedings : ... Annual International Conference of the IEEE Engineering in Medicine and Biology Society. IEEE Engineering in Medicine and Biology Society. Annual Conference* **2011**, 87-90, doi:10.1109/iembs.2011.6089903 (2011).

57 Pollack, I. F., Claassen, D., al-Shboul, Q., Janosky, J. E. & Deutsch, M. Low-grade gliomas of the cerebral hemispheres in children: an analysis of 71 cases. *Journal of neurosurgery* **82**, 536-547, doi:10.3171/jns.1995.82.4.0536 (1995).

58 Griffin, T. W., Beaufait, D. & Blasko, J. C. Cystic cerebellar astrocytomas in childhood. *Cancer* **44**, 276-280 (1979).

59 Pencalet, P. *et al.* Benign cerebellar astrocytomas in children. *Journal of neurosurgery* **90**, 265-273, doi:10.3171/jns.1999.90.2.0265 (1999).

60 Smoots, D. W., Geyer, J. R., Lieberman, D. M. & Berger, M. S. Predicting disease progression in childhood cerebellar astrocytoma. *Child's nervous system : ChNS : official journal of the International Society for Pediatric Neurosurgery* **14**, 636-648, doi:10.1007/s003810050290 (1998).

61 Desai, K. I., Nadkarni, T. D., Muzumdar, D. P. & Goel, A. Prognostic factors for cerebellar astrocytomas in children: a study of 102 cases. *Pediatric neurosurgery* **35**, 311-317, doi:10.1159/000050443 (2001).

62 Fisher, P. G. *et al.* Outcome analysis of childhood low-grade astrocytomas. *Pediatric blood & cancer* **51**, 245-250, doi:10.1002/pbc.21563 (2008).

63 Gajjar, A. *et al.* Low-grade astrocytoma: a decade of experience at St. Jude Children's Research Hospital. *Journal of clinical oncology : official journal of the American Society of Clinical Oncology* **15**, 2792-2799, doi:10.1200/jco.1997.15.8.2792 (1997).

64 Sutton, L. N. *et al.* Postoperative surveillance imaging in children with cerebellar astrocytomas. *Journal of neurosurgery* **84**, 721-725, doi:10.3171/jns.1996.84.5.0721 (1996).

65 Fisher, B. J., Leighton, C. C., Vujovic, O., Macdonald, D. R. & Stitt, L. Results of a policy of surveillance alone after surgical management of pediatric low grade gliomas. *International journal of radiation oncology, biology, physics* **51**, 704-710 (2001).

66 Merchant, T. E., Conklin, H. M., Wu, S., Lustig, R. H. & Xiong, X. Late effects of conformal radiation therapy for pediatric patients with low-grade glioma: prospective evaluation of cognitive, endocrine, and hearing deficits. *Journal of clinical oncology : official journal of the American Society of Clinical Oncology* **27**, 3691-3697, doi:10.1200/jco.2008.21.2738 (2009).

67 Gnekow, A. K. *et al.* Long-term follow-up of the multicenter, multidisciplinary treatment study HIT-LGG-1996 for low-grade glioma in children and adolescents of the German Speaking Society of Pediatric Oncology and Hematology. *Neuro-oncology* **14**, 1265-1284, doi:10.1093/neuonc/nos202 (2012).

68 Kool, M. *et al.* Genome sequencing of SHH medulloblastoma predicts genotype-related response to smoothened inhibition. *Cancer cell* **25**, 393-405, doi:10.1016/j.ccr.2014.02.004 (2014).

69 Krishnatry, R. *et al.* Clinical and treatment factors determining long-term outcomes for adult survivors of childhood low-grade glioma: A population-based study. *Cancer* **122**, 1261-1269, doi:10.1002/cncr.29907 (2016).

70 Kahlenberg, C. A. *et al.* Seizure prognosis of patients with low-grade tumors. *Seizure* **21**, 540-545, doi:https://doi.org/10.1016/j.seizure.2012.05.014 (2012).

71 Kerkhof, M. & Vecht, C. J. Seizure characteristics and prognostic factors of gliomas. *Epilepsia* **54 Suppl 9**, 12-17, doi:10.1111/epi.12437 (2013).

72 Kurzwelly, D., Herrlinger, U. & Simon, M. Seizures in patients with low-grade gliomas--incidence, pathogenesis, surgical management, and pharmacotherapy. *Advances and technical standards in neurosurgery* **35**, 81-111 (2010).

73 Ruda, R., Bello, L., Duffau, H. & Soffietti, R. Seizures in low-grade gliomas: natural history, pathogenesis, and outcome after treatments. *Neuro-oncology* **14 Suppl 4**, iv55-64, doi:10.1093/neuonc/nos199 (2012).

74 Armstrong, G. T. *et al.* Survival and long-term health and cognitive outcomes after low-grade glioma. *Neuro-oncology* **13**, 223-234, doi:10.1093/neuonc/noq178 (2011).

75 Welsh, S. J. & Corrie, P. G. Management of BRAF and MEK inhibitor toxicities in patients with metastatic melanoma. *Therapeutic advances in medical oncology* **7**, 122-136, doi:10.1177/1758834014566428 (2015).

76 Puzanov, I., Burnett, P. & Flaherty, K. T. Biological challenges of BRAF inhibitor therapy. *Molecular oncology* **5**, 116-123, doi:10.1016/j.molonc.2011.01.005 (2011).

77 Gnekow, A. K. *et al.* A European randomised controlled trial of the addition of etoposide to standard vincristine and carboplatin induction as part of an 18-

month treatment programme for childhood (</=16 years) low grade glioma - A final report. *European journal of cancer (Oxford, England : 1990)* **81**, 206-225, doi:10.1016/j.ejca.2017.04.019 (2017).

78 Kim, K. B. *et al.* Phase II study of the MEK1/MEK2 inhibitor Trametinib in patients with metastatic BRAF-mutant cutaneous melanoma previously treated with or without a BRAF inhibitor. *Journal of clinical oncology : official journal of the American Society of Clinical Oncology* **31**, 482-489, doi:10.1200/jco.2012.43.5966 (2013).

79 Liu, M. *et al.* Efficacy and safety of BRAF inhibition alone versus combined BRAF and MEK inhibition in melanoma: a meta-analysis of randomized controlled trials. *Oncotarget* **8**, 32258-32269, doi:10.18632/oncotarget.15632 (2017).

80 Azizi, A. A. & Schouten-van Meeteren, A. Y. N. Current and emerging treatment strategies for children with progressive chiasmatic-hypothalamic glioma diagnosed as infants: a web-based survey. *Journal of neuro-oncology* **136**, 127-134, doi:10.1007/s11060-017-2630-6 (2018).

81 Greger, J. G. *et al.* Combinations of BRAF, MEK, and PI3K/mTOR inhibitors overcome acquired resistance to the BRAF inhibitor GSK2118436 dabrafenib, mediated by NRAS or MEK mutations. *Molecular cancer therapeutics* **11**, 909-920, doi:10.1158/1535-7163.mct-11-0989 (2012).

82 Kool, M. *et al.* Molecular subgroups of medulloblastoma: an international meta-analysis of transcriptome, genetic aberrations, and clinical data of WNT, SHH, Group 3, and Group 4 medulloblastomas. *Acta neuropathologica* **123**, 473-484, doi:10.1007/s00401-012-0958-8 (2012).

83 Taylor, M. D. *et al.* Molecular subgroups of medulloblastoma: the current consensus. *Acta neuropathologica* **123**, 465-472, doi:10.1007/s00401-011-0922-z (2012).

84 Northcott, P. A. *et al.* Medulloblastomics: the end of the beginning. *Nature reviews. Cancer* **12**, 818-834, doi:10.1038/nrc3410 (2012).

85 Sturm, D. *et al.* New Brain Tumor Entities Emerge from Molecular Classification of CNS-PNETs. *Cell* **164**, 1060-1072, doi:10.1016/j.cell.2016.01.015 (2016).

86 Reinhardt, A. *et al.* Anaplastic astrocytoma with piloid features, a novel molecular class of IDH wildtype glioma with recurrent MAPK pathway, CDKN2A/B and ATRX alterations. *Acta neuropathologica*, doi:10.1007/s00401-018-1837-8 (2018).

87 Capper, D. *et al.* Characterization of R132H mutation-specific IDH1 antibody binding in brain tumors. *Brain pathology (Zurich, Switzerland)* **20**, 245-254, doi:10.1111/j.1750-3639.2009.00352.x (2010).

88 Chan, K. M. *et al.* The histone H3.3K27M mutation in pediatric glioma reprograms H3K27 methylation and gene expression. *Genes & development* **27**, 985-990, doi:10.1101/gad.217778.113 (2013).

89 Hasselblatt, M. *et al.* High-resolution genomic analysis suggests the absence of recurrent genomic alterations other than SMARCB1 aberrations in atypical teratoid/rhabdoid tumors. *Genes, chromosomes & cancer* **52**, 185-190, doi:10.1002/gcc.22018 (2013).

90 Margol, A. S. & Judkins, A. R. Pathology and diagnosis of SMARCB1-deficient tumors. *Cancer genetics* **207**, 358-364, doi:10.1016/j.cancergen.2014.07.004 (2014).

91 Pajtler, K. W. *et al.* Molecular Classification of Ependymal Tumors across All CNS Compartments, Histopathological Grades, and Age Groups. *Cancer cell* **27**, 728-743, doi:10.1016/j.ccell.2015.04.002 (2015).

92 Parker, M. *et al.* C11orf95-RELA fusions drive oncogenic NF-kappaB signalling in ependymoma. *Nature* **506**, 451-455, doi:10.1038/nature13109 (2014).

93 Schneppenheim, R. *et al.* Germline nonsense mutation and somatic inactivation of SMARCA4/BRG1 in a family with rhabdoid tumor predisposition syndrome. *American journal of human genetics* **86**, 279-284, doi:10.1016/j.ajhg.2010.01.013 (2010).

94 Venneti, S. *et al.* Evaluation of histone 3 lysine 27 trimethylation (H3K27me3) and enhancer of Zest 2 (EZH2) in pediatric glial and glioneuronal tumors shows decreased H3K27me3 in H3F3A K27M mutant glioblastomas. *Brain pathology (Zurich, Switzerland)* **23**, 558-564, doi:10.1111/bpa.12042 (2013).

95 Wu, G. *et al.* Somatic histone H3 alterations in pediatric diffuse intrinsic pontine gliomas and non-brainstem glioblastomas. *Nature genetics* **44**, 251-253, doi:10.1038/ng.1102 (2012).

96 Yan, H. *et al.* IDH1 and IDH2 mutations in gliomas. *The New England journal of medicine* **360**, 765-773, doi:10.1056/NEJMoa0808710 (2009).

97 Louis, D. N. *et al.* The 2016 World Health Organization Classification of Tumors of the Central Nervous System: a summary. *Acta neuropathologica* **131**, 803-820, doi:10.1007/s00401-016-1545-1 (2016).

98 DeWitt, J. C., Mock, A. & Louis, D. N. The 2016 WHO classification of central nervous system tumors: what neurologists need to know. *Current opinion in neurology* **30**, 643-649, doi:10.1097/wco.0000000000000490 (2017).

99 Komori, T. The 2016 WHO Classification of Tumours of the Central Nervous System: The Major Points of Revision. *Neurologia medico-chirurgica* **57**, 301-311, doi:10.2176/nmc.ra.2017-0010 (2017).

100 van den Bent, M. J. & Chang, S. M. Grade II and III Oligodendroglioma and Astrocytoma. *Neurologic clinics* **36**, 467-484, doi:10.1016/j.ncl.2018.04.005 (2018).

101 Hirose, T. [2016 WHO Classification of Tumors of CNS: A Paradigm Shift from Histologic to Molecular Classification]. *Brain and nerve = Shinkei kenkyu no shinpo* **70**, 543-550, doi:10.11477/mf.1416201036 (2018).

102 Kim, B. S. *et al.* Clinical outcomes of intracranial solitary fibrous tumor and hemangiopericytoma: analysis according to the 2016 WHO classification of central nervous system tumors. *Journal of neurosurgery*, 1-13, doi:10.3171/2017.7.jns171226 (2018).

103 Kobyakov, G. L., Absalyamova, O. V., Poddubskiy, A. A., Lodygina, K. S. & Kobyakova, E. A. [The 2016 WHO classification of primary central nervous system tumors: a clinician's view]. *Zhurnal voprosy neirokhirurgii imeni N. N. Burdenko* **82**, 88-96, doi:10.17116/neiro201882388 (2018).

104 Wen, P. Y. & Huse, J. T. 2016 World Health Organization Classification of Central Nervous System Tumors. *Continuum (Minneapolis, Minn.)* **23**, 1531-1547, doi:10.1212/con.0000000000000536 (2017).

105 Hovestadt, V. *et al.* Robust molecular subgrouping and copy-number profiling of medulloblastoma from small amounts of archival tumour material using high-

density DNA methylation arrays. *Acta neuropathologica* **125**, 913-916, doi:10.1007/s00401-013-1126-5 (2013).

106 Mazor, T. *et al.* DNA Methylation and Somatic Mutations Converge on the Cell Cycle and Define Similar Evolutionary Histories in Brain Tumors. *Cancer cell* **28**, 307-317, doi:10.1016/j.ccell.2015.07.012 (2015).

107 Olar, A. *et al.* Global epigenetic profiling identifies methylation subgroups associated with recurrence-free survival in meningioma. *Acta neuropathologica* **133**, 431-444, doi:10.1007/s00401-017-1678-x (2017).

108 Rohrich, M. *et al.* Methylation-based classification of benign and malignant peripheral nerve sheath tumors. *Acta neuropathologica* **131**, 877-887, doi:10.1007/s00401-016-1540-6 (2016).

109 Sahm, F. *et al.* DNA methylation-based classification and grading system for meningioma: a multicentre, retrospective analysis. *The Lancet. Oncology* **18**, 682-694, doi:10.1016/s1470-2045(17)30155-9 (2017).

110 Sturm, D. *et al.* Paediatric and adult glioblastoma: multiform (epi)genomic culprits emerge. *Nature reviews. Cancer* **14**, 92-107, doi:10.1038/nrc3655 (2014).

111 Heyn, H. & Esteller, M. DNA methylation profiling in the clinic: applications and challenges. *Nature Reviews Genetics* **13**, 679, doi:10.1038/nrg3270 (2012).

112 Taschner, C. A. *et al.* Freiburg Neuropathology Case Conference. *Clinical Neuroradiology* **28**, 461-466, doi:10.1007/s00062-018-0712-2 (2018).

113 Worst, B. C. *et al.* Next-generation personalised medicine for high-risk paediatric cancer patients - The INFORM pilot study. *European journal of cancer (Oxford, England : 1990)* **65**, 91-101, doi:10.1016/j.ejca.2016.06.009 (2016).

114 Robinson, D. R., Wu, Y. M. & Lin, S. F. The protein tyrosine kinase family of the human genome. *Oncogene* **19**, 5548-5557, doi:10.1038/sj.onc.1203957 (2000).

115 Zwick, E., Bange, J. & Ullrich, A. Receptor tyrosine kinase signalling as a target for cancer intervention strategies. *Endocrine-related cancer* **8**, 161-173 (2001).

116 Song, Z., Wang, M. & Zhang, A. Alectinib: a novel second generation anaplastic lymphoma kinase (ALK) inhibitor for overcoming clinically-acquired resistance. *Acta Pharmaceutica Sinica B* **5**, 34-37, doi:https://doi.org/10.1016/j.apsb.2014.12.007 (2015).

117 Morris, S. W. *et al.* Fusion of a kinase gene, ALK, to a nucleolar protein gene, NPM, in non-Hodgkin's lymphoma. *Science (New York, N.Y.)* **267**, 316-317 (1995).

118 Toyokawa, G. & Seto, T. Anaplastic lymphoma kinase rearrangement in lung cancer: its biological and clinical significance. *Respiratory investigation* **52**, 330-338, doi:10.1016/j.resinv.2014.06.005 (2014).

119 Revannasiddaiah, S., Thakur, P., Bhardwaj, B., Susheela, S. P. & Madabhavi, I. Pulmonary adenocarcinoma: implications of the recent advances in molecular biology, treatment and the IASLC/ATS/ERS classification. *Journal of thoracic disease* **6**, S502-525, doi:10.3978/j.issn.2072-1439.2014.05.19 (2014).

120 Rikova, K. *et al.* Global Survey of Phosphotyrosine Signaling Identifies Oncogenic Kinases in Lung Cancer. *Cell* **131**, 1190-1203, doi:https://doi.org/10.1016/j.cell.2007.11.025 (2007).

121 Soda, M. *et al.* Identification of the transforming EML4-ALK fusion gene in non-small-cell lung cancer. *Nature* **448**, 561-566, doi:10.1038/nature05945 (2007).

122 Inamura, K. *et al.* EML4-ALK fusion is linked to histological characteristics in a subset of lung cancers. *Journal of thoracic oncology : official publication of the*

International Association for the Study of Lung Cancer **3**, 13-17, doi:10.1097/JTO.0b013e31815e8b60 (2008).

123 Katayama, R. *et al.* Mechanisms of acquired crizotinib resistance in ALK-rearranged lung Cancers. *Science translational medicine* **4**, 120ra117, doi:10.1126/scitranslmed.3003316 (2012).

124 Solomon, B., Wilner, K. D. & Shaw, A. T. Current status of targeted therapy for anaplastic lymphoma kinase-rearranged non-small cell lung cancer. *Clinical pharmacology and therapeutics* **95**, 15-23, doi:10.1038/clpt.2013.200 (2014).

125 Shaw, A. T. & Engelman, J. A. ALK in lung cancer: past, present, and future. *Journal of clinical oncology : official journal of the American Society of Clinical Oncology* **31**, 1105-1111, doi:10.1200/jco.2012.44.5353 (2013).

126 Shaw, A. T. *et al.* Clinical features and outcome of patients with non-small-cell lung cancer who harbor EML4-ALK. *Journal of clinical oncology : official journal of the American Society of Clinical Oncology* **27**, 4247-4253, doi:10.1200/jco.2009.22.6993 (2009).

127 Rodig, S. J. *et al.* Unique clinicopathologic features characterize ALK-rearranged lung adenocarcinoma in the western population. *Clinical cancer research : an official journal of the American Association for Cancer Research* **15**, 5216-5223, doi:10.1158/1078-0432.ccr-09-0802 (2009).

128 Weickhardt, A. J. *et al.* Diagnostic assays for identification of anaplastic lymphoma kinase-positive non-small cell lung cancer. *Cancer* **119**, 1467-1477, doi:10.1002/cncr.27913 (2013).

129 Roskoski, R., Jr. Anaplastic lymphoma kinase (ALK): structure, oncogenic activation, and pharmacological inhibition. *Pharmacological research* **68**, 68-94, doi:10.1016/j.phrs.2012.11.007 (2013).

130 Alshareef, A. Novel Molecular Challenges in Targeting Anaplastic Lymphoma Kinase in ALK-Expressing Human Cancers. *Cancers* **9**, doi:10.3390/cancers9110148 (2017).

131 Sakamoto, H. *et al.* CH5424802, a selective ALK inhibitor capable of blocking the resistant gatekeeper mutant. *Cancer cell* **19**, 679-690, doi:10.1016/j.ccr.2011.04.004 (2011).

132 Grobner, S. N. *et al.* The landscape of genomic alterations across childhood cancers. *Nature* **555**, 321-327, doi:10.1038/nature25480 (2018).

133 Cui, J. *Case History: Xalkori™ (Crizotinib), a Potent and Selective Dual Inhibitor of Mesenchymal Epithelial Transition (MET) and Anaplastic Lymphoma Kinase (ALK) for Cancer Treatment*. (2013).

134 Cui, J. J. *et al.* Structure based drug design of crizotinib (PF-02341066), a potent and selective dual inhibitor of mesenchymal-epithelial transition factor (c-MET) kinase and anaplastic lymphoma kinase (ALK). *Journal of medicinal chemistry* **54**, 6342-6363, doi:10.1021/jm2007613 (2011).

135 Shaw, A. T. *et al.* Effect of crizotinib on overall survival in patients with advanced non-small-cell lung cancer harbouring ALK gene rearrangement: a retrospective analysis. *The Lancet. Oncology* **12**, 1004-1012, doi:10.1016/s1470-2045(11)70232-7 (2011).

136 Kodama, T., Tsukaguchi, T., Yoshida, M., Kondoh, O. & Sakamoto, H. Selective ALK inhibitor alectinib with potent antitumor activity in models of crizotinib resistance. *Cancer letters* **351**, 215-221, doi:10.1016/j.canlet.2014.05.020 (2014).

137 Kinoshita, K. *et al.* 9-substituted 6,6-dimethyl-11-oxo-6,11-dihydro-5H-benzo[b]carbazoles as highly selective and potent anaplastic lymphoma kinase inhibitors. *Journal of medicinal chemistry* **54**, 6286-6294, doi:10.1021/jm200652u (2011).

138 Watanabe, S. *et al.* Progression-Free and Overall Survival of Patients With ALK Rearrangement-Positive Non-Small Cell Lung Cancer Treated Sequentially With Crizotinib and Alectinib. *Clinical lung cancer* **17**, 528-534, doi:10.1016/j.cllc.2016.05.001 (2016).

139 Friboulet, L. *et al.* The ALK inhibitor ceritinib overcomes crizotinib resistance in non-small cell lung cancer. *Cancer discovery* **4**, 662-673, doi:10.1158/2159-8290.cd-13-0846 (2014).

140 Sun, H., Li, Y., Li, D. & Hou, T. Insight into crizotinib resistance mechanisms caused by three mutations in ALK tyrosine kinase using free energy calculation approaches. *Journal of chemical information and modeling* **53**, 2376-2389, doi:10.1021/ci400188q (2013).

141 Ignatius Ou, S. H. *et al.* Next-generation sequencing reveals a Novel NSCLC ALK F1174V mutation and confirms ALK G1202R mutation confers high-level resistance to alectinib (CH5424802/RO5424802) in ALK-rearranged NSCLC patients who progressed on crizotinib. *Journal of thoracic oncology : official publication of the International Association for the Study of Lung Cancer* **9**, 549-553, doi:10.1097/jto.0000000000000094 (2014).

142 Peters, S. *et al.* Alectinib versus Crizotinib in Untreated ALK-Positive Non-Small-Cell Lung Cancer. *The New England journal of medicine* **377**, 829-838, doi:10.1056/NEJMoa1704795 (2017).

143 Zou, H. Y. *et al.* PF-06463922 is a potent and selective next-generation ROS1/ALK inhibitor capable of blocking crizotinib-resistant ROS1 mutations. *Proceedings of the National Academy of Sciences of the United States of America* **112**, 3493-3498, doi:10.1073/pnas.1420785112 (2015).

144 Gainor, J. F. & Shaw, A. T. Emerging paradigms in the development of resistance to tyrosine kinase inhibitors in lung cancer. *Journal of clinical oncology : official journal of the American Society of Clinical Oncology* **31**, 3987-3996, doi:10.1200/jco.2012.45.2029 (2013).

145 Ou, S. H., Tan, J., Yen, Y. & Soo, R. A. ROS1 as a 'druggable' receptor tyrosine kinase: lessons learned from inhibiting the ALK pathway. *Expert review of anticancer therapy* **12**, 447-456, doi:10.1586/era.12.17 (2012).

146 Collier, T. L. *et al.* Brain Penetration of the ROS1/ALK Inhibitor Lorlatinib Confirmed by PET. *Molecular imaging* **16**, 1536012117736669, doi:10.1177/1536012117736669 (2017).

147 Johnson, T. W. *et al.* Discovery of (10R)-7-amino-12-fluoro-2,10,16-trimethyl-15-oxo-10,15,16,17-tetrahydro-2H-8,4-(m etheno)pyrazolo[4,3-h][2,5,11]-benzoxadiazacyclotetradecine-3-carbonitrile (PF-06463922), a macrocyclic inhibitor of anaplastic lymphoma kinase (ALK) and c-ros oncogene 1 (ROS1) with preclinical brain exposure and broad-spectrum potency against ALK-resistant mutations. *Journal of medicinal chemistry* **57**, 4720-4744, doi:10.1021/jm500261q (2014).

148 Begley, D. J., Pontikis, C. C. & Scarpa, M. Lysosomal storage diseases and the blood-brain barrier. *Current pharmaceutical design* **14**, 1566-1580 (2008).

149 Schiffmann, R. Therapeutic approaches for neuronopathic lysosomal storage disorders. *Journal of inherited metabolic disease* **33**, 373-379, doi:10.1007/s10545-010-9047-0 (2010).
150 Smith, Q. R. in *The Blood-Brain Barrier: Biology and Research Protocols* (ed Sukriti Nag) 193-208 (Humana Press, 2003).
151 Abbott, N. J., Dolman, D. E. & Patabendige, A. K. Assays to predict drug permeation across the blood-brain barrier, and distribution to brain. *Current drug metabolism* **9**, 901-910 (2008).
152 Hammad, S. Advances in 2D and 3D in vitro systems for hepatotoxicity testing. *EXCLI journal* **12**, 993-996 (2013).
153 Knobeloch, D. *et al.* Human hepatocytes: isolation, culture, and quality procedures. *Methods in molecular biology (Clifton, N.J.)* **806**, 99-120, doi:10.1007/978-1-61779-367-7_8 (2012).
154 Zellmer, S. *et al.* Transcription factors ETF, E2F, and SP-1 are involved in cytokine-independent proliferation of murine hepatocytes. *Hepatology (Baltimore, Md.)* **52**, 2127-2136, doi:10.1002/hep.23930 (2010).
155 Godoy, P. *et al.* Extracellular matrix modulates sensitivity of hepatocytes to fibroblastoid dedifferentiation and transforming growth factor beta-induced apoptosis. *Hepatology (Baltimore, Md.)* **49**, 2031-2043, doi:10.1002/hep.22880 (2009).
156 Godoy, P. *et al.* Dexamethasone-dependent versus -independent markers of epithelial to mesenchymal transition in primary hepatocytes. *Biological chemistry* **391**, 73-83, doi:10.1515/bc.2010.010 (2010).
157 Godoy, P., Schug, M., Bauer, A. & Hengstler, J. G. Reversible manipulation of apoptosis sensitivity in cultured hepatocytes by matrix-mediated manipulation of signaling activities. *Methods in molecular biology (Clifton, N.J.)* **640**, 139-155, doi:10.1007/978-1-60761-688-7_7 (2010).
158 Perlman, R. L. Mouse models of human disease: An evolutionary perspective. *Evolution, medicine, and public health* **2016**, 170-176, doi:10.1093/emph/eow014 (2016).
159 Monaco, G., van Dam, S., Casal Novo Ribeiro, J. L., Larbi, A. & de Magalhaes, J. P. A comparison of human and mouse gene co-expression networks reveals conservation and divergence at the tissue, pathway and disease levels. *BMC evolutionary biology* **15**, 259, doi:10.1186/s12862-015-0534-7 (2015).
160 Waterston, R. H. *et al.* Initial sequencing and comparative analysis of the mouse genome. *Nature* **420**, 520-562, doi:10.1038/nature01262 (2002).
161 Workman, P. *et al.* Guidelines for the welfare and use of animals in cancer research. *British journal of cancer* **102**, 1555-1577, doi:10.1038/sj.bjc.6605642 (2010).
162 Lilienblum, W. *et al.* Alternative methods to safety studies in experimental animals: role in the risk assessment of chemicals under the new European Chemicals Legislation (REACH). *Archives of toxicology* **82**, 211-236, doi:10.1007/s00204-008-0279-9 (2008).
163 Ghallab, A. In vitro test systems and their limitations. *EXCLI journal* **12**, 1024-1026 (2013).

5. References

164 Tice, R. R., Austin, C. P., Kavlock, R. J. & Bucher, J. R. Improving the human hazard characterization of chemicals: a Tox21 update. *Environmental health perspectives* **121**, 756-765, doi:10.1289/ehp.1205784 (2013).

165 Miller, J. A., Horvath, S. & Geschwind, D. H. Divergence of human and mouse brain transcriptome highlights Alzheimer disease pathways. *Proceedings of the National Academy of Sciences of the United States of America* **107**, 12698-12703, doi:10.1073/pnas.0914257107 (2010).

166 Chan, E. T. *et al.* Conservation of core gene expression in vertebrate tissues. *Journal of biology* **8**, 33, doi:10.1186/jbiol130 (2009).

167 de Magalhaes, J. P. & Church, G. M. Analyses of human-chimpanzee orthologous gene pairs to explore evolutionary hypotheses of aging. *Mechanisms of ageing and development* **128**, 355-364, doi:10.1016/j.mad.2007.03.004 (2007).

168 Tacutu, R., Budovsky, A., Yanai, H. & Fraifeld, V. E. Molecular links between cellular senescence, longevity and age-related diseases - a systems biology perspective. *Aging* **3**, 1178-1191, doi:10.18632/aging.100413 (2011).

169 Liao, B. Y. & Zhang, J. Evolutionary conservation of expression profiles between human and mouse orthologous genes. *Molecular biology and evolution* **23**, 530-540, doi:10.1093/molbev/msj054 (2006).

170 Vandamme, T. F. Use of rodents as models of human diseases. *Journal of pharmacy & bioallied sciences* **6**, 2-9, doi:10.4103/0975-7406.124301 (2014).

171 Navone, N. M. *et al.* Movember GAP1 PDX project: An international collection of serially transplantable prostate cancer patient-derived xenograft (PDX) models. *The Prostate*, doi:10.1002/pros.23701 (2018).

172 Capasso, A. *et al.* Dual compartmental targeting of cell cycle and angiogenic kinases in colorectal cancer models. *Anti-cancer drugs*, doi:10.1097/cad.0000000000000673 (2018).

173 Nitschinsk, K., Idris, A. & McMillan, N. Patient derived xenografts as models for head and neck cancer. *Cancer letters* **434**, 114-119, doi:10.1016/j.canlet.2018.07.023 (2018).

174 Deng, M. *et al.* Effective elimination of adult B-lineage acute lymphoblastic leukemia by disulfiram/copper complex in vitro and in vivo in patient-derived xenograft models. *Oncotarget* **7**, 82200-82212, doi:10.18632/oncotarget.9413 (2016).

175 Lampreht Tratar, U., Horvat, S. & Cemazar, M. Transgenic Mouse Models in Cancer Research. *Frontiers in oncology* **8**, 268, doi:10.3389/fonc.2018.00268 (2018).

176 Lwin, T. M., Hoffman, R. M. & Bouvet, M. Advantages of patient-derived orthotopic mouse models and genetic reporters for developing fluorescence-guided surgery. *Journal of surgical oncology*, doi:10.1002/jso.25150 (2018).

177 Tentler, J. J. *et al.* Patient-derived tumour xenografts as models for oncology drug development. *Nature reviews. Clinical oncology* **9**, 338-350, doi:10.1038/nrclinonc.2012.61 (2012).

178 Hidalgo, M. *et al.* Patient-derived xenograft models: an emerging platform for translational cancer research. *Cancer discovery* **4**, 998-1013, doi:10.1158/2159-8290.cd-14-0001 (2014).

179 Kelly, J. J. *et al.* Oligodendroglioma cell lines containing t(1;19)(q10;p10). *Neuro-oncology* **12**, 745-755, doi:10.1093/neuonc/noq031 (2010).

180 Grippo, M. C., Penteado, P. F., Carelli, E. F., Cruz-Hofling, M. A. & Verinaud, L. Establishment and partial characterization of a continuous human malignant glioma cell line: NG97. *Cellular and molecular neurobiology* **21**, 421-428 (2001).

181 Twombly, R. First clinical trials of endostatin yield lukewarm results. *Journal of the National Cancer Institute* **94**, 1520-1521 (2002).

182 Kulke, M. H. *et al.* A phase II study of troglitazone, an activator of the PPARgamma receptor, in patients with chemotherapy-resistant metastatic colorectal cancer. *Cancer journal (Sudbury, Mass.)* **8**, 395-399 (2002).

183 Seitz, G., Armeanu-Ebinger, S., Warmann, S. & Fuchs, J. Animal models of extracranial pediatric solid tumors. *Oncology letters* **4**, 859-864, doi:10.3892/ol.2012.852 (2012).

184 Dobbin, Z. C. *et al.* Using heterogeneity of the patient-derived xenograft model to identify the chemoresistant population in ovarian cancer. *Oncotarget* **5**, 8750-8764, doi:10.18632/oncotarget.2373 (2014).

185 Cassidy, J. W., Caldas, C. & Bruna, A. Maintaining Tumor Heterogeneity in Patient-Derived Tumor Xenografts. *Cancer research* **75**, 2963-2968, doi:10.1158/0008-5472.can-15-0727 (2015).

186 Adams, J. M. & Cory, S. Transgenic models of tumor development. *Science (New York, N.Y.)* **254**, 1161-1167 (1991).

187 Sharpless, N. E. & Depinho, R. A. The mighty mouse: genetically engineered mouse models in cancer drug development. *Nature reviews. Drug discovery* **5**, 741-754, doi:10.1038/nrd2110 (2006).

188 Recurrent MET fusion genes represent a drug target in pediatric glioblastoma. *Nature medicine* **22**, 1314-1320, doi:10.1038/nm.4204 (2016).

189 Misuraca, K. L., Hu, G., Barton, K. L., Chung, A. & Becher, O. J. A Novel Mouse Model of Diffuse Intrinsic Pontine Glioma Initiated in Pax3-Expressing Cells. *Neoplasia (New York, N.Y.)* **18**, 60-70, doi:10.1016/j.neo.2015.12.002 (2016).

190 Svoboda, D. S., Clark, A., Park, D. S. & Slack, R. S. Induction of protein deletion through in utero electroporation to define deficits in neuronal migration in transgenic models. *Journal of visualized experiments : JoVE*, 51983, doi:10.3791/51983 (2015).

191 Chen, F., Becker, A. J. & LoTurco, J. J. Contribution of tumor heterogeneity in a new animal model of CNS tumors. *Molecular cancer research : MCR* **12**, 742-753, doi:10.1158/1541-7786.mcr-13-0531 (2014).

192 Sreedharan, S. *et al.* Mouse Models of Pediatric Supratentorial High-grade Glioma Reveal How Cell-of-Origin Influences Tumor Development and Phenotype. *Cancer research* **77**, 802-812, doi:10.1158/0008-5472.can-16-2482 (2017).

193 Hambardzumyan, D., Amankulor, N. M., Helmy, K. Y., Becher, O. J. & Holland, E. C. Modeling Adult Gliomas Using RCAS/t-va Technology. *Translational oncology* **2**, 89-95 (2009).

194 Wang, W., Dong, B. & Yang, F. Avian Retrovirus-Mediated Tumor-Specific Gene Knockout. *Current protocols in molecular biology* **121**, 23.17.21-23.17.27, doi:10.1002/cpmb.54 (2018).

195 Friedmann-Morvinski, D. & Singer, O. Overexpression Models: Lentiviral Modeling of Brain Cancer. *Current protocols in mouse biology* **3**, 121-139, doi:10.1002/9780470942390.mo110271 (2013).

5. References

196 Taniguchi, Y., Young-Pearse, T., Sawa, A. & Kamiya, A. In utero electroporation as a tool for genetic manipulation in vivo to study psychiatric disorders: from genes to circuits and behaviors. *The Neuroscientist : a review journal bringing neurobiology, neurology and psychiatry* **18**, 169-179, doi:10.1177/1073858411399925 (2012).

197 Kim, D., Alptekin, B. & Budak, H. CRISPR/Cas9 genome editing in wheat. *Functional & integrative genomics* **18**, 31-41, doi:10.1007/s10142-017-0572-x (2018).

198 Bourgeois, F. T. *et al.* Pediatric versus adult drug trials for conditions with high pediatric disease burden. *Pediatrics* **130**, 285-292, doi:10.1542/peds.2012-0139 (2012).

199 Lindkvist, J., Airaksinen, M., Kaukonen, A. M., Klaukka, T. & Hoppu, K. Evolution of paediatric off-label use after new significant medicines become available for adults: a study on triptans in Finnish children 1994-2007. *British journal of clinical pharmacology* **71**, 929-935, doi:10.1111/j.1365-2125.2010.03881.x (2011).

200 Waller, D. G. Off-label and unlicensed prescribing for children: have we made any progress? *British journal of clinical pharmacology* **64**, 1-2, doi:10.1111/j.1365-2125.2007.02987.x (2007).

201 Kolb, E. A. *et al.* Initial testing (stage 1) of AZD6244 (ARRY-142886) by the Pediatric Preclinical Testing Program. *Pediatric blood & cancer* **55**, 668-677, doi:10.1002/pbc.22576 (2010).

202 Sato, Y. *et al.* Stable integration and conditional expression of electroporated transgenes in chicken embryos. *Developmental biology* **305**, 616-624, doi:10.1016/j.ydbio.2007.01.043 (2007).

203 Dyer, M. A. Mouse models of childhood cancer of the nervous system. *Journal of clinical pathology* **57**, 561-576 (2004).

204 Bandopadhayay, P. *et al.* MYB-QKI rearrangements in angiocentric glioma drive tumorigenicity through a tripartite mechanism. *Nature genetics* **48**, 273-282, doi:10.1038/ng.3500 (2016).

205 Infarinato, N. R. *et al.* The ALK/ROS1 Inhibitor PF-06463922 Overcomes Primary Resistance to Crizotinib in ALK-Driven Neuroblastoma. *Cancer discovery* **6**, 96-107, doi:10.1158/2159-8290.cd-15-1056 (2016).

206 Nair, A. B. & Jacob, S. A simple practice guide for dose conversion between animals and human. *Journal of basic and clinical pharmacy* **7**, 27-31, doi:10.4103/0976-0105.177703 (2016).

207 Kerr, J. F., Wyllie, A. H. & Currie, A. R. Apoptosis: a basic biological phenomenon with wide-ranging implications in tissue kinetics. *British journal of cancer* **26**, 239-257 (1972).

208 Casciola-Rosen, L., Rosen, A., Petri, M. & Schlissel, M. Surface blebs on apoptotic cells are sites of enhanced procoagulant activity: implications for coagulation events and antigenic spread in systemic lupus erythematosus. *Proceedings of the National Academy of Sciences of the United States of America* **93**, 1624-1629 (1996).

209 van Engeland, M., Ramaekers, F. C., Schutte, B. & Reutelingsperger, C. P. A novel assay to measure loss of plasma membrane asymmetry during apoptosis of adherent cells in culture. *Cytometry* **24**, 131-139, doi:10.1002/(sici)1097-0320(19960601)24:2<131::aid-cyto5>3.0.co;2-m (1996).

210 Vermes, I., Haanen, C., Steffens-Nakken, H. & Reutelingsperger, C. A novel assay for apoptosis. Flow cytometric detection of phosphatidylserine expression on early apoptotic cells using fluorescein labelled Annexin V. *Journal of immunological methods* **184**, 39-51 (1995).

211 Gopinathan, A., Morton, J. P., Jodrell, D. I. & Sansom, O. J. GEMMs as preclinical models for testing pancreatic cancer therapies. *Disease models & mechanisms* **8**, 1185-1200, doi:10.1242/dmm.021055 (2015).

212 Becher, O. J. & Holland, E. C. Genetically engineered models have advantages over xenografts for preclinical studies. *Cancer research* **66**, 3355-3358, discussion 3358-3359, doi:10.1158/0008-5472.can-05-3827 (2006).

213 Gopinathan, A. & Tuveson, D. A. The use of GEM models for experimental cancer therapeutics. *Disease models & mechanisms* **1**, 83-86, doi:10.1242/dmm.000570 (2008).

214 Zhang, Y. *et al.* Study human pancreatic cancer in mice: how close are they? *Biochimica et biophysica acta* **1835**, 110-118, doi:10.1016/j.bbcan.2012.11.001 (2013).

215 Au - Feng, W. *et al.* CRISPR-mediated Loss of Function Analysis in Cerebellar Granule Cells Using In Utero Electroporation-based Gene Transfer. *JoVE*, e57311, doi:doi:10.3791/57311 (2018).

216 Zuckermann, M. *et al.* Somatic CRISPR/Cas9-mediated tumour suppressor disruption enables versatile brain tumour modelling. *Nature communications* **6**, 7391, doi:10.1038/ncomms8391 (2015).

217 Dyer, M. A. & Cepko, C. L. Regulating proliferation during retinal development. *Nature reviews. Neuroscience* **2**, 333-342, doi:10.1038/35072555 (2001).

218 Basch, M. L., Selleck, M. A. & Bronner-Fraser, M. Timing and competence of neural crest formation. *Developmental neuroscience* **22**, 217-227, doi:10.1159/000017444 (2000).

219 Livesey, F. J. & Cepko, C. L. Vertebrate neural cell-fate determination: lessons from the retina. *Nature reviews. Neuroscience* **2**, 109-118, doi:10.1038/35053522 (2001).

220 Grande, E., Bolos, M. V. & Arriola, E. Targeting oncogenic ALK: a promising strategy for cancer treatment. *Molecular cancer therapeutics* **10**, 569-579, doi:10.1158/1535-7163.mct-10-0615 (2011).

221 Luo, S. Y. & Lam, D. C. Oncogenic driver mutations in lung cancer. *Translational Respiratory Medicine* **1**, 6, doi:10.1186/2213-0802-1-6 (2013).

222 Faehling, M. *et al.* Oncogenic driver mutations, treatment, and EGFR-TKI resistance in a Caucasian population with non-small cell lung cancer: survival in clinical practice. *Oncotarget* **8**, 77897-77914, doi:10.18632/oncotarget.20857 (2017).

223 Li, S. *et al.* Comprehensive Characterization of Oncogenic Drivers in Asian Lung Adenocarcinoma. *Journal of Thoracic Oncology* **11**, 2129-2140, doi:https://doi.org/10.1016/j.jtho.2016.08.142 (2016).

224 Zhou, J. X. *et al.* Oncogenic driver mutations in patients with non-small-cell lung cancer at various clinical stages. *Annals of oncology : official journal of the European Society for Medical Oncology* **24**, 1319-1325, doi:10.1093/annonc/mds626 (2013).

5. References

225 Sholl, L. M. *et al.* Multi-institutional Oncogenic Driver Mutation Analysis in Lung Adenocarcinoma: The Lung Cancer Mutation Consortium Experience. *Journal of thoracic oncology : official publication of the International Association for the Study of Lung Cancer* **10**, 768-777, doi:10.1097/jto.0000000000000516 (2015).

226 Kwak, E. L. *et al.* Anaplastic lymphoma kinase inhibition in non-small-cell lung cancer. *The New England journal of medicine* **363**, 1693-1703, doi:10.1056/NEJMoa1006448 (2010).

227 Zhu, Z. & Chai, Y. Crizotinib resistance overcome by ceritinib in an ALK-positive non-small cell lung cancer patient with brain metastases: A case report. *Medicine* **96**, e8652, doi:10.1097/md.0000000000008652 (2017).

228 Casaluce, F. *et al.* Resistance to Crizotinib in Advanced Non-Small Cell Lung Cancer (NSCLC) with ALK Rearrangement: Mechanisms, Treatment Strategies and New Targeted Therapies. *Current clinical pharmacology* **11**, 77-87 (2016).

229 Weiss, M. B. *et al.* Deletion of p53 in human mammary epithelial cells causes chromosomal instability and altered therapeutic response. *Oncogene* **29**, 4715-4724, doi:10.1038/onc.2010.220 (2010).

230 Kuerbitz, S. J., Plunkett, B. S., Walsh, W. V. & Kastan, M. B. Wild-type p53 is a cell cycle checkpoint determinant following irradiation. *Proceedings of the National Academy of Sciences of the United States of America* **89**, 7491-7495 (1992).

231 Agarwal, M. L., Agarwal, A., Taylor, W. R. & Stark, G. R. p53 controls both the G2/M and the G1 cell cycle checkpoints and mediates reversible growth arrest in human fibroblasts. *Proceedings of the National Academy of Sciences of the United States of America* **92**, 8493-8497 (1995).

232 Lukin, D. J., Carvajal, L. A., Liu, W. J., Resnick-Silverman, L. & Manfredi, J. J. p53 Promotes cell survival due to the reversibility of its cell-cycle checkpoints. *Molecular cancer research : MCR* **13**, 16-28, doi:10.1158/1541-7786.mcr-14-0177 (2015).

233 Levin, S. Apoptosis, necrosis, or oncosis: what is your diagnosis? A report from the Cell Death Nomenclature Committee of the Society of Toxicologic Pathologists. *Toxicological sciences : an official journal of the Society of Toxicology* **41**, 155-156, doi:10.1006/toxs.1997.2432 (1998).

234 Levin, S. *et al.* The nomenclature of cell death: recommendations of an ad hoc Committee of the Society of Toxicologic Pathologists. *Toxicologic pathology* **27**, 484-490, doi:10.1177/019262339902700419 (1999).

235 Majno, G. & Joris, I. Apoptosis, oncosis, and necrosis. An overview of cell death. *The American journal of pathology* **146**, 3-15 (1995).

236 Fink, S. L. & Cookson, B. T. Apoptosis, pyroptosis, and necrosis: mechanistic description of dead and dying eukaryotic cells. *Infection and immunity* **73**, 1907-1916, doi:10.1128/iai.73.4.1907-1916.2005 (2005).

237 Lee, S. Y. Temozolomide resistance in glioblastoma multiforme. *Genes & Diseases* **3**, 198-210, doi:https://doi.org/10.1016/j.gendis.2016.04.007 (2016).

238 Hottinger, A. F., Stupp, R. & Homicsko, K. Standards of care and novel approaches in the management of glioblastoma multiforme. *Chinese journal of cancer* **33**, 32-39, doi:10.5732/cjc.013.10207 (2014).

239 Weller, M., Cloughesy, T., Perry, J. R. & Wick, W. Standards of care for treatment of recurrent glioblastoma--are we there yet? *Neuro-oncology* **15**, 4-27, doi:10.1093/neuonc/nos273 (2013).

240 Friedman, H. S., Kerby, T. & Calvert, H. Temozolomide and treatment of malignant glioma. *Clinical cancer research : an official journal of the American Association for Cancer Research* **6**, 2585-2597 (2000).

241 Fernandes, C. in *Glioblastoma* (Codon Publications, 2017).

242 Tseng, W. L., Hsu, H. H., Chen, Y. & Tseng, S. H. Tumor Recurrence in a Glioblastoma Patient after Discontinuation of Prolonged Temozolomide Treatment. *Asian journal of neurosurgery* **12**, 727-730, doi:10.4103/ajns.AJNS_39_15 (2017).

243 Wenger, K. J. *et al.* Bevacizumab as a last-line treatment for glioblastoma following failure of radiotherapy, temozolomide and lomustine. *Oncology letters* **14**, 1141-1146, doi:10.3892/ol.2017.6251 (2017).

5. References

6. Publications

Ismer B., Clarke M., Stoler I., Bandopadhayay P., Tatevossian R., Worst B., Balasubramanian P., Olsen T. K., Brandal P., Farrell M., Cryan J., Capra M., Karremann M., Schittenhelm J., Schuhmann M., Ebinger M., Kerl K., Pietsch T., Mackay A., Driever P. H., Kramm C., Preusser M., Haberler C., Korshunov A., Witt O., Sahm F., von Deimling A., Pfister S. M., Jones, C., Ligon K. L., Capper D., Ellison D.*, Jones D. T. W.*. *In preparation*

Ismer B.*, Jones D. T.W.*, Schrimpf D., Reuss D., Stichel D., Casalini B., Schittenhelm J., Stephan F., Winther-Kristensen B., Sehested A. M., Scheie D., Korshunov A., Milde T., Pajtler K., Herold-Mende C., Witt O., Wick W., Pfister S. M., von Deimling A., Sahm F. *In preparation*

6. Publications

7. Acknowledgements

First of all I would like to thank Dr. David Jones and Dr. Jan Gronych for choosing me as your PhD Student at the summer selection 2015 and thereby allowing me to carry out the above work and develop myself further scientifically. Thank you for believing in me and supporting me throughout my PhD time at the DKFZ. I would like to thank David especially for always being so understanding, kind, funny and easy to persuade into doing a triathlon with me. Scientifically and athletically you challenged me to always try my best and I really appreciate your support and your believe in me! Thank you!

The same gratitude goes out to Prof. Stefan Pfister and Prof. Peter Lichter, who supported me during my time in their divisions, both in my PhD and my fundraising projects. I really appreciate all four of you giving me the support and freedom to be who I am.

Thank you very much also to my TAC members, Prof. Christel Herold-Mende and Prof. Peter Angel, who always gave me constructive feedback on the progress of my project. I would like to thanks Prof. Peter Angel also for organising three amazing DKFZ-MOST meetings in Tel Aviv and Heidelberg and for making my PhD project very collaborative. This brings me to my collaboration partners at Tel Aviv University, Israel, Dr. Dinorah Friedmann-Morvinski and Itai Moshe. Thank you both for such a nice and effective collaboration and for bringing our project forward together. It was nice visiting you in Israel and I enjoyed welcoming you in Heidelberg.

Thank you everyone in the groups of G702, B062 and B060 who introduced me to new methods, techniques or laboratory equipment. Without this great support I could have not done the work I did. The atmosphere in our big group is amazing, thank you for making my time here so enjoyable and never not wanting to come to work in the morning. Thank you especially to Dr. Daisuke Kawauchi for bringing the *in utero* electroporation method into the lab, my animal experiments and results would have not been the same without it! A huge thank you goes out to the big office on the fourth floor, you are fun and cool people and are always good for a laugh or a joke. I will miss our little competitions in and in front of the office.

7. Acknowledgements

Furthermore, I cannot forget the amazing friends I made during my PhD time. Sonja Krausert and Jasmin Mangei, thank you for being such amazing friends and joining in to all those hard, but enjoyable sporting competitions. Go, Tri girls! I could not have asked for any better training partners, relay team members and friends! You are amazing and I will miss you most!

I would also like to thank Kathrin Schramm, Marc Zuckermann, Alex Sommerkamp and Kati Lappalainen for some great (and not always scientific) discussions and making me laugh about some of the things either one of us said. I don't think I will ever meet people like you again. Thank you to Norman Mack, Dany Sohn, Britta Statz and Benni Schwalm for always being fun to work and socialise with. I learnt so much from you guys!

Katia Fundter, I owe so much to you! Sharing my passion for the KiTZ and the fundraising aspect of it and coming up and executing such great ideas we had in our KiTZ Club meetings! Thank you Katia, for meeting with me in August 2016, that was a great start to something big! I will never forget it! The whole KiTZ Club made my time here more enjoyable and made me better at project management, which was a great balance to my work in the lab. I would also like to thank Sarina Thomas and Kati Deumelandt for making my selection and the Israel trips respectively enjoyable and unforgettable.

Zum Schluss möchte ich mich bei meiner tollen Familie bedanken, die mich auf all meinen Wegen immer unterstützt hat! Egal was war, ihr wart immer für mich da und das weiß ich sehr zu schätzen! Ich weiß nicht, wo ich heute ohne euch wäre und möchte mich von ganzem Herzen bei euch für alles bedanken: Mama, Omi & Opi, Tante Christel und Oliver. Danke für die wunderbarste Kindheit, die ich mir je hätte vorstellen können! Ich hoffe, dass ich euch eines Tages all dies zurückgeben kann. Another person and therewith his family came into my life 7 years ago and since then, I cannot imagine living my life without you Honig. You are my best friend and soul mate and I am looking forward to finally spending my future with you. Although times were not always straight forward, we managed to get where we are now with the support of our families and us being us. Thank you also to Pam, Paul, Gemma and Greg, you are the other half of my family. Thank you for everything and for welcoming me into your family and treating me like I am part of yours. A huge kiss and cuddle also to my dearest buddy Theo and

Summer, you always make me smile and make me forget about any bad day I had. I will always be there for you and look after you!

Der wichtigste Dank geht aber an eine Person, die ich leider nicht immer dann anrufen oder besuchen kann, wenn ich sie gerade brauche. Trotzdem ist sie immer bei mir und unterstützt mich und glaubt an mich mehr als jeder andere. Onkel Kai, ohne dich wäre ich nicht hier angekommen wo ich jetzt bin, ohne dich hätte ich vielleicht niemals hier angefangen und ohne dich hätte ich nie meinen Traum in der Krebsforschung zu arbeiten verwirklichen können! Ich vermisse dich von ganzem Herzen. Danke, dass du mich immer ermutigst alles zu schaffen was ich mir vornehme, dass du mir immer gut zusprichst, wenn ich Zweifel habe, dass du mir gezeigt hast was Lebensfreude und Lebenswillen ist und danke, dass du mir gezeigt hast, dass es sich lohnt für Dinge zu kämpfen egal wie (gut) die Chancen stehen. Ich habe dir so viel zu verdanken und habe aber leider keine Chance mehr bekommen es dir so zu zeigen wie du es verdient hättest.

Danke, dass du der beste Onkel warst, den ich mir je hätte wünschen können. Ich liebe dich bis zum großen Wagen und zurück!